

THE MECHANICAL PROPERTIES OF
HIGH STRENGTH LOW ALLOY STEELS

THE MECHANICAL PROPERTIES OF
HIGH STRENGTH LOW ALLOY STEELS

By

ANDJELKO R. FILIPOVIC, Dipl. Ing.

A Thesis

Submitted to the School of Graduate Studies
in Partial Fulfilment of the Requirements
for the Degree
Master of Engineering

McMaster University

January, 1976

MASTER OF ENGINEERING
(Metallurgy and Materials Science)

McMASTER UNIVERSITY
Hamilton, Ontario

TITLE: The Mechanical Properties of High Strength Low
Alloy Steels

AUTHOR: Andjelko R. Filipovic, Dipl. Ing. (University of
Belgrade, Yugoslavia)

SUPERVISOR: Professor J.D. Embury

NUMBER OF PAGES: ix, 124

SCOPE AND CONTENTS:

The relationships between the mechanical properties, fracture and forming characteristics and the microstructural features has been investigated in commercially available HSLA steels. In addition, attention has been focussed on the behaviour of these materials subjected to a reverse straining, as a very important characteristic for pipeline applications.

ACKNOWLEDGMENTS

It is indeed a pleasure to express my gratitude to those members of the Department of Metallurgy and Materials Science who assisted in this work. I am greatly indebted to my supervisor, Dr. J.D. Embury for his assistance in this program and in providing advice and encouragement throughout the duration of the work.

Many thanks are also extended to Dr. J.L. Duncan and Dr. R. Sowerby, whose interest also contributed to the success of this work. Furthermore, I wish to acknowledge the assistance and valuable discussions to Mr. G.D. Moan and other members of the research group.

I wish to express the appreciation of Mr. H. Herø, who during his stay at McMaster University, contributed significantly to this work.

I would also like to thank Mr. T. Bryner for work done on the micrographs.

Thanks are also due to Mrs. Annette Neumayer for the accurate typing of this thesis.

Special gratitude is extended to my wife, Dusanka, for her patience and understanding throughout the course of this work.

FIGURE CAPTIONS

- Figure 1 Diagram illustrating the correlation between yield strength and transformation temperature for different finishing temperatures (Ref. 1).
- Figure 2 Schematic CCT diagram for low carbon steel. Broken lines indicate transformation path for different rolling schedules.
CCR: Conventional Controlled Rolling
CR: Continuous Rolling
AC: Air Cool
WQ: Water Quench (From Ref. 2)
- Figures 3 and 4 Composite micrographs showing the microstructures of acicular ferrite Ipsco 3/8" steel.
- Figures 5 and 6 Composite micrographs showing the microstructures of polygonal ferrite Molycorp X-80, 5/8" steel.
- Figure 7 Composite micrographs showing the microstructure of Molycorp X-80, 1/4" steel.
- Figure 8 Composite micrographs showing the microstructure of INCO 787, 1/2" steel.
- Figure 9 Schematic drawing of the tensile sample.
- Figure 10 Typical tensile test load-elongation diagrams of:
a) the Molycorp X-80, 1/4"
b) the INCO 787, 1/2"
c) the Molycorp X-80, 5/8"
d) the Ipsco 3/8"
- Figure 11 The variation of the flow stress and the work-hardening rate with true strain.
- Figure 12 Schematic drawing of the V-notched plane strain sample.
- Figure 13 Schematic drawing of the unnotched plane strain sample (From Ref. 12).
- Figure 14 Photographs of the Balanced Biaxial Tensile sample of:
a) the Ipsco 3/8" steel
b) the Molycorp X-80, 5/8" steel
- Figure 15 Schematic drawing of the Biaxial Tension Test.
- Figure 16 The autographic punch load - punch travel diagram from the Balanced Biaxial Tension Test.

- Figure 17 Forming Limit Diagrams for the tested HSLA steels.
- Figure 18 Schematic drawing of the Stretch-Bend Test.
- Figure 19 The autographic punch load - punch travel diagrams from the Stretch-Bend Test, for smaller punches.
- Figure 20 The Stretch-Bend formability diagram of all HSLA steels tested.
- Figure 21 Schematic drawing illustrating the condition of the local necking and void link-up.
- Figure 22 Composite micrographs showing details of failure of the tensile specimen of Ipsco, 3/8" steel.
- Figure 23 Schematic drawing showing the cumulative events of strain localization, formation of shear bands, and nucleation of shear crack in relation to the processes of void nucleation and growth.
- Figure 24 Composite micrographs showing void nucleated at non-ferritic constituents and the development of the shear bands between the voids.
- Figure 25 Composite micrographs showing details of the failure of the tensile sample of Molycorp X-80, 1/4" steel.
- Figure 26 Composite micrographs showing details of failure of the tensile sample of Molycorp X-80, 5/8" steel.
- Figure 27 Composite micrographs showing details of failure of the tensile sample of INCO 787, 1/2" steel.
- Figure 28 Composite micrographs showing the failure of the biaxially stretched samples of Ipsco 3/8" and Molycorp X-80, 5/8" steels.
- Figure 29 Composite photographs showing the crack propagation in the stretch-bend test.
- Figure 30 Composite micrographs showing the voiding process at the M/A constituents and the path of the shear band in the stretch-bend test of Molycorp X-80, 5/8" steel.
- Figure 31 Composite micrographs showing delamination along the rolling axis and shear across the stretch-bend specimen of Ipsco 3/8" steel.
- Figure 32 Composite micrographs showing details in the shear band formed during the stretch-bend test of Molycorp X-80, 5/8" steel.

- Figure 33 Composite micrograph showing the delamination in the Ipsco 3/8" material for the specimens perpendicular and parallel to the rolling direction.
- Figure 34 Schematic drawing showing the processing steps and associated strain distributions developed in UOE pipemaking processes.
- Figure 35 Relationship between $\frac{1}{BEP}$ and $\frac{1}{f^2}$ for various steels. (From ref. 24).
- Figure 36 Relationship between $\frac{\sigma_B}{\sigma_{for}}$ and f^2 for various steels (From ref. 24).
- Figure 37 The effect of volume fraction of second-phase particles on the BEP in steels (From Ref. 24).
- Figure 38 The effect of the shape of second-phase particles on the BEP for eutectoid steel.
- Figure 39 The effect of the grain size on the BEP for C-Mn steel (From Ref. 24).
- Figure 40 Schematic illustration of methods commonly used to account for the Bauschinger Effect.
- Figure 41 Schematic diagram showing the method used to evaluate the BEP.
- Figure 42 Schematic drawing of the sample used in the BE experiments.
- Figure 43 Photographs showing the BEP gripping system.
- Figure 44 Schematic drawing showing the BEP loops and the method used to evaluate the BEP for the range of strains.
- Figures 45 to 56 Relationship between the BEP and forward strain, for the materials and the procedures stated on the diagrams.
- Figure 57 Relationships between the BEP and $\frac{1}{f^2}$ for various carbon steels (From Ref. 24) and $\frac{1}{f^2}$ for the tested HSLA steels, in as-received conditions.
- Figure 58 Summarized results for the BEP of Molycorp X-80, 5/8" steel at various conditions and the testing procedures, as stated on the diagram.
- Figure 59 Summarized results for the BEP for Ipsco 3/8" steel for various conditions and the testing procedures, as stated on the diagram.

Figure 60 The initial yielding characteristics for Molycorp X-80, 5/8" steel for different orientations of the sample tested in tension and compression.

TABLE OF CONTENTS

	Page
CHAPTER 1 INTRODUCTION	1
CHAPTER 2 THE CHARACTERIZATION OF MATERIALS	7
a) Microstructural Features of Ipsco- Climax 3/8" HSLA Steel	9
b) Microstructural Features of Molycorp X-80 Steels	13
c) Microstructural Features of INCO 787 Steel	14
CHAPTER 3 BASIC MECHANICAL PROPERTIES	20
CHAPTER 4 THE ASSESSMENT OF FORMABILITY	27
1) The Keeler-Goodwin Forming Limit Diagram (FLD)	30
b) Plane strain tensile tests	30
c) The balanced biaxial tension test	36
2) The Stretch-Bend Test	42
CHAPTER 5 METALLOGRAPHIC STUDIES OF FAILURE	49
1) Failure Mechanisms in Uniaxial Tensile Tests	50
2) Failure Mechanisms in Biaxial Tension	62
3) Failure Mechanisms in Stretch-Bend Test	65
CHAPTER 6 REVERSE STRAINING AND THE BAUSCHINGER EFFECT	75
1) Theoretical Aspects of the Bauschinger Effect	78
2) Factors Influencing the Bauschinger Effect	85
3) Methods of Measuring the Bauschinger Effect	89

	Page
4) Experimental Details	92
5) Experimental Results	98
CHAPTER 7 CONCLUSIONS	121
REFERENCES	123

CHAPTER 1
INTRODUCTION

The development of strong, tough, easily weldable steels with yield stresses greater than 80 ksi for pipeline, pressure vessels, the automotive industry and structural applications at an economically attractive cost has been perhaps the most commercially significant achievement by metallurgists in the last decade.

The general requirements for this class of steels are high (50 - 100 ksi) yield strength, adequate toughness, weldability and formability, corrosion resistance and economy of production.

In order to attain high yield strength and adequate toughness there are several different approaches in practice characterized by the following factors:

- The use of alloying elements such as Nb, V, Ti which promote both grain refinement of the austenite and precipitation hardening in the ferrite.
- The ability to process the austenite phase by hot deformation in a controlled manner involving both the degree and the temperature of deformation and the subsequent cooling rate.

- In addition to the control of the alloy content, the trend has been to improve weldability by reducing the carbon content.
- The demand for an isotropic structural HSLA material has led to the practice of inclusion control, using both desulphurization practices and sulphide shape modification.

Much effort has been made to produce steels with an ultrafine grain size ($1-5 \mu$). Reduction in transformation temperature increases ferrite nucleation and reduces the grain size of steel. Also, at a greater degree of undercooling more free energy is available to produce plate and needle morphologies. Hence, the faster growing acicular products dominate in the structure at lower transformation temperatures. The grain size obtained by reducing transformation temperatures may be further refined by finishing the rolling at lower temperatures. Figure 1 shows the grain size as a function of the transformation temperature for different finishing temperatures⁽¹⁾. Most controlled rolled steels presently produced are based on this practice. Other methods of refining grain size involve use of NbCN particles.

Beside the grain refinement, which acts as the principal strengthening mechanism in this family of HSLA steels, precipitation hardening, substructural strengthening and solid-solution strengthening also contribute to the higher yield strength.

As a result of different approaches there are a number

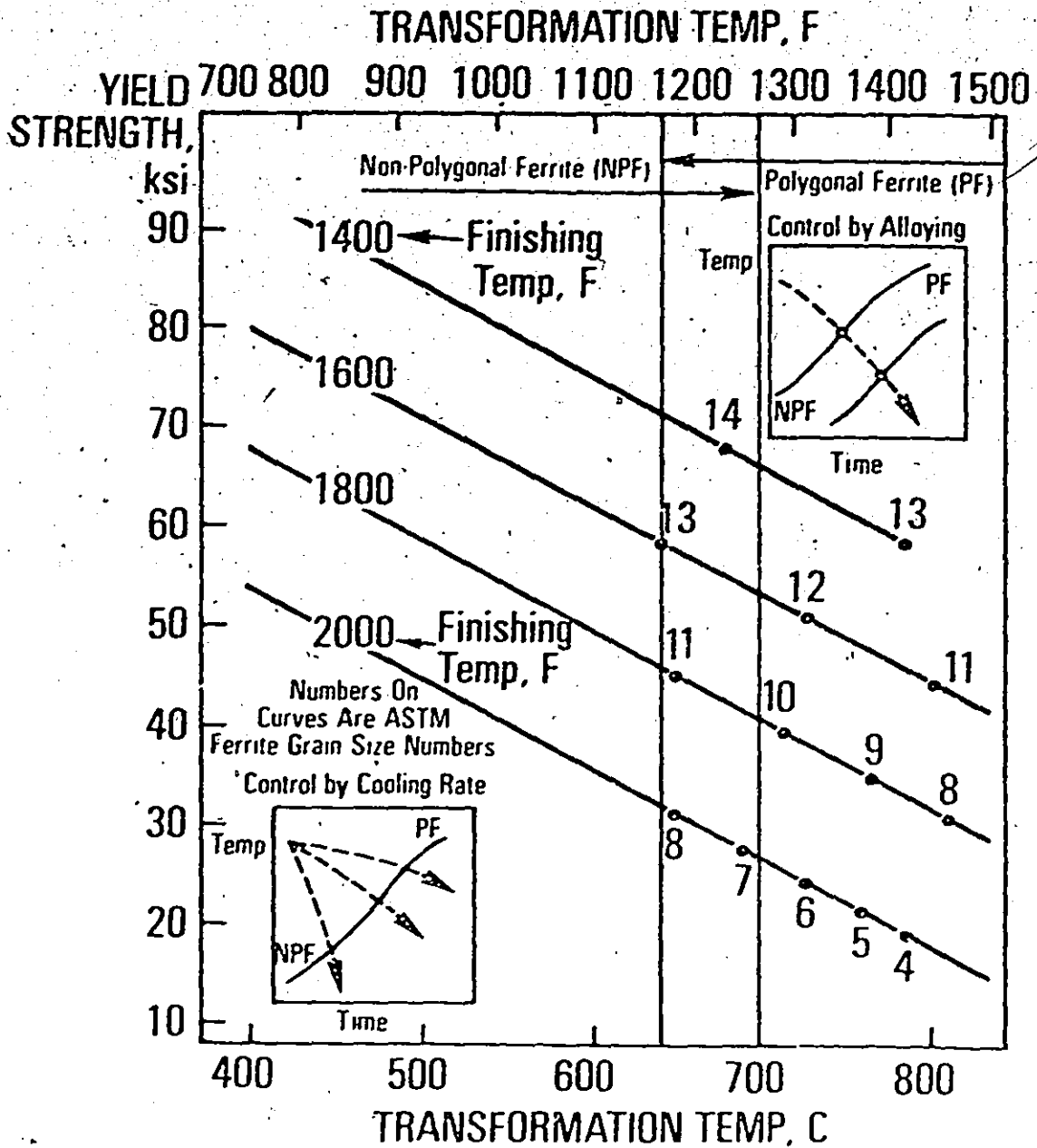


Figure 1.

of grades of the HSLA steels which can be divided into the following categories:

- Quenched and tempered HSLA steels
- Acicular ferrite HSLA steels
- Polygonal ferrite, pearlite reduced HSLA steels
- Precipitation hardened HSLA steels

In the past for many engineering applications, the specification and comparison of materials have been based only on tensile properties such as the yield strength or the strain to failure. However, specific requirements vary for each application. For example, an important property for automotive industry is the formability of strip material, whereas, for structural uses the weldability of heavy plate sections is more important. For the pipeline application, the important characteristics are high yield strength, fracture toughness, weldability and economy of production. Many fabrication processes such as UOE pipe-making process, subject the material to strain reversals, which may lead to reduction in the strength due to the Bauschinger effect. It is important to be able to predict the influence of the microstructural constituents, not only on the yield strength, but also on such features as the form of yielding and the behaviour of materials in the reverse flow.

So far, the results of these developments have shown the need:

1. to understand the complex phase transformation occurring during continuous cooling of the thermomechanically

processed low alloy steels,

2. to give a detailed description of the complex transformation products,
3. to correlate the microstructural parameters with the mechanical behaviour of the materials.

A better understanding and definition of the major material parameters could lead to more suitable specifications for each particular application of HSLA steels.

The materials used in this study were chosen so that the influence of a variety of microstructural variables on fracture and formability could be studied. The materials included both acicular and polygonal ferrites and precipitation hardened ferritic structures with various distributions of both non-metallic inclusions and non-ferritic phases.

The objective of this study was to establish the relationship between basic mechanical properties, fracture and forming characteristics and the microstructural features. In addition, an effort has been made to define the behaviour of these materials in reverse straining, as a very important characteristic for pipeline applications.

For clarity of presentation, this study is divided into chapters which deal with the following topics:

2. The characteristics of the materials
3. The basic mechanical properties
4. The assessment of formability
5. The metallographic studies of failure

6. The reverse straining behaviour and the Baushinger effect

7. Conclusions

The present study was concluded on the commercially available materials. Because of the large amount needed and the reproducibility of these materials in a wide range of section sizes, an adequate characterization of these HSLA steels is of great importance for the present industry. The advantage of this study is the use of high volume commercially produced materials, but disadvantages are the difficulties to quantitatively characterize materials because of the lack of knowledge of the material histories from ingot to the finally produced plate.

Some of the experimental work concerned with basic mechanical properties and formability was performed in conjunction with Mr. H. Herø, during his stay at McMaster University.

TABLE I
CHEMICAL COMPOSITIONS

<u>Alloy Designation</u>	<u>C</u>	<u>S</u>	<u>O</u>	<u>Mn</u>	<u>Mo</u>	<u>Nb</u>	<u>Ni</u>	<u>Cu</u>	<u>Si</u>	<u>Al</u>	<u>Processing</u>	<u>Average Grain Size mm x 10⁻³</u>
Ipsco 3/8"	0.063	0.023	0.002	1.6	0.25	0.05	-	-	0.06	0.02	hot rolled and finished at 1600°F	2.6
Molycorp X-80, 1/4"	0.059	0.002	0.003	1.71	0.14	0.10	-	-	0.66	0.06	soaked at 2350°F and hot rolled finishing at 1650°F	3.2
Molycorp X-80, 5/8"	0.063	0.001	0.009	1.71	0.14	0.10	-	-	0.67	0.06	soaked at 2350°F and hot rolled finishing at 1450°F	5.3
INCO 787 1/2"	0.034	0.011	0.002	0.44	0.21	0.045	0.89	1.16	0.28	-	hot rolled normalized from 1650°F and aged 1 hour at 1000°F	12.5

CHAPTER 2

THE CHARACTERIZATION OF THE MATERIALS

In order to give an adequate description of the microstructural features of HSLA steels, it is necessary to consider the effect of both the composition and the thermo-mechanical history on the transformation of austenite under continuous cooling conditions.

In general, the addition of alloying elements and the controlled rolling practice lead to the production of fine-grained ferrite transformation products, from austenite finished at low temperature. The continuous cooling transformations can be predicted with the aid of the diagram in Figure 2 which gives the conditions in which polygonal and non-polygonal ferrite structures are produced⁽²⁾. In addition to the morphology and scale of the ferrite, redistribution of carbon during transformation plays an important role in the formation of non-ferritic products. Carbon may be in the form of small alloy carbides, precipitated either at the transformation interface or in the ferrite. Also, the rejection of carbon from the growing ferrite may result in the formation of regions of retained austenite or martensite⁽³⁾. The amount and distribution of the austenite-martensite constituent

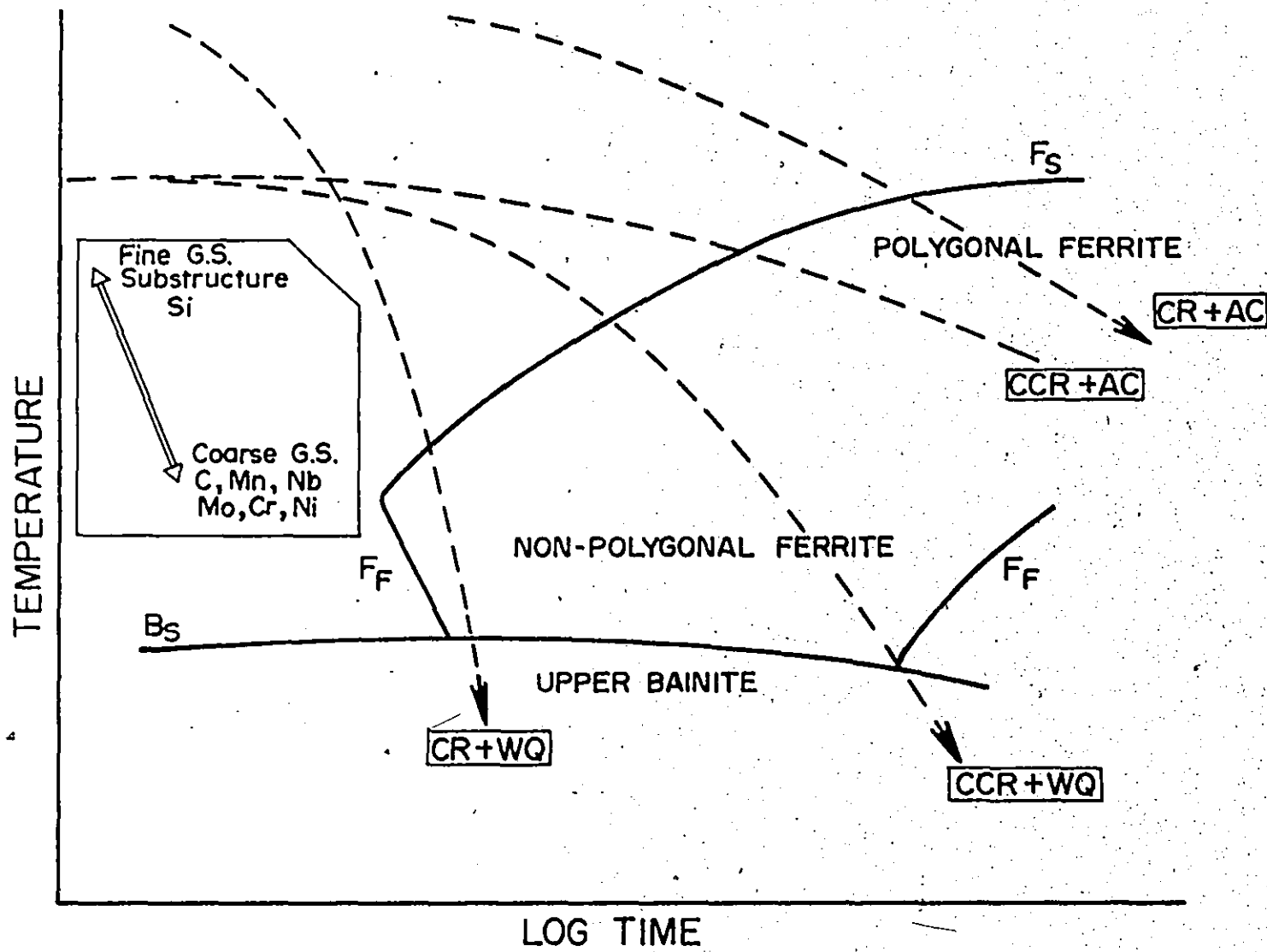


Fig. 2.

depends on the thermal history, on the kinetics of the transformation and on factors such as the homogeneity of the distribution of some alloying elements, e.g. manganese.

The amount and the distribution of this complex microconstituent appears to be very important, because, as shown later, the austenite-martensite microconstituent plays a major role in determining the yielding characteristics and energy absorption in HSLA steels.

It was decided that the study of the microstructure of these steels would be limited to the use of

- a) Optical microscopy, and
- b) Scanning Electron Microscopy.

The use of Transmission Electron Microscopy was excluded because of time considerations. It was felt that a thorough TEM study of these materials would itself be a major project.

For clarity, the study of the microstructural features of tested HSLA steels is divided into sections dealing with:

- a) Microstructural features of Ipsco-Climax HSLA steel,
- b) Microstructural features of Molycorp X-80 HSLA steels,
- c) Microstructural features of INCO 787 HSLA steel.

a) Microstructural features of Ipsco-Climax 3/8" HSLA Steel

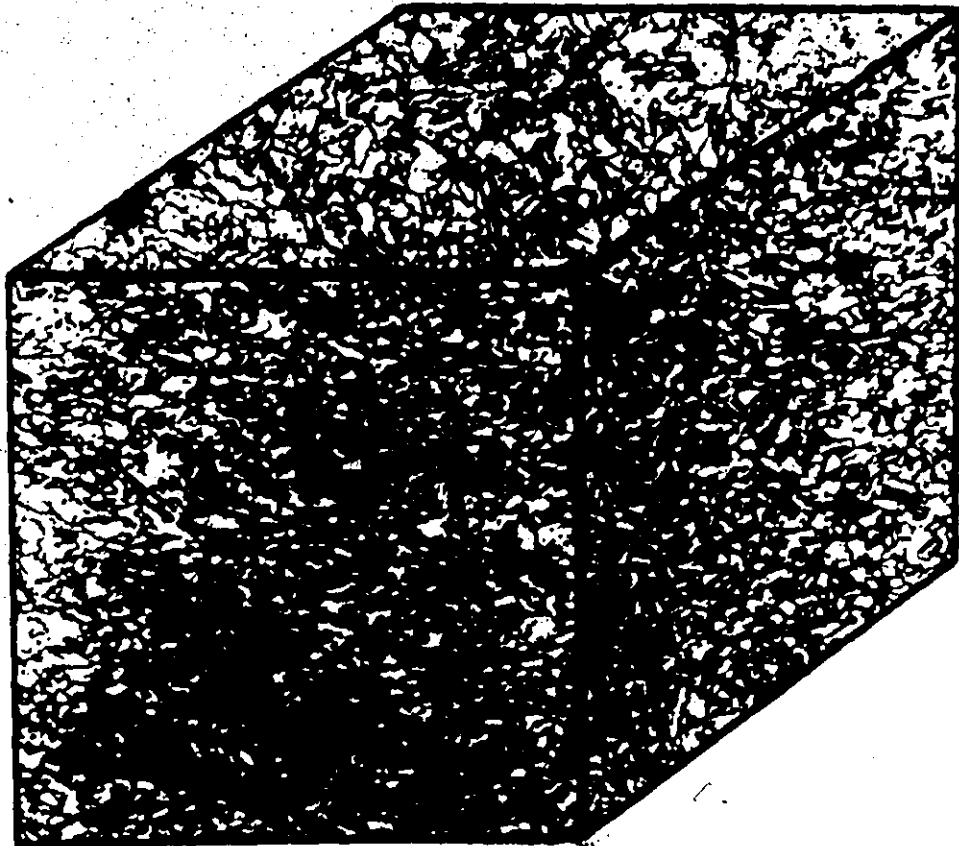
The original development of Ipsco Mn-Mo-Nb steel (in later text Ipsco steel), was proposed by Ipsco-Climax-Molybdenum Company and is based on the concept of combining transformation strengthening with precipitation strengthening in an acicular ferrite matrix⁽⁴⁾. This concept involved the use

of low carbon contents for improved toughness, weldability and formability, alloying with Manganese, Molybdenum and Niobium in order to suppress the γ - α transformation temperature and subsequently form a predominantly high strength, fine-grained acicular ferrite structure.

The microstructure of Ipsco steel, shown in Figures 3 and 4, consists of an acicular ferrite matrix with small amounts of cementite and austenite-martensite islands. According to the literature⁽⁵⁾, the acicular ferrite is composed of groups of parallel ferrite laths arranged in colonies with a small lattice misorientation between individual laths and a high dislocation density. The microstructure of the acicular ferrite is too complex to permit a quantitative estimate of the dislocation density or the extent of precipitation, by TEM.

The main features visible on the optical and on the Scanning Electron Microscope (SEM) micrographs are the general scale of the structure with grain size of the order of 2 - 3 μm , and the absence of a network of prior austenite grain boundaries (an important distinction between acicular ferrite and bainite structures).

As far as chemical composition is concerned, the major alloying element in this steel, Manganese, is added to reduce the ferrite-pearlite transformation temperature, forming fine-grained acicular ferrite and also to act as a solid-solution strengthening component. Molybdenum is used primarily for its effect on the continuous-cooling transformation characteristics. As it is more effective in retarding ferrite than



R. D.

50 μ

IPSCO-CLIMAX, 3/8"

Fig. 3.



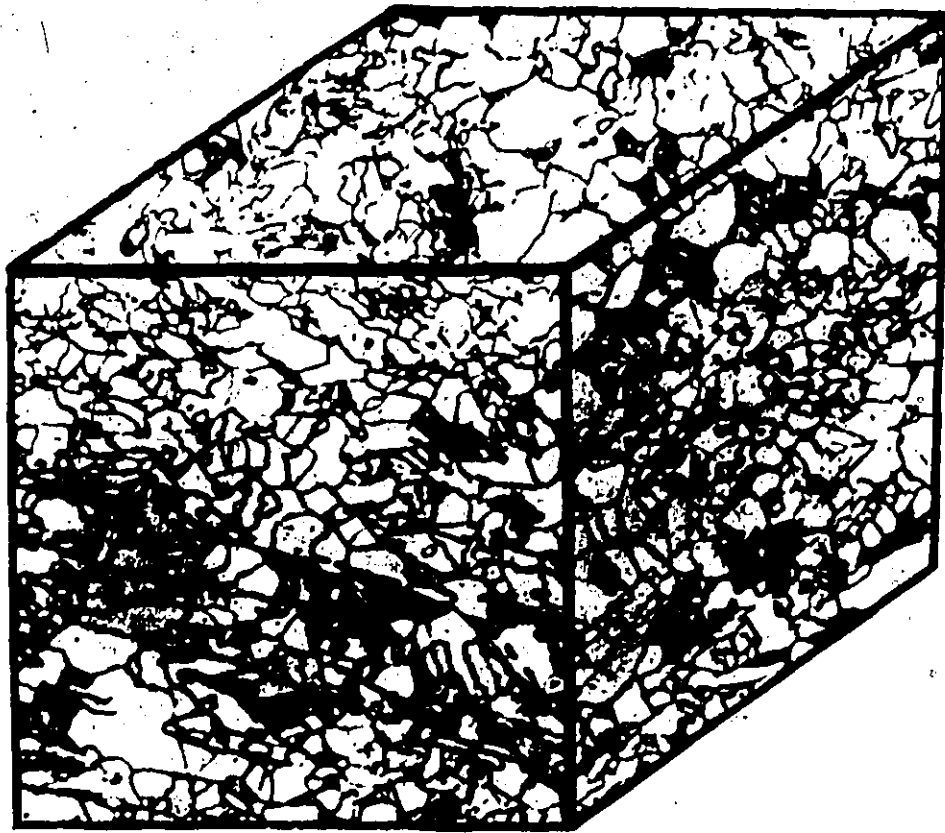
IPSCO - CLIMAX 3/8"

Fig. 4

bainite, it acts in conjunction with manganese to produce fine-grained acicular ferrite. Niobium, the most effective alloy element for refining grain size of all controlled-rolled steels, lowers the austenite-ferrite transformation temperature and also contributes to the precipitation strengthening by precipitation of niobium carbide nitrides - Nb(C,N). Low Carbon was specified since only 0.01 to 0.02% is required for Nb(C,N) precipitation, and any increase above this level is detrimental to the mechanical properties and to the welding behaviour. However, it is not practical to specify carbon contents lower than ~ 0.06% for steelmaking. This steel has a high Sulphur content (0.020% S) and thus, a high volume fraction of manganese sulphide inclusions are observed in the microstructure. These inclusions, highly elongated during rolling, are distributed in the planes parallel to the rolling planes.

b) Microstructural features of Molycorp X-80 Steels

The chemical composition of these steels was proposed by Molybdenum Corporation of America⁽⁶⁾ as an economical means of obtaining steels with mechanical properties suitable for construction of large diameter pipes for use in the Arctic. It is a low-carbon Mn-Si steel containing 0.10% Nb, produced by control-rolling followed by accelerated cooling and ageing. In these HSLA Nb-Mn-Si steels, the inclusion content was reduced to very low values by a combination of desulphurization and deoxidation. In addition, the shape of the remaining sulphides was controlled by the use of rare earth elements



R. D.

50 μ

MOLYCORP X-80 , 5/8"

Fig. 1



AS RECEIVED



ANNEALED AT 550°C/1H

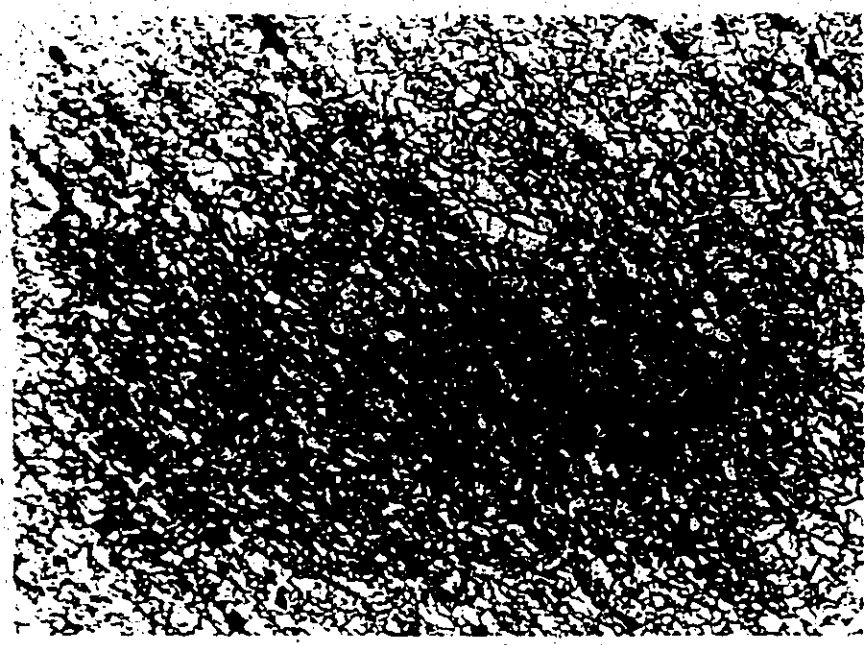
The microstructures of these steels are presented in Figures 6 and 7. The main constituents are polygonal fine-grained ferrite with statistically distributed "pearlite" regions in 5/8" thick plate, and a banded ferrite-pearlite structure in 1/4" plate, Figure 7. Careful optical and SEM investigations show that in 5/8" plate, the "pearlite" regions consist of very complex transformation products such as mixtures of blocks of retained austenite and high carbon martensite⁽³⁾.

In addition to the formation of carbides, the rejection of carbon from the growing ferrite results in the formation of regions of retained austenite or martensite. The amount and distribution of the austenite-martensite constituents depend both on the thermal history and kinetics of the transformation and on factors such as the homogeneity of the distribution of the substitutional alloying elements. Further investigations have indicated that these complex austenite-martensite regions may be accompanied by residual stresses in neighboring regions.

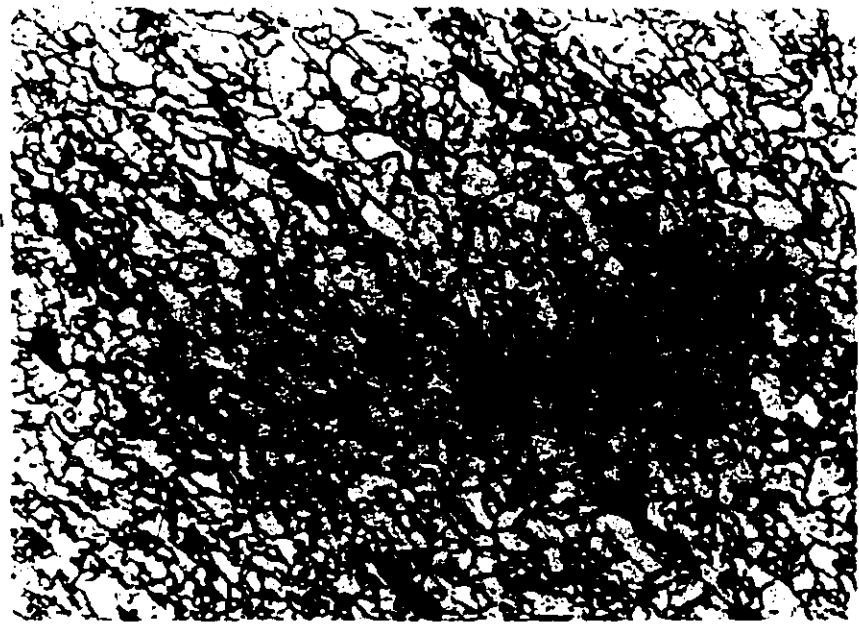
Control rolled 1/4" plate is characterized by a fine ferrite-pearlite banded structure accompanied with cementite⁽⁷⁾ distributed at the grain boundaries and often in the pearlite banded planes.

c) Microstructural features of INCO 787 Steel

INCO 787 was developed from a Ni-Cu-Nb steel base using methods designed to meet the requirements for gas transmission pipeline, especially those to be built and operated in areas of extreme climatic conditions⁽⁸⁾. The alloying procedure



x 200



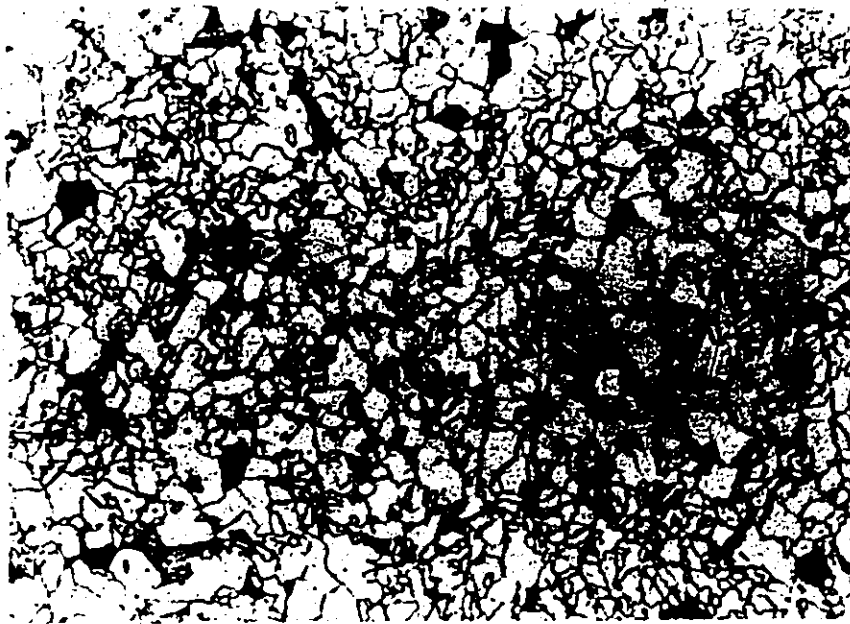
x 800

Molycorp X-80, 1/4"

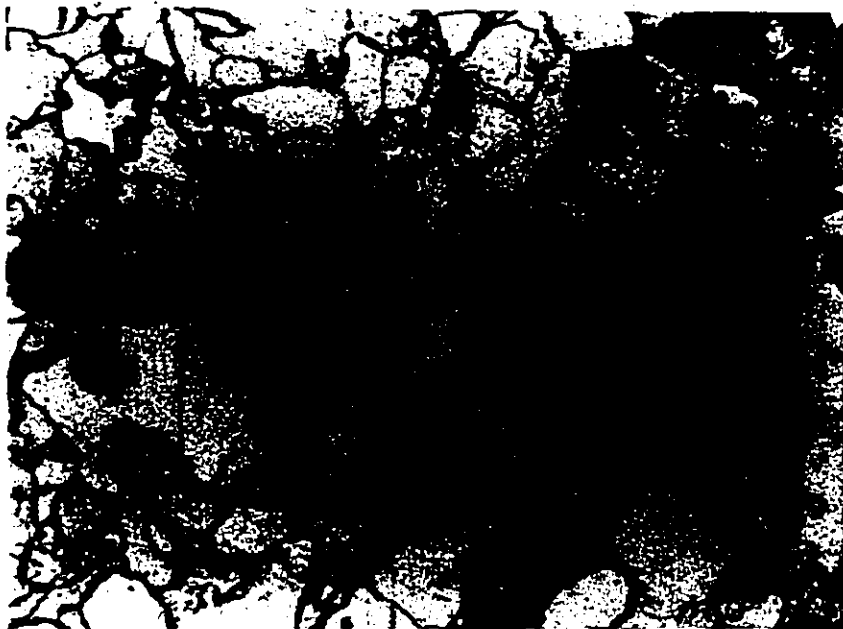
Figure 7.

allowed both strength and toughness to be increased while retaining excellent weldability. In view of the applications for which the steel was intended, much of the development work involved 1/2" plate in a) the as-rolled, b) rolled and aged, c) normalized and aged, and d) quenched and aged conditions. Thus, the steel is versatile and appears to be suitable for a number of structural and general engineering applications in a wide range of section sizes. Small amounts of Cr and Mo are added to delay auto-ageing on cooling after hot rolling. Copper provides age-hardening by precipitation of the copper-rich epsilon phase in ferrite⁽⁹⁾. However, when copper is present in amounts greater than 0.4%, it tends to cause surface cracking during hot rolling, known as "hot shortness". Nickel additions in the ratio of about 1Ni:2Cu are required to minimize this effect.

The microstructure of this material, shown in Figure 8 consists of relatively coarse polygonal ferrite with a small amount of pearlite. The average grain size of ferrite in the as-received condition is relatively coarse, and after normalizing at 900°C for 1 hour and ageing at 540°C for 1 hour, a remarkable change in grain size is observed, giving an average grain size of ~ 12 - 15 μm with considerable reduction of pearlite content.



x 200



x 800

INCO 787, 1/2"

Figure 8.

TABLE II

H. S. L. A. GRAIN SIZE DIAMETERS

Material	Average Grain Size (Micron)	
	Rolling Direction	Thickness Direction
X-80, 1/4"	3.6	2.6
X-80, 5/8"	6.3	4.5
Inco 787, 1/2"	14.5	11.3
Ipsco, 3/8"	2.2	2.5

CHAPTER 3

BASIC MECHANICAL PROPERTIES

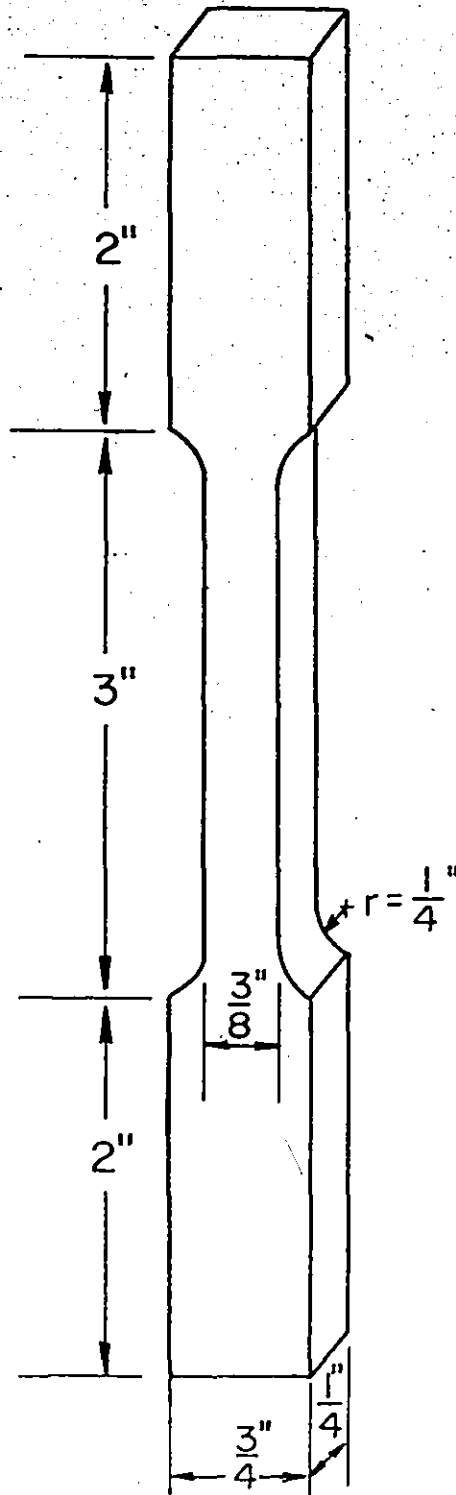
Tensile tests have been performed on all the test materials using 0.207" x 0.375" flat samples, shown schematically in Figure 9. The tests were performed on a 10,000 lb. Instron testing machine, using a crosshead speed of 0.05 ins/min. The specimens were taken parallel and perpendicular to the rolling direction of the plate, and a one inch Instron strain gauge extensometer was used to record changes in the length.

For determination of the plastic strain ratio, the results for through-width and through-thickness deformation were taken from the samples deformed at about 13-15% and r-values were calculated. The strain to fracture ϵ_f^* was calculated using measurements of the reduction in area. To evaluate the strain hardening index, n, the tensile true stress-true strain data were fitted by the empirical power-law equation

$$\bar{\sigma} = \sigma_0 \bar{\epsilon}^n$$

In Table II are listed all tensile parameters determined, and Figure 10 shows representative stress-strain curves for the materials.

Both Molycorp X-80, 1/4" plate and INCO 787 1/2" exhibit



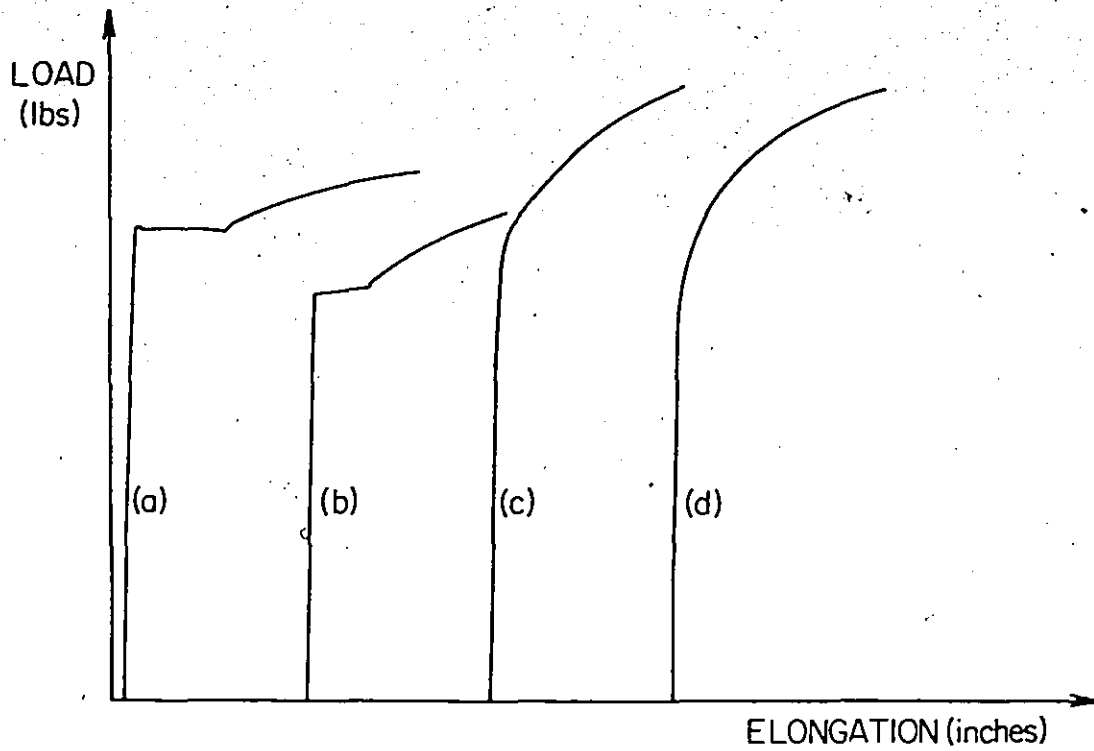
SCALE 1:1

Fig. 9.

TABLE III
MECHANICAL PROPERTIES

<u>Alloy Designation</u>	<u>Orientation Long = L Trans = T</u>	<u>Lower Yield Stress or 0.2% Offset</u>	<u>Tensile Strength ksi</u>	<u>Fracture Stress ksi</u>	<u>Fracture Strain ϵ_f^*</u>	<u>R.A. %</u>	<u>r Value</u>	<u>Luders Strain %</u>	<u>Uniform Strain ϵ_u</u>	<u>Strain to Instability ϵ^*</u>	<u>n</u>	<u>σ_0 ksi</u>	<u>Total Elong. %</u>
Ipsco 3/8"	T	69.1	99.1	160.5	0.71	51	0.83	0	0.08	0.10	0.125	145	21
	L	67.1	95.4	187.3	1.08	66	0.69	0	0.13	0.14	0.125	141	26
Molycorp X-80, 1/4"	T	82.5	95.2	180.2	1.09	66	0.66	3	0.16	0.15	0.145	146	N/A
	L	81.8	94.0	210.0	1.27	72	0.64	3	0.14	N/A	0.155	148	36
Molycorp X-80, 5/8"	T	74.0	106.4	187.1	0.89	58	0.77	0	0.13	0.14	0.140	162	27
	L	71.0	103.3	180.6	0.85	57	0.84	0	0.13	0.13	0.135	154	24
INCO 787 1/2" (Normalized and Aged)	L	65.3	85.4	200.5	1.37	75	0.85	2	0.14	0.15	0.160	134	32
	T	59.0	80.7	177.0	1.27	72	1.00	1	0.18	0.17	0.165	127	34

N/A - Not Available



- a) Molycorp X-80, 1/4"
- b) INCO 787, 1/2"
- c) Molycorp X-80, 5/8"
- d) Ipsco-Climax, 3/8"

Figure 10.

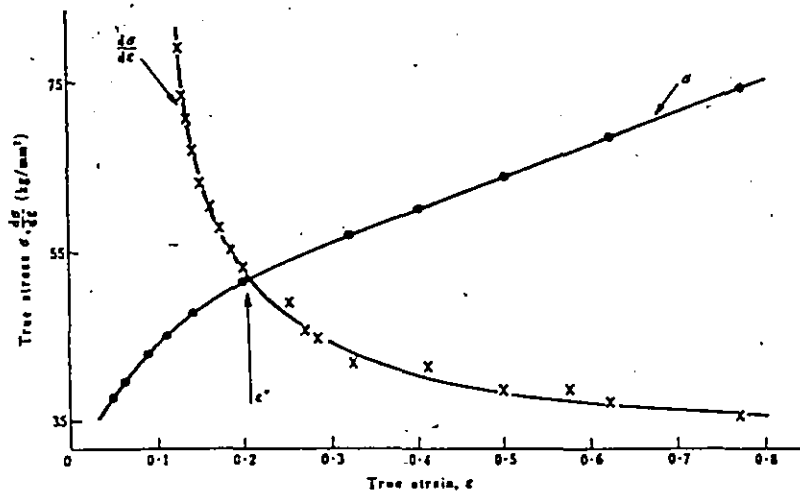


Figure 11 - A diagram showing the variation of flow stress and work hardening rate with true strain (from ref. 5)

a discontinuous yielding with large Luders elongations and square-type stress-strain curve. The acicular-ferrite Ipsco 3/8" steel is a typical representative of materials with continuous yielding and rounded stress-strain curves. Molycorp X-80, 5/8" plate shows behaviour intermediate between the square to the round type of stress-strain curves.

The work-hardening exponents, n , (computed using the above equation) for all the tested materials are very low and lie between 0.12 and 0.16, giving the corresponding values for the uniform strains in the range of 0.13 - 0.18. In order to define more accurately uniform strain, true stress, σ , -true strain, ϵ , and $d\sigma/d\epsilon - \epsilon$ were plotted and the intersection between the falling $d\sigma/d\epsilon$ versus ϵ and the rising σ versus ϵ determined, giving a value of ϵ^* at which necking begins. The values for ϵ^* are listed in Table II and an example of such diagram is shown on Figure 11.

It can be observed that the determined values of the strain hardening exponent, n , are in all cases comparable in magnitude with the uniform strain prior to necking, $\epsilon_u = n$.

Soon after necking started, the tensile samples failed along shear zones within the neck with low total true strains to failure. Due to the banded microstructure, in Molycorp X 80, 1/4" plate, characteristic central delamination was observed and is discussed in Chapter 5.

It has been difficult to find adequate correlation between the strain to failure and other material characteristics, particularly comparing the very clean, Molycorp X 80, 5/8"

plate and the Ipsco 3/8" steel which has a high sulphur content.

Despite very low sulphur content in Molycorp X-80, 5/8" (S = 0.001%) and rare earth treatment for inclusion modification, the failure strains of the order of 0.85 - 0.89 are considerably lower than the true strains to failure for Ipsco material with high sulphur content and almost without inclusion shape control. In order to find explanation for this behaviour, the metallographic studies of failure were employed and a more detailed description is given in Chapter 5.

From the data presented in Table II, a significant planar anisotropy is observed, and this could be due to:

- a) the distribution of non-ferritic phases parallel to the rolling direction,
- b) the presence of polarized residual stresses due to rolling at low temperatures,
- c) a crystallographic texture.

Significant reduction in ductility for these fine-grained materials could arise due to the processing at low temperatures which leaves a high dislocation density and hence reduces the work hardening capacity of the matrix. More quantitative discussion on this problem is given in Chapters 4 and 5 dealing with formability and failure mechanisms, respectively

CHAPTER 4

THE ASSESSMENT OF FORMABILITY

Relatively little is known about the formability of hot rolled HSLA steels for the simple reason that their application in roles requiring such knowledge has been rather limited.

The higher strength of HSLA steels has been utilized mostly to achieve higher working stresses of welded flat sections or simple structural shapes, and little forming was involved. The automotive industry is currently trying to reduce the weight of basic automotive components without sacrificing the impact resistance of the vehicle frame. This has placed emphasis on the HSLA steels with high strength to weight ratios. The higher strength steels permit the design of impact resistant systems with a lower section modulus and hence, more compact and lighter assembly.

Formability is a key factor which establishes the allowable part contours for HSLA steel components which dictates the engineer's latitude in designing automotive parts with good rigidity.

The forming of different parts from sheet metal is characterized generally by two different deformation modes, drawing and stretching. During pure drawing, material deforms

without thinning such that the ratio of principal strains is 1:-1. On the other side of the pure stretching formation mode, the sheet thins so that the principal strains increase positively the ratio 1:1. Between these extreme deformation modes, there exists plane strain in which the minor principal strain is zero.

Formability and ductility are qualitative material characteristics. In general, ductility is the ability of a material to deform plastically without fracture, and formability can be defined more precisely as a measure of the maximum deformation of a material without the occurrence of cracking or surface deterioration. Ductility can be expressed as:

- a) the uniform percentage elongation of a specified gauge length, or the strain at fracture in tensile test, and
- b) the total percentage elongation measured over a specified gauge length.

Fracture strain measured from reduction in area is often regarded as a more reliable index of ductility, but its disadvantages are that it is not always easy to measure the reduction in area and to define and take into account the complex stress state occurring in the necked zone.

In this study, an attempt was made to understand the relationship existing between the parameters derived from uniaxial tensile tests and performance of the material under complex stress conditions in order to define the influence of the microstructural parameters on the formability. This is

made more complicated by the continuations of strengthening mechanisms and the anisotropy of mechanical properties. In all forming methods, manufactured parts are made from sheet by stretching, drawing, or a combination of both. The properties required for good stretchability are not the same as those that impart good drawability. In general, stretch formability (stretchability) is dependent on the strain hardening capacity of the material and drawability reflects the anisotropy of the flow stress and the crystallographic texture. Cognizance must be taken of the influence of the ductility of the material and its ability to distribute strain homogeneously. There are several parameters which can be chosen to express an index of ductility. Some authors⁽¹⁰⁾ have related the uniform strain prior to necking to the behaviour in stretching operations, and others⁽¹¹⁾ have related this parameter to the press formability. The alternative ductility parameter, true strain to fracture, has also been used to correlate with behaviour in bending and spinning operations.

In order to determine the characteristics of the HSLA steels in forming operations under complex stress states, there are two approaches available:

- 1) The Keeler-Goodwin Forming Limit Diagram, and
- 2) The Stretch-Bend Test

These will be discussed in turn.

1) THE KEELER-GOODWIN FORMING LIMIT DIAGRAM (FLD)

In order to construct the FLD for each material, data from several tests were necessary. These were:

- a) The uniaxial tensile test
- b) The plane strain tensile test
- c) The balanced-biaxial tensile test

The uniaxial tensile test was described in the previous chapter. The other tests will now be discussed.

b) Plane strain tensile tests

In order to obtain an approximate limit strain under plane strain conditions, two attempts were made, using specimens with different geometries.

In the first attempt, the plane strain specimens were 2" x 7" strips, surface ground to 0.12" with two samples oriented in each the rolling and the transverse directions of the tested materials.

To generate plane strain conditions during tensile testing, the 45° through-thickness V-notch was machined in the middle of each sample. The design of such samples is shown in Figure 12. For the strain measurements, a circular grid pattern of 0.05" diameter was printed on the surface, using a photoresist technique.

Test pieces were tested in tension, close to fracture and plane strain limits were computed from deformed grid circles located close to the actual site of cracking, if cracking occurred or from the grid circles located in the

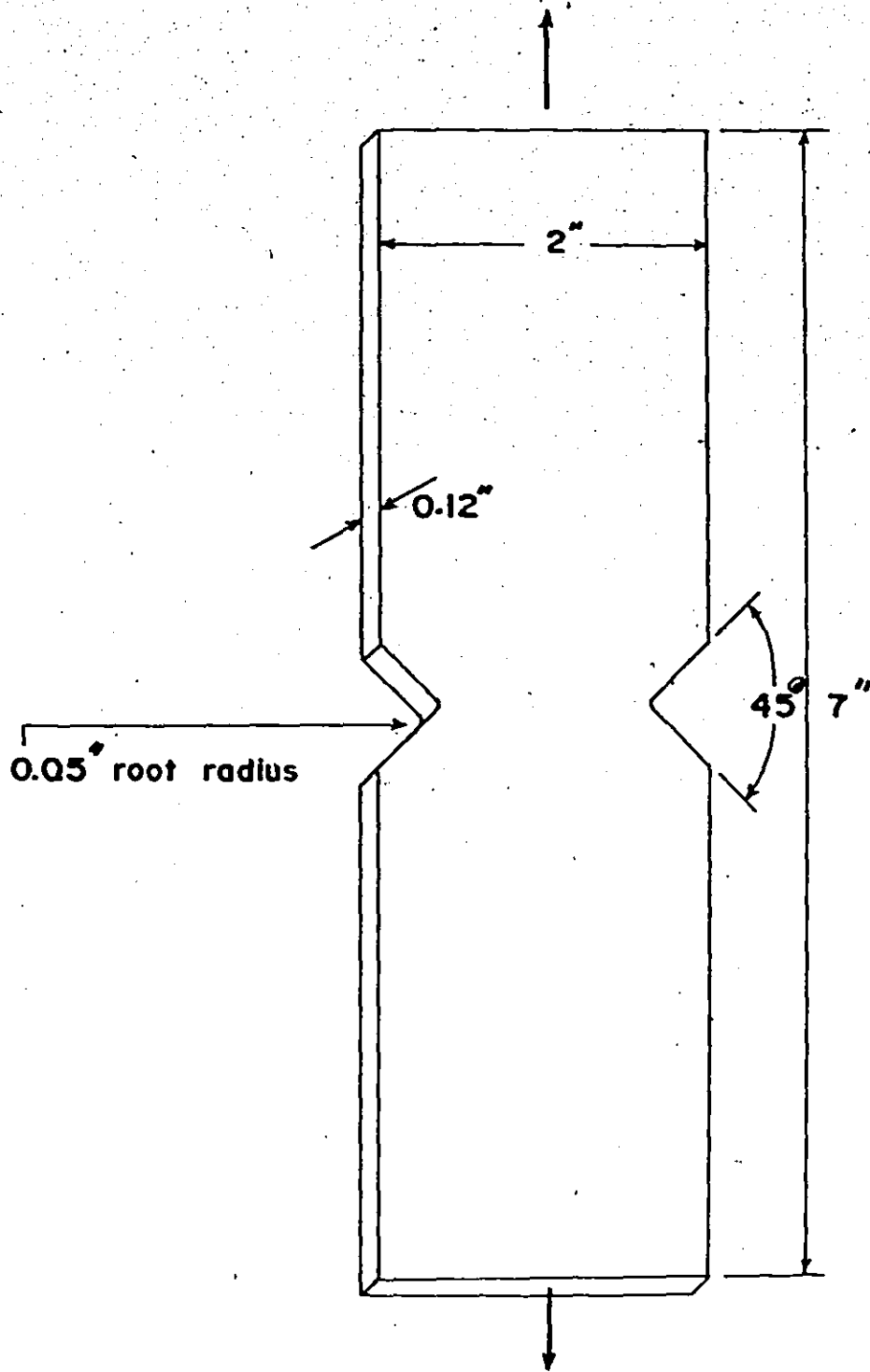


Figure 12.

groove, if the experiment has been stopped before cracking occurred.

From those strain measurements shown in Table IV and Figure 17 for the HSLA steels under plane strain, the limit condition was found to be relatively low, of the order of 0.1 or less.

Analyzing all the parameters employed in this test, it was found that:

- i) Relatively sharp notches have an effect on the stress concentration and strain distribution through the width of the sample, and
- ii) Because of high strain gradients in the deformed region, and the relatively large grid circle used for the strain determination, the strain computed in this way would rather represent some mean value of the overall strain in the deformed region and cannot be compared with the other limit strains used in this work for the determination of the FLD.

In order to eliminate the influence of those effects, another design for the plane strain tension sample, shown in Figure 13 was chosen.⁽¹²⁾

The shoulders of the sample are thick enough to remain elastic during the tensile test. The ratio w/l is large enough to achieve an approximate plane strain in the centre region. The ratio l/t is large enough so that a notch effect is not created. This solution constitutes a design for an unnotched plane strain tension specimen.

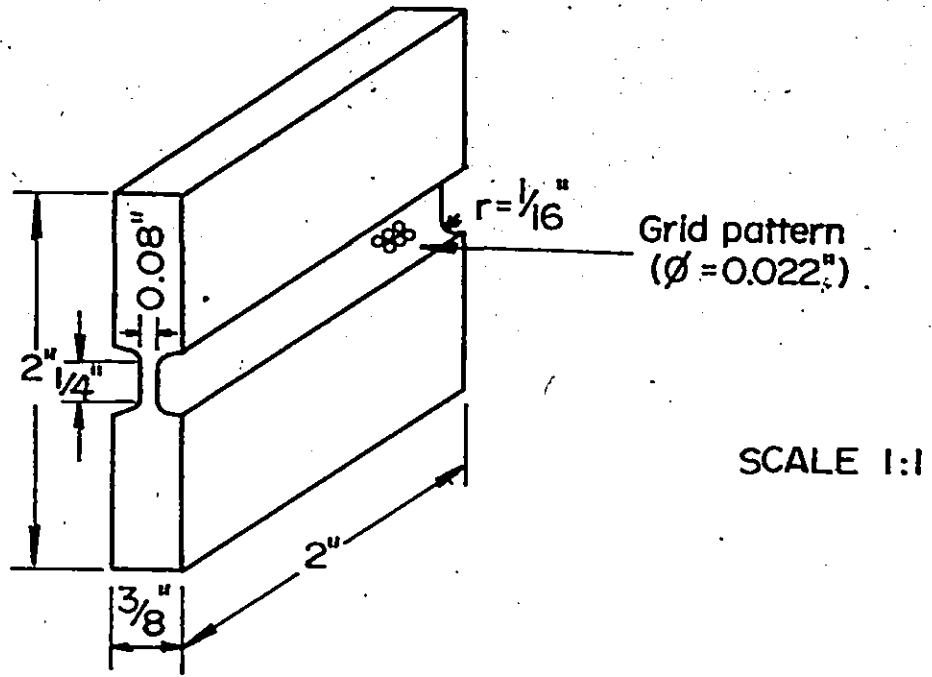


Fig. 13.

TABLE IV

PLANE STRAIN TEST

<u>Material</u>	<u>Orientation Relative to RD</u>	<u>V-Notched Specimens</u>		<u>Unnotched Specimens</u>	
		<u>Range of the Strain Obtained</u>	<u>"Representative" Strain</u>	<u>Elongation $\frac{\Delta d}{d_0} \cdot 100$ (%)</u>	<u>Plane Strain $\epsilon = \ln \frac{d}{d_0}$</u>
<u>Ipsco, 3/8"</u>	parallel to RD	0.101 - 0.114	0.11	22.45	0.227
	perpendicular to RD	0.079 - 0.110	0.08	14.03	0.131
<u>Molycorp X-80, 5/8"</u>	parallel to RD	0.108 - 0.147	0.12	24.11	0.216
	perpendicular to RD	0.120 - 0.179	0.12	20.09	0.183
<u>Molycorp X-80, 1/4"</u>	parallel to RD	0.125 - 0.185	0.15	-	-
	perpendicular to RD	0.126 - 0.147	0.14	-	-
<u>INCO 787 1/2"</u>	parallel to RD	0.013 - 0.157	0.13	-	-
	perpendicular to RD	0.098 - 0.178	0.14	-	-

Two test pieces in both transverse and rolling directions were machined from two of the tested materials: - Ipsco 3/8" and Molycorp X-80, 5/8". A circular grid pattern of 0.022" diameter was printed onto the reduced section of the plane strain tension specimen, employing photoresist technique, and used for the determination of the strain in longitudinal and transversal directions. The plane strain tension tests were carried out on TINIUS OLSEN 60,000 lbs. tensile testing machine because the expected load was greater than the capacity of the Instron tensile testing machine available. The crosshead speed was controlled by a main hydraulic valve and the plan was to keep the crosshead speed in the range 0.01 - 0.001 ins/min. The maximum load was recorded and the crosshead was stopped, in some cases just before complete fracture occurred, and in the other cases, surface cracking and complete fracture occurred simultaneously before extensive development of the neck.

The plane strains were computed from deformed grid circles. In the cases where complete fracture occurred, the circles measured were located close to but not at the actual sites of cracking. For the tests which were stopped before complete fracture, the measured circles were located in the groove. The final dimensions of the deformed circles were measured to an accuracy of 0.0001" using a toolmaker's microscope. Knowing the original average grid diameters, longitudinal ϵ_l (strains in the length direction of the sample) and transverse ϵ_t strains were computed both as natural and logarithmic strains.

The results of this experiment are shown in Table IV and Figure 17.

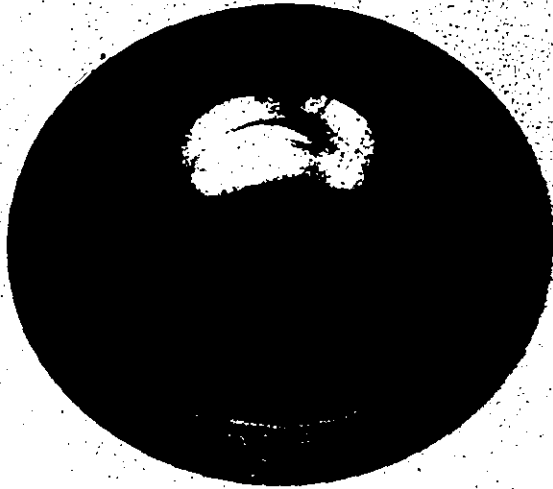
The overall results produced under these conditions for unnotched specimen design lie much above those for V-notch type samples. This arises because the unnotched specimen has a more homogeneous strain distribution through the width.

The measured strain of a notched sample represents some strain between zero and the fracture strain, depending on the size and position of the measured grid circle and the strain gradient. The results of this test are taken from the developed groove or from the sites close to fracture surface, and lie in the region above the strain at instability and below the strain to failure.

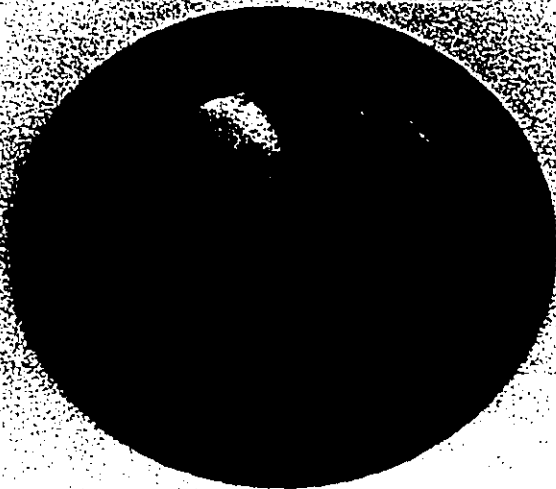
c) The balanced biaxial tension test

Earlier studies of failure in biaxially stretched sheets showed that the largest tensile strain before local thinning may be larger than the strain for necking in simple tension and may even increase as the degree of biaxiality increases. This discovery led to the development of the forming limit diagram in use today by the sheet metal industry. In order to determine the behaviour of HSLA steels under biaxial stress states, for the proportional straining path ($f = \epsilon_2/\epsilon_1$) close to unity, the balanced biaxial tension test was conducted.

For this experiment, two samples from each tested material were prepared. The samples, 0.18" thick by 10" diameter blanks were tested on a 200 ton hydraulic press. In order to induce a biaxial stretching, a groove 0.032" deep by 1.5" diameter was carefully machined in the centre of each sample on both surfaces (Figure 14). In this test, schematically shown in Figure 15, the blank was rigidly clamped around the perimeter and the central region deformed using a 5" diameter flat punch. In order to measure strains, a circular grid pattern was printed on both surfaces of the groove. A light film of multi-purpose oil, SAE 140 was applied to both sides of a 0.003" thick polyethylene sheet and this sheet was placed over the contact area between the blank and the punch to reduce friction. The sample was deformed at a crosshead speed of 0.5 in/min. and an autographic plot of punch load versus punch travel was recorded. An example of such a diagram is shown in Figure 16 and the data are presented in Table V.

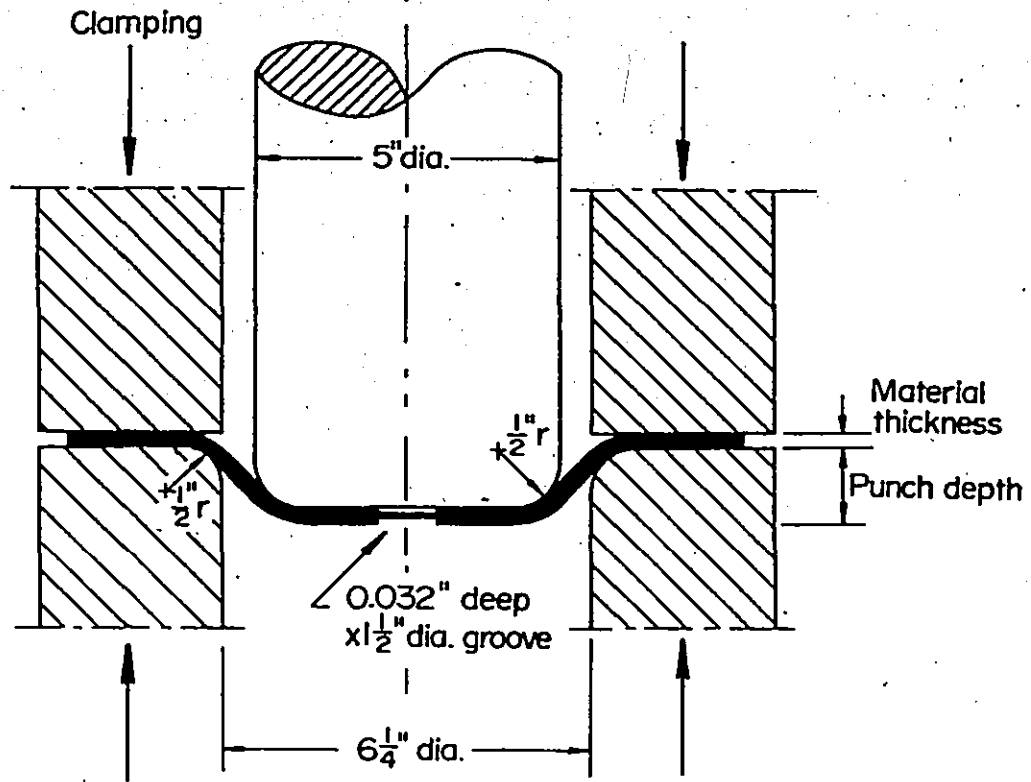


a)



b)

Figure 14.



Schematic Drawing of the Biaxial Tension Test

Figure 15.

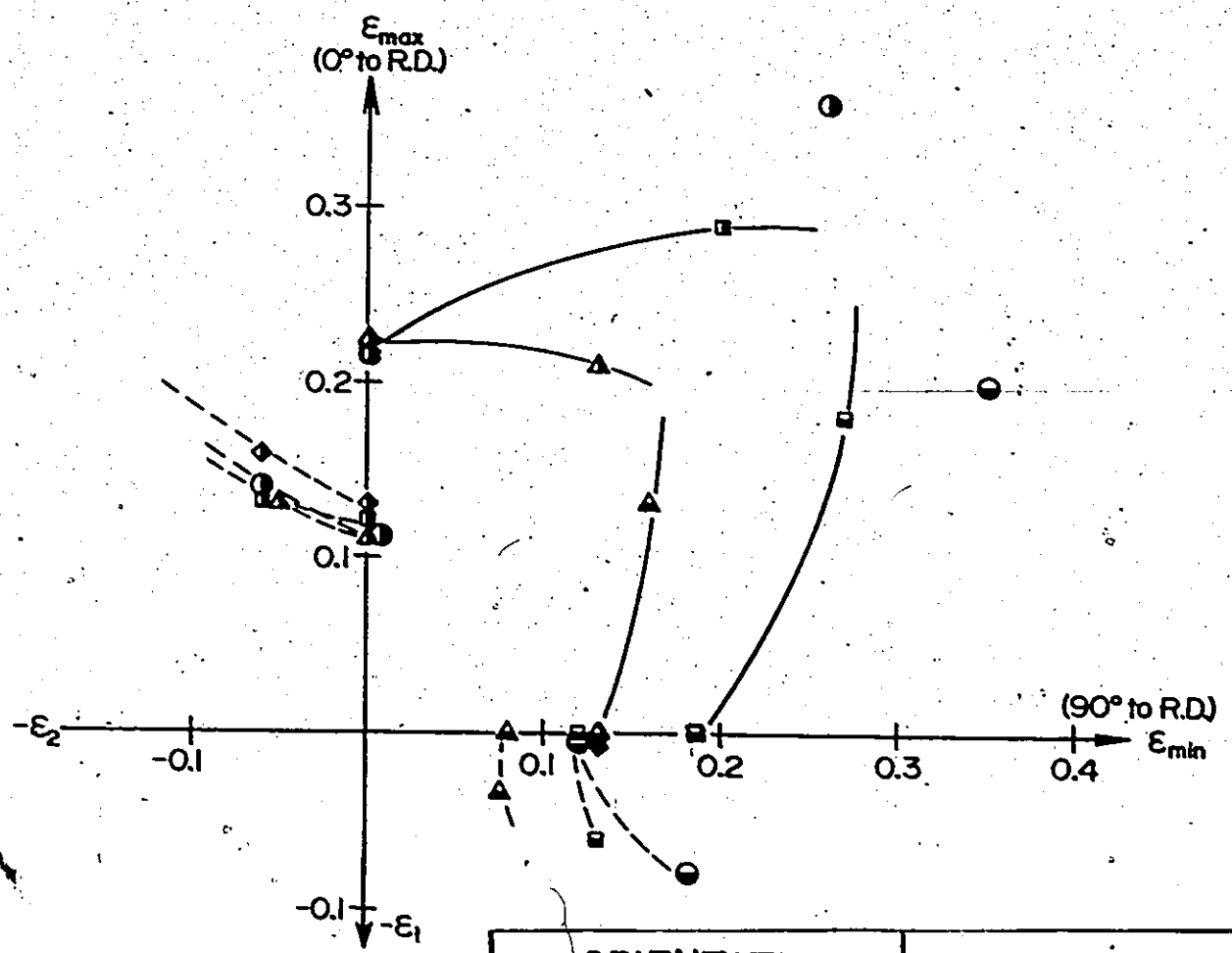
TABLE V
BALANCED BIAxIAL TENSION

<u>Material</u>	<u>Punch Depth (ins.)</u>	<u>Fracture Load (lb. f x 10³)</u>
Molycorp	1.33	186.0
X-80, 5/8"	1.33	180.8
Ipsco, 3/8"	1.14	147.2
	1.12	144.4
INCO 787, 1/2"	1.43	167.0
Normalized and aged	1.42	170.0

Strains were measured on a grid circle close to the fracture sites and the results are shown in Table V and on the Forming Limit Diagram in Figure 17. All the results are discussed later in this chapter, and metallographic studies of failure are presented in Chapter 5.

In the Ipsco material, failure occurred in the direction parallel to the rolling direction, initiated by the sulphide inclusion. As indicated in the Table V, the total strain at failure was small. In the Molycorp X-80, 5/8" plate, failure occurred at slightly higher strains, and is predominantly shear and not connected to the directionality of the plate. The forming limit in both cases increases slightly as the imposed strain ratio, $f = \epsilon_2/\epsilon_1$ changes from zero (plane strain) toward unity (balanced biaxial tension).

Using all the data from uniaxial tension, plane strain and balanced biaxial tensile tests at the imposed strain ratios $f = -1/2, 0$ and 1 , respectively, Keeler-Goodwin⁽¹³⁾ forming limit curves are constructed for the tested materials, as shown in Figure 17. It can be seen that the results for uniaxial tensile tests are lower than the other results. This could be understood if it is known that these data represent uniform strain limits, shown as a broken line on the FLD, Figure 17. These data are in good agreement with the work-hardening exponents, n , computed earlier. The data from plane strain, tensile, unnotched type of samples, and balanced biaxial tensile tests are represented in the FLD as full lines, and are at a higher level, representing maximum forming



ORIENTATION		MATERIAL
0° to RD	90° to RD	
▲	▲	IPSCO 3/8"
◆	◆	MOLYCORP X-80, 1/4"
■	■	MOLYCORP X-80, 5/8"
●	●	INCO 787, 1/4"

Fig. 17.

potential under these stress conditions.

The major strain, ϵ_1 , is the strain parallel to the rolling direction and the minor strain, ϵ_2 , is the transverse strain. Using the data presented in Figure 17 we can see the greatest difference in forming limits between the rolling and transverse directions for the Ipsco, 3/8" plate, acicular ferrite steel with a considerable fraction of elongated sulphide inclusions in the rolling direction. On the other hand, the directionality of the forming properties are not pronounced in the polygonal ferrite Molycorp X-80, 5/8" plate.

All the forming limit curves for the tested HSLA steels show, in general, low forming potentials, predicting difficulties in the forming of more complex components.

2) THE STRETCH-BEND TEST

Directionality of properties and poor transverse formability are frustrating characteristics of controlled rolled HSLA steels with the elongated manganese sulphide inclusions. The stretch-bend test was developed for the evaluation of the formability of lighter gauge HSLA steels and for monitoring the effect of inclusion control techniques on the transverse ductility⁽¹⁴⁾. In this test, schematically shown in Figure 18, a strip is rigidly clamped at each end and bent by transverse loading at the centre, using a radiussed punch. At the start, the tensile stress is applied on an outer surface and the inner surface is subjected to the compressive stress, while in between, there exists a neutral surface of

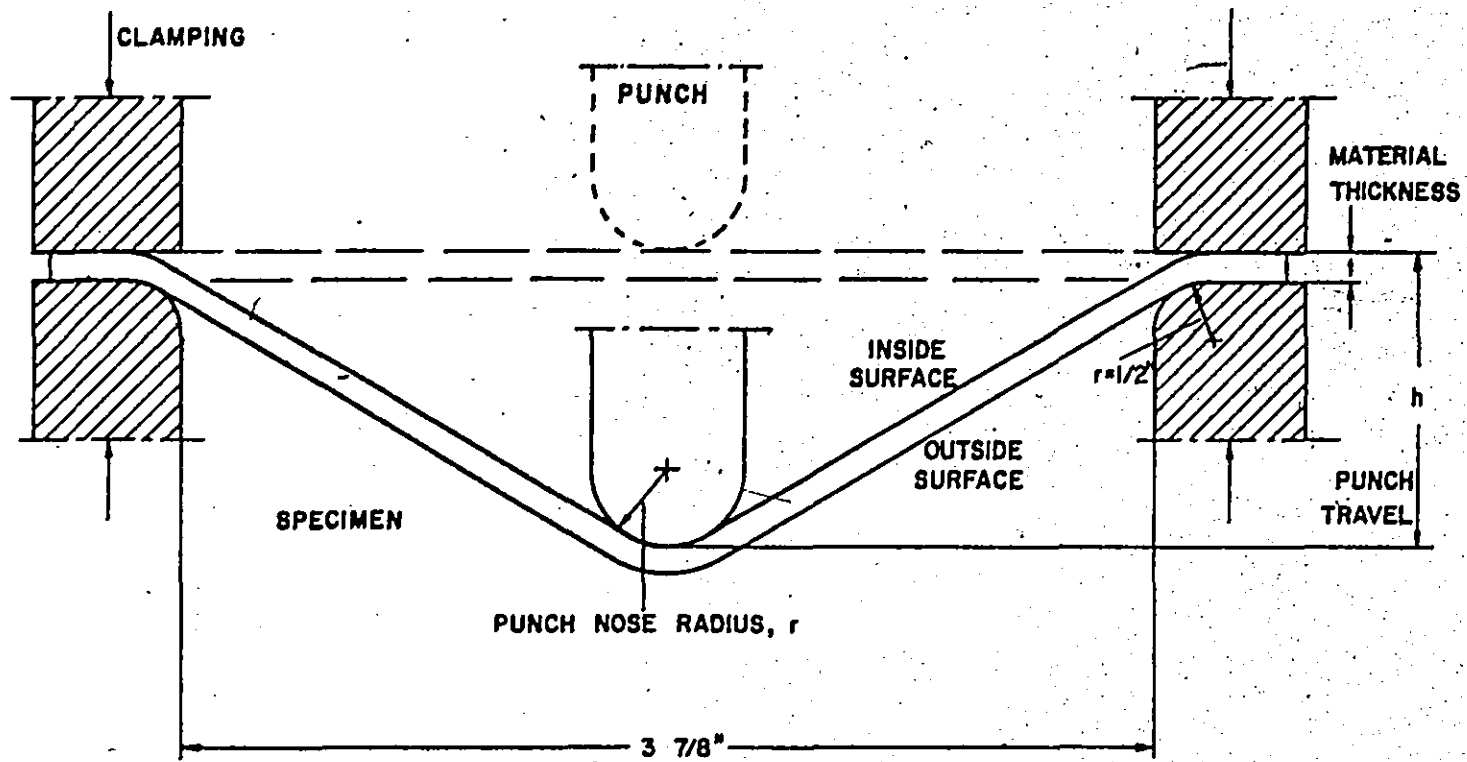


Fig. 18.

unstrained fibres. As the test progresses, the outer surface remains in tension. The inner surface compressive strain continuously decreases. Eventually, it becomes a tensile strain, when the neutral surface coincides with the inner specimen surface. Beyond this point, both major surface strain are tensile and increase rapidly, approaching each other. In order to measure strains, a circular grid pattern was printed on both surfaces of the sample, using the photoresist technique. The ends of the sample were rigidly clamped. A light film of multi-purpose E.P. gear oil, SAE 140 was applied on both sides of a 0.003" thick polyethylene sheet and this sheet was placed on the test piece over the area of contact with the punch. The sample was deformed by the punch moving at a speed of 0.5 in/min. An autographic plot of punch load versus punch travel was obtained and an example of such a diagram is shown in Figure 19.

Using larger radius punches, a gradual shattering and slight decrease were observed on the punch load - punch travel plot just before fracture and sudden load drop.

Using the smaller punches, the sharp load drop immediately follows the maximum load, as indicated in Figure 19. It was observed that, consistently after the load drop, audible cracking occurred on the outer surface and in the middle of the bent portion of the sample as shown in Figure

Strains were measured on grid circles close to the fracture sites. In this test three radiused punches 3/16", 3/8" and 3/4" were employed. The results of this experiment

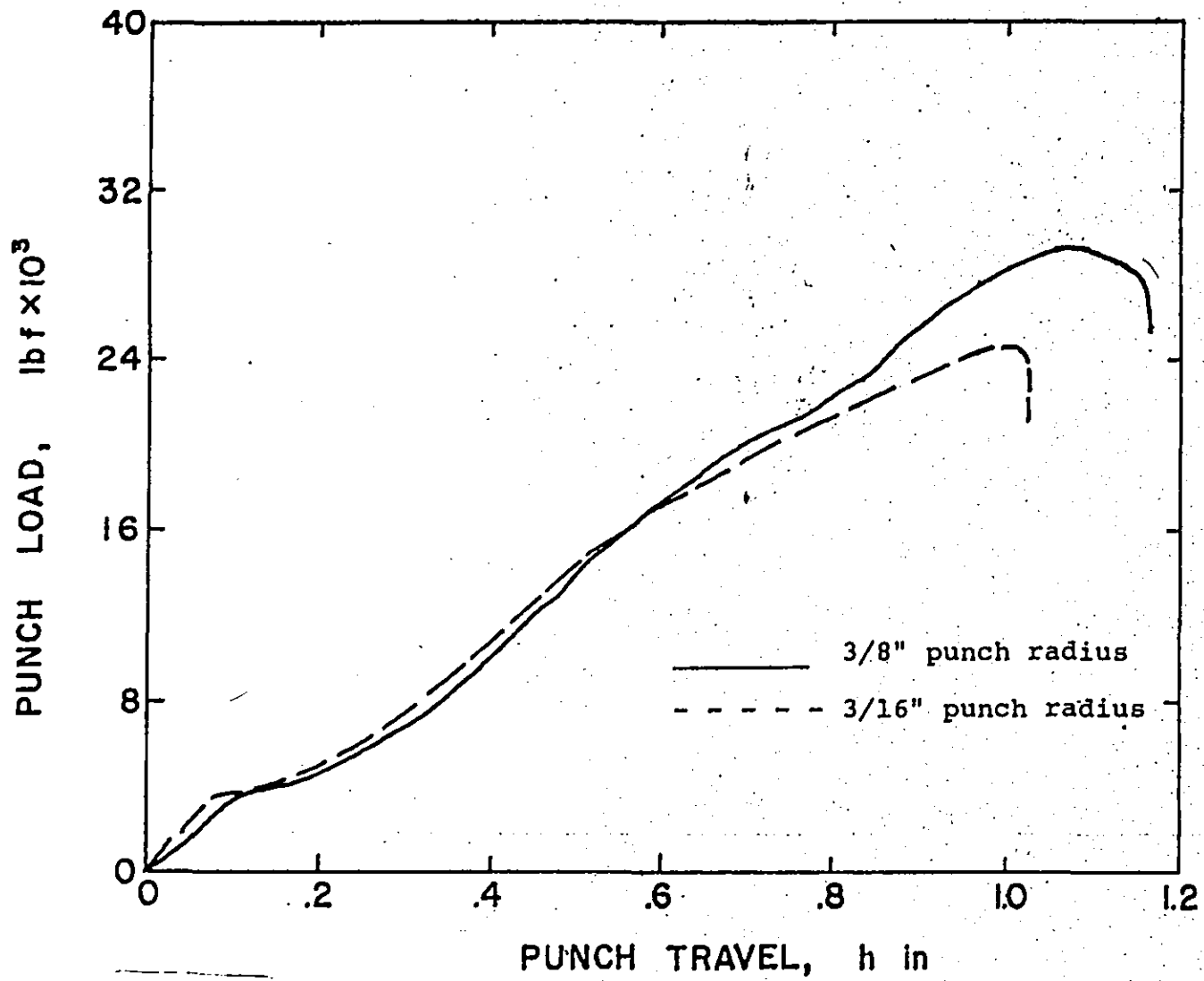


Fig. 19. Autographic load-deflection plot from stretch-bend tests with smaller punches

are presented in Table VI and Figure 20.

As seen from the results, the stretch-bend test gives a good correlation with the forming characteristics and the ductility observed in the other experiments. It has been a very sensitive method of evaluating the transverse formability and the effectiveness of sulphide shape control. The straining process is concentrated on the intersection of the transverse and longitudinal axis of symmetry and failure originates here on the outer surface, spreading through the sample along a loci of velocity discontinuities.

Metallographic studies of the failure under stretch-bend conditions are discussed in the next chapter.

Thus, in general, the forming potential of these complex materials is influenced not only by non-metallic inclusions, but also by the presence of hard, rigid, non-deformable phases such as M/A constituents in the Molycorp X-80, 5/8"

Also, in the materials such as Ipsco 3/8" at a low finishing temperature, the work-hardening capacity of the matrix is reduced due to high dislocation density in as-received condition and the material behaves as if already prestrained. Thus, the low-temperature rolling, favorable for production of fine grain and high yield strength materials, reduces the forming potential by reduction of work-hardening capacity of the matrix.

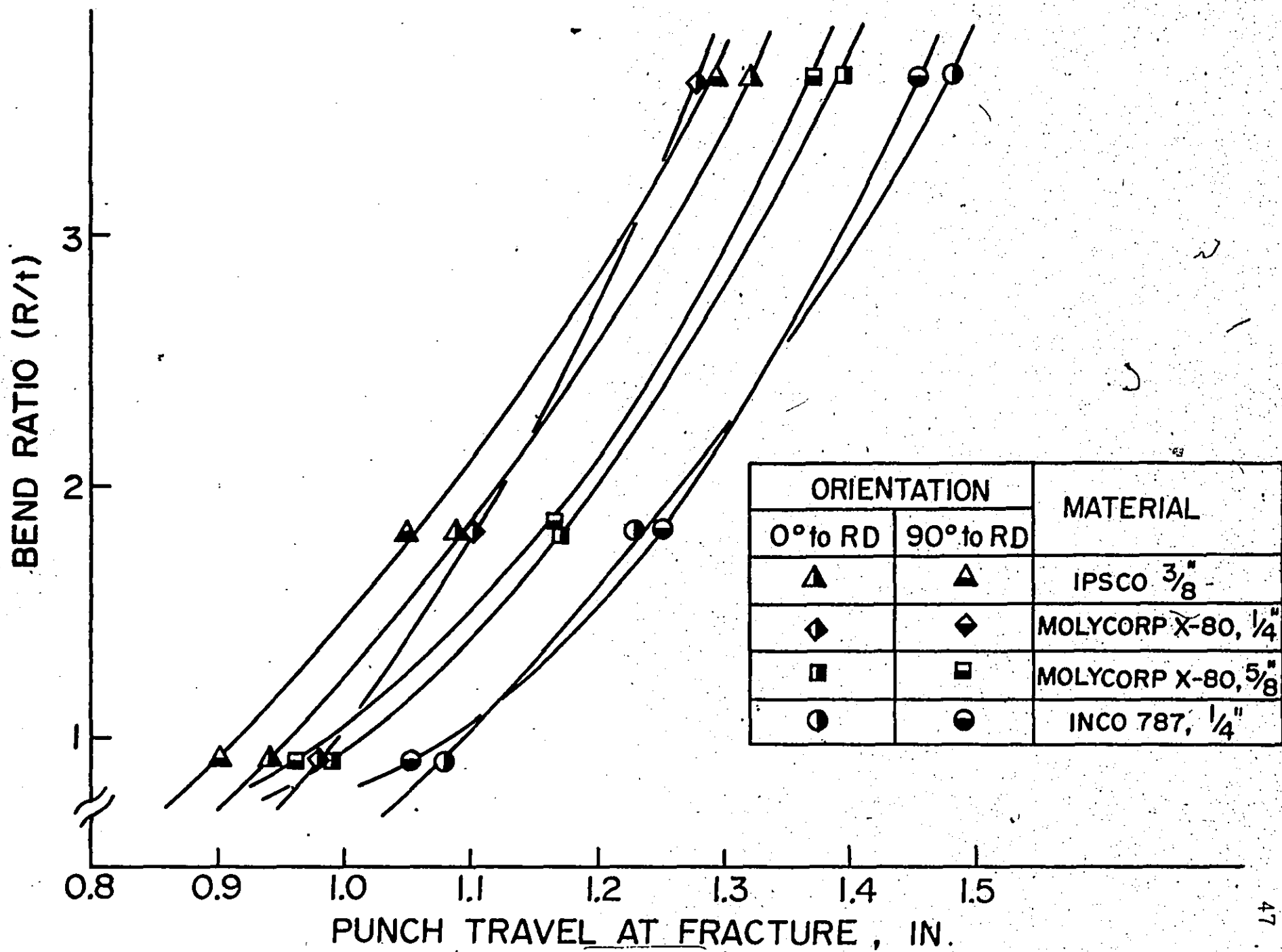


Fig. 20

TABLE VI

STRETCH-BEND TEST

<u>Material</u>	<u>Orientation Relative to RD</u>	<u>Punch Radius R = 3/16" Ratio R/T = 0.906</u>	<u>Punch Radius R = 3/8" Ratio R/T = 1.812</u>	<u>Punch Radius R = 3/4" Ratio R/T = 3.624</u>	<u>Strain Hardening Index n</u>
<u>Ipsco 3/8"</u>	parallel to RD	0.94	1.09	1.32	0.125
	perpendicular to RD	0.90	1.05	1.29	0.125
<u>Molycorp X-80, 1/4"</u>	parallel to RD	0.98	1.10	1.28	0.155
	perpendicular to RD	N/A	N/A	N/A	0.145
<u>Molycorp X-80, 5/8"</u>	parallel to RD	0.99	1.17	1.39	0.135
	perpendicular to RD	0.96	1.17	1.37	0.140
<u>INCO 787 1/2"</u>	parallel to RD	1.08	1.23	1.48	0.160
	perpendicular to RD	1.05	1.25	1.45	0.165

N/A - Not Available

CHAPTER 5

METALLOGRAPHIC STUDIES OF FAILURE

As stated earlier in the metallographic section, the HSLA steels used in the present work exhibit a wide range of microstructural features such as:

- inclusions
- grain size and shape
- ferrite morphology
- carbide distribution
- presence of M/A constituents.

In this chapter, an effort is made to relate the process of failure in various stress states to detailed microstructural features. In order to clarify this, the discussion is divided into sections dealing with:

- 1) Failure mechanisms in uniaxial tensile tests
- 2) Failure mechanisms in biaxial tension
- 3) Failure mechanisms in stretch-bend tests.

The characterization of failure modes of HSLA steels under different stress states and their relationship to microstructural features become very important in terms of component design and material selection. In such complex HSLA systems, as deformation progresses and the distribution of strain

becomes critical, failure can ensue in the region of localized plastic strain.

As a result of microstructural features of the tested HSLA steels, possible failure mechanisms could involve:

- a) local brittle failure of non-metallic inclusions or hard, rigid phases,
- b) void formation at the interface between hard phases and the matrix,
- c) void formation in intensively deformed shear bands,
- d) void growth and joining,
- e) delamination along weak planes, and
- f) failure by localized shear.

In some cases a number of failure modes may be involved in the final failure mechanism, but often, as a result of competition between them, some of the failure modes are very pronounced. A more detailed description of the failure mechanisms and their relation to the microstructural features is given in this chapter.

1) FAILURE MECHANISMS IN UNIAXIAL TENSILE TESTS

Introduction

The failure of most ductile polycrystalline materials begins by void nucleation, growth and linkage in the neck region, and is completed by very rapid shear fracture along planes of maximum shear stress. This type of failure leaves the characteristic cup-and-cone fracture appearance. In this case, the high energy absorption failure process is void

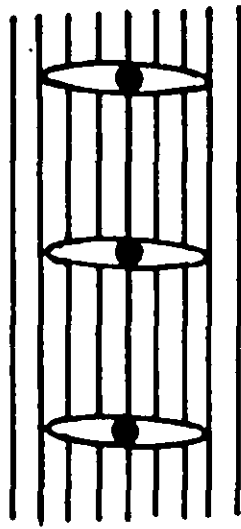
growth and linkage, which are spread over a large volume of material. When the critical conditions for localized shear are reached, relaxation or unloading of the system occurs by the formation of localized shear bands, which have a very high propagation rate through the material. The overall ductility or strain to failure is a function of the failure modes involved in final stages of deformation. The critical conditions for each failure mode depend strongly on the stress-strain relationship of the system, particularly on the local work-hardening rate and the strain rate sensitivity. In systems with a negative strain rate sensitivity and an inhomogeneous strain distribution, the sites with a higher strain rate (due to reduction in local work-hardening capacity) could become origins for the formation of localized shear bands at low overall strain.

In the competition between continuing plasticity and voiding at the particle-matrix interface, Argon et al⁽¹⁵⁾ indicate that the process of void initiation can be quantitatively described in terms of critical stresses at the matrix-particle interface. Very often, for the material with a low volume fraction of particles homogeneously distributed, the strain to cause voiding is of the order of one-half of the true strain to failure. But, for closely spaced inclusions, local plastic fields interact and reduce the critical strain for void nucleation. Hence, the critical conditions for void nucleation depend not only on the volume fraction, but also on the distribution and local spacing of the particles.

An elementary treatment of the influence of microstructural parameters on the process of void growth is shown in the geometrical model, Figure 21, proposed by Brown and Embury⁽¹⁶⁾. In this model, they indicated that the growth strain, ϵ_g , should be related to the inverse square of the volume fraction of inclusions and second phase particles, and is relatively insensitive to the inclusion size. However, size, shape and particularly distribution of the inclusions, as mentioned earlier, seem to have an important effect on the local work-hardening rate and strain distribution during void growth, and on the strain localization during the void linkage process.

In general, in HSLA steels the delamination failure mode is often found, particularly in the steels with a high content of non-metallic inclusions, or with a banded structure. Most often, delamination fracture occurred along planes of weakness parallel to the rolling plane. Some authors⁽¹⁷⁾ have suggested that a strong (100) texture component in the rolling plane could be responsible for delamination by cleavage fracture, at low temperatures.

Delamination is frequently observed to be accompanied by inclusions, segregation and non-ferritic products distributed along certain planes during solidification, transformation or mechanical working. In high sulphur steel, delamination occurs along stringers of MnS, as observed in Ipsco 3/8", while in a very clean steel, delamination failure occurs along the ferrite grain boundaries. Herø et al⁽⁷⁾ explained this



$$2r_0(1 + \epsilon_g) = r_0 \left(\sqrt{\frac{2\pi}{3f}} - \sqrt{\frac{8}{3}} \right)$$

$$\begin{aligned} \epsilon_r &= \ln \frac{A_0}{A_f} \\ &= \ln(1 + \epsilon_g + \epsilon_n) \\ &= \ln \left(\sqrt{\frac{\pi}{6f}} - \sqrt{\frac{2}{3}} + \epsilon_0 \right) \end{aligned}$$

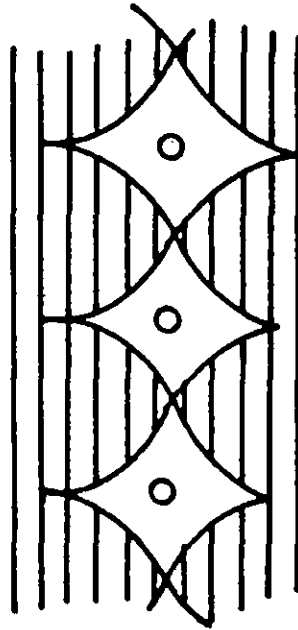


Fig. 21

by the presence of grain boundary cementite. They suggested that the failure mechanism involved nucleation and growth of voids at the grain boundary carbides, and their linking under the action of the transverse stresses developed in the neck.

Results of this Study

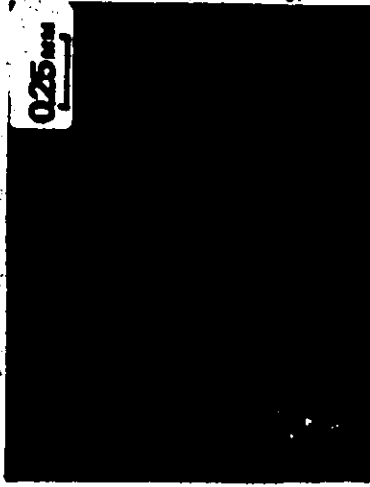
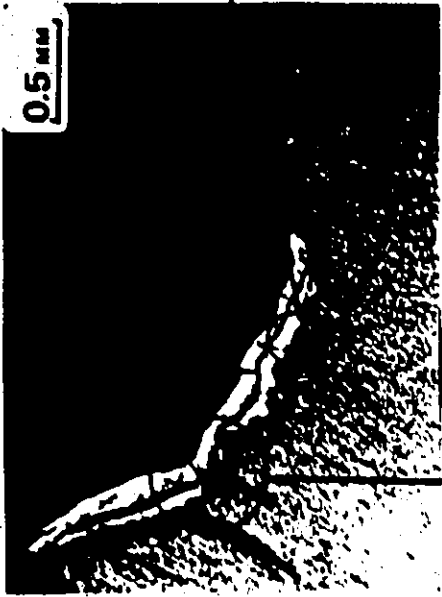
In this work, an effort was made to characterize the failure modes for the tested materials, and where it was possible, to relate this to the microstructural features.

Careful optical metallography and Scanning Electron Microscopy (in text SEM) were employed, and, in order to preserve fracture edges, in some cases the fracture surfaces were nickel-plated prior to mounting and polishing.

In the Ipsco 3/8" tensile sample, Figure 22, the usual cup-and-cone fracture appearance is found.

In this material with a relatively high inclusion content (with high volume fraction of elongated sulphide inclusion) extreme void nucleation, void growth and splitting occurs prior to complete failure by shear, as shown in Figure 22. It was found that all the voiding and splitting originates at non-metallic inclusions, such as MnS, and at the complex islands composed of the mixture of retained austenite and martensite.

However, for the other HSLA steels, where desulphurization practice and sulphide shape control were applied to reduce the influence of the sulphides to a minimum, the expected gain in ductility was not observed. In these cases, some other microstructural features have a marked influence on the



IPSCO-CLIMAX, 3/8"

FIGURE 22

fracture properties. Some authors^(18,19) have emphasized the importance of the melting practice in the control of volume fraction, distribution and nature of oxide particles. In addition to oxides, an important feature in low sulphur, low carbon HSLA steels appears to be the presence of large amounts of martensitic and retained austenitic (M/A) aggregates⁽²⁰⁾. Careful metallographic studies of deformed samples show that these M/A constituents, distributed as islands, act as void nucleation sites in ductile failure, Figure 23. These non-ferritic phases act as rigid inclusions, reducing the ductility and producing local internal stresses, which have an influence on the homogeneity of the flow processes.

The critical conditions for shear band formation and propagation are reached at low plastic strains. This leads to the catastrophic fracture by shear. This is not expected in these types of HSLA steels since they are very clean, having very low non-metallic inclusions. Tensile samples which failed by this mechanism exhibit a very small cup region (if at all) and show very large shear lips.

During the failure process by shear, there are often secondary shear bands associated with the fracture. These bands do not totally penetrate the sample and are usually representative of the main fracture mode. An example of such a shear band is shown in Figure 24. In this case, in the shear band, produced between two large voids, and parallel to the major fracture surface, the shear strain, γ , is of the order of 1. Relatively little theoretical work has been done

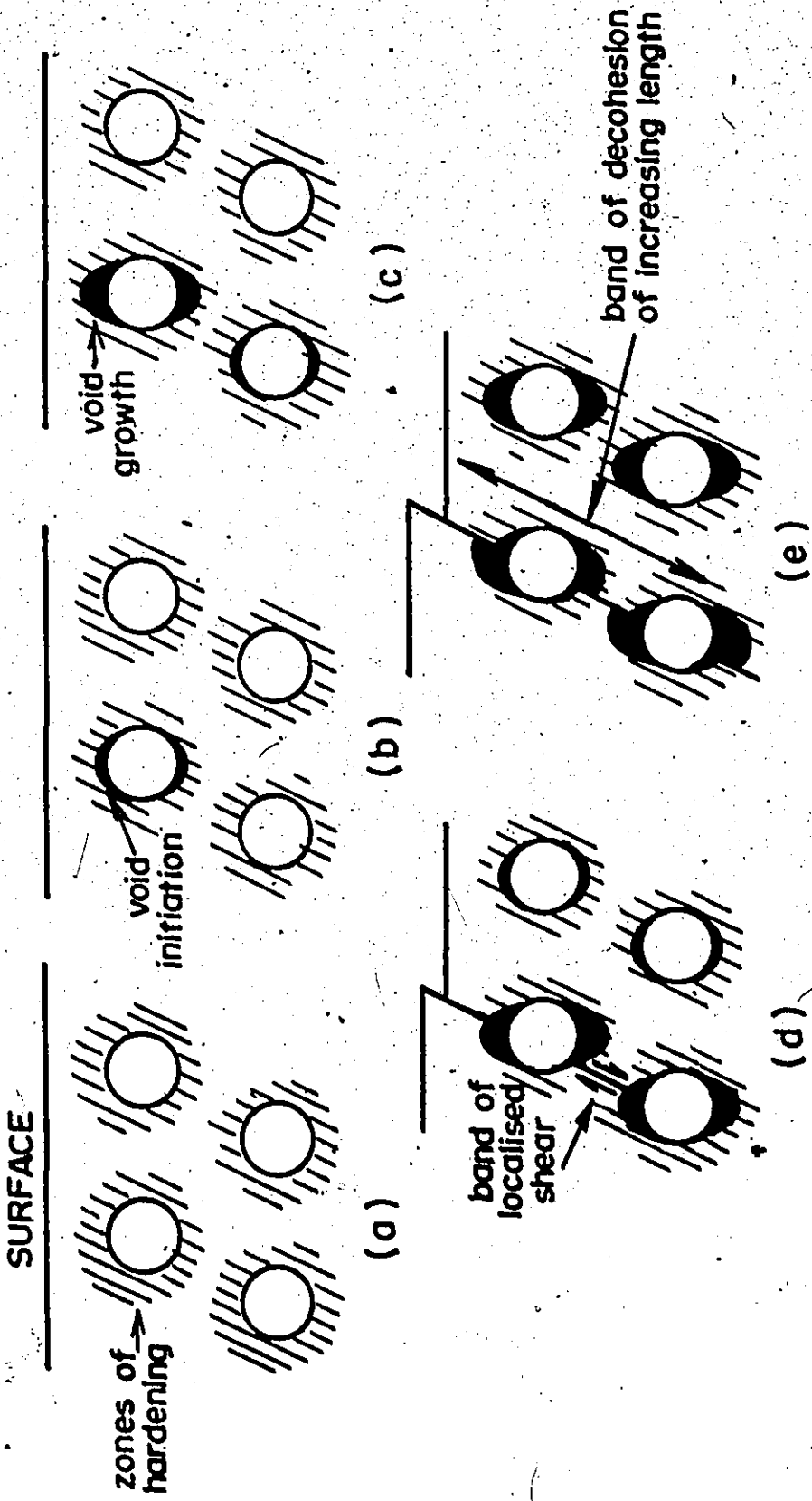


FIG. 23.

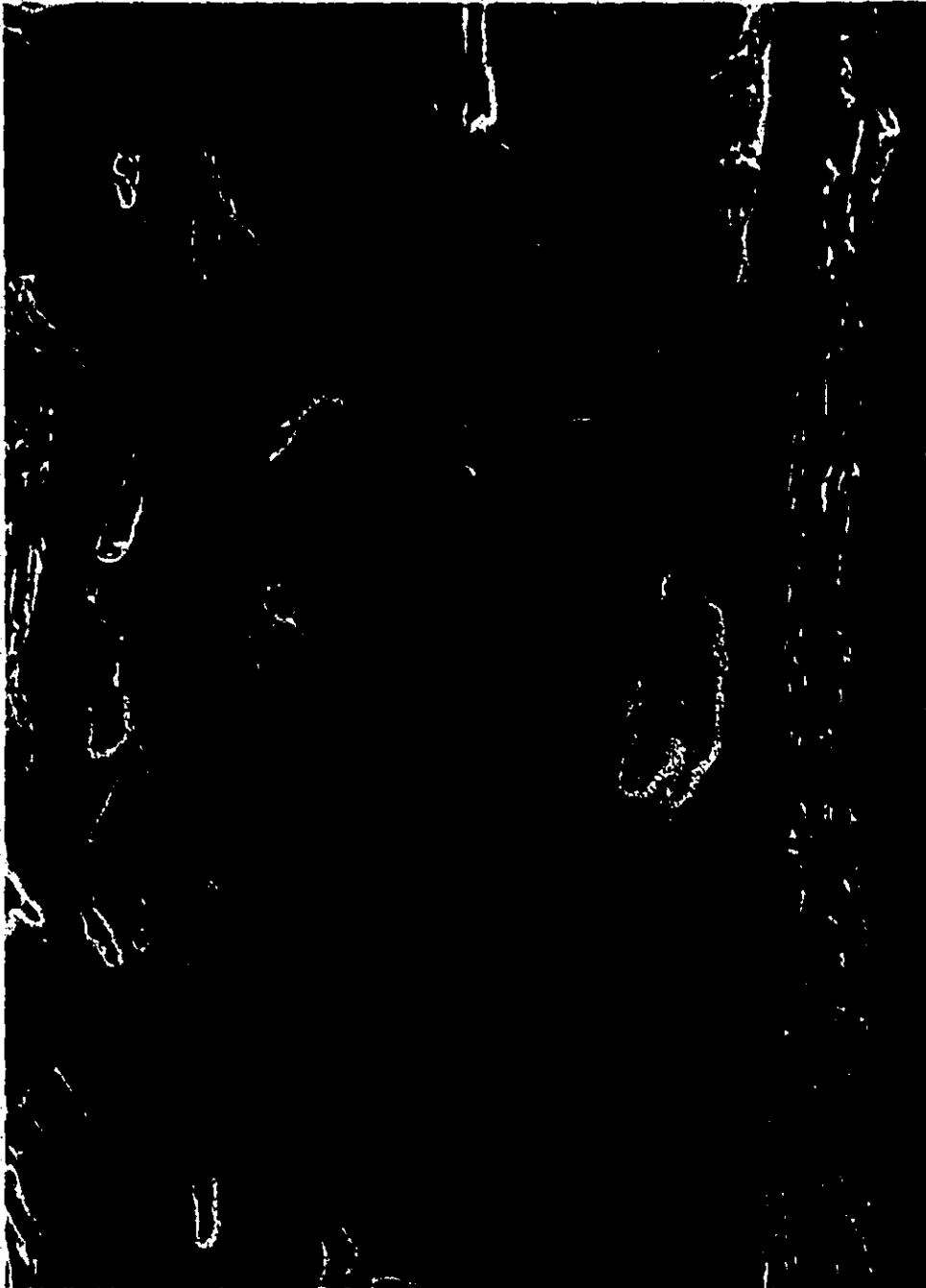


Fig. 24

to analyze the competition between void growth and localized shear as a function of microstructure and stress states. A better understanding of these complex processes would give the answer to many questions concerning the ductility of the high strength materials, such as HSLA steels tested in this work.

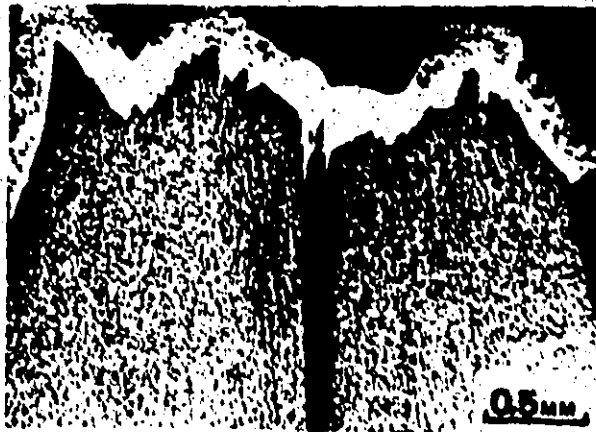
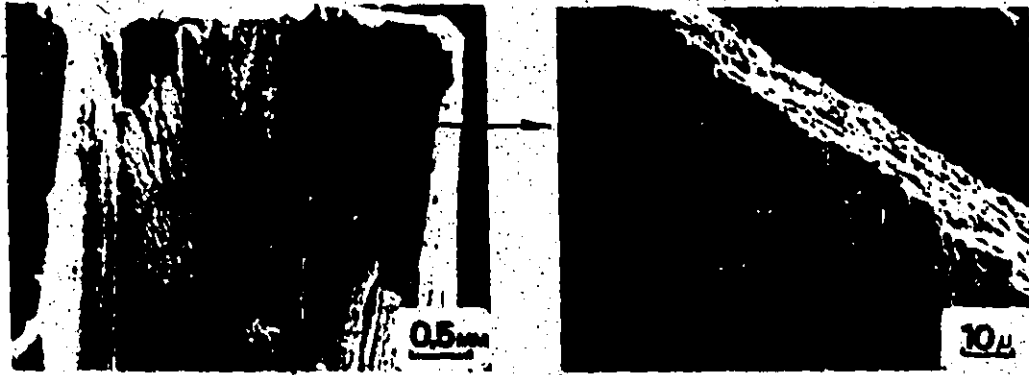
As evidence that the failure process by shear is very common in almost all types of HSLA steels, under different stress conditions, a number of micrographs and fractographs will be discussed.

As mentioned earlier, only the fracture surface for the Ipsco material could be classified as cup-and-cone type, accompanied by delamination along MnS inclusions.

For Molycorp X-80, 1/4" plate, in the neck region, after delamination along the pearlite bands, fracture occurred mostly by shear of separate fragments, such as one shown in Figure 25.

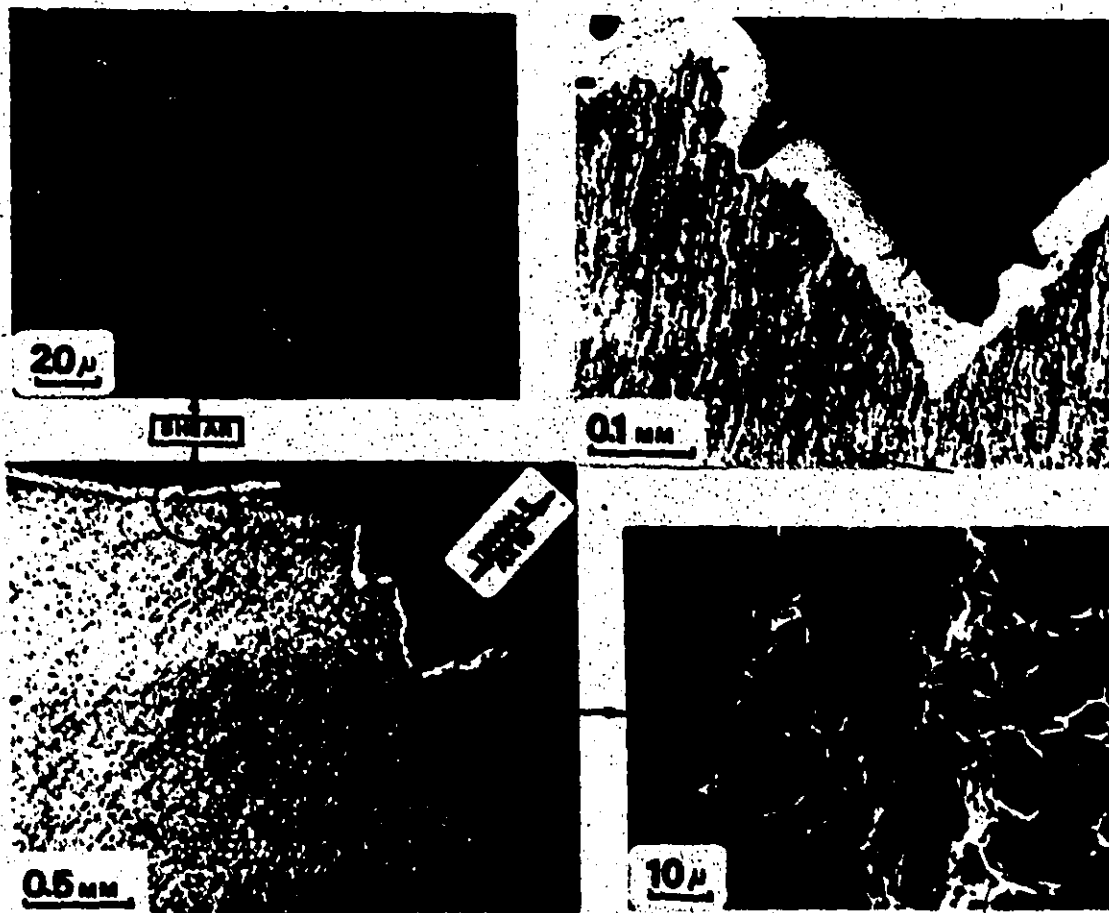
For Molycorp X-80, 5/8" plate and INCO 787, 1/2" plate, the failure mechanisms can be discussed together. Optical micrographs of the cross-section along the tensile sample and across the fracture surface, and SEM fractographs are shown in Figure 26 and Figure 24.

As discussed earlier, after void nucleation at hard particles and their growth, the tensile sample fails by catastrophic shear along the planes of maximum shear stress. This produces a characteristic fracture appearance - the rather uniformly ordered array of elongated dimples oriented parallel to a single direction as a result of the deformation in the



MOLYCORP X-80, 1/4"

Fig. 25



MOLYCORP X-80, 5/8"

Fig. 26

shear band. The micrograph of the tensile Molycrop X-80, 5/8" sample in Figure 24 shows that, well within the neck, the shear band segments are short and in a zig-zag pattern, to avoid moving very far from the most highly stressed region of the material. For the INCO 787 tensile sample, with better strain distribution in the diffuse neck, the band segments are longer. The SEM fractograph in Figure 27 shows the intersection of two shear bands.

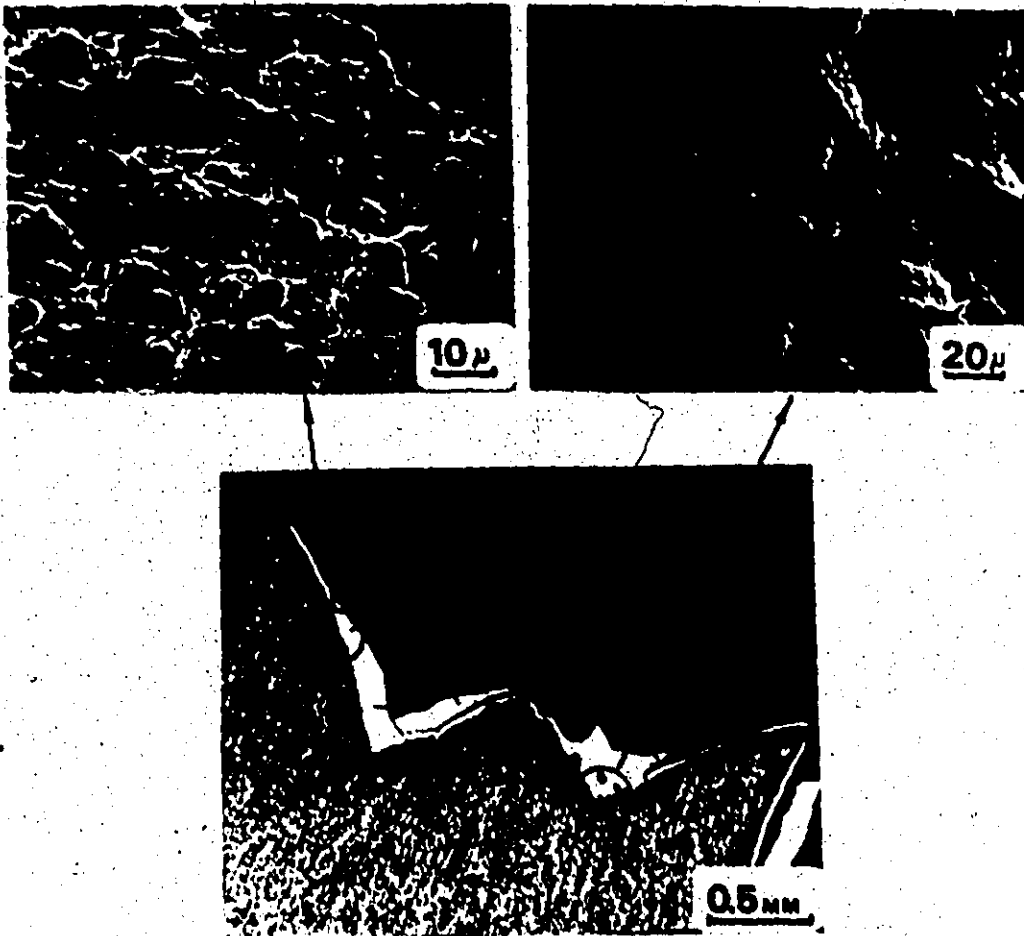
2) FAILURE MECHANISMS IN BIAXIAL TENSION

In order to determine the influence of the stress states on the fracture appearance in HSLA steels, the samples used for the determination of the Forming Limit Diagram, were carefully examined in the SEM. The fracture appearance of some biaxial stretched samples is shown in Figure 28.

Due to major microstructural differences, the attention is confined to the Ipsco 3/8" and Molycorp X-80, 5/8", which are taken to be representative of the various types of the materials used.

Due to the lower forming potential in the transverse direction, after in-plane splitting along elongated inclusions, the Ipsco sample fails along the rolling direction. The SEM fractograph clearly shows extensive splitting along MnS inclusions.

In Molycorp X-80, 5/8" balanced biaxially stretched sample, voiding occurred at hard phases, followed by shear failure, propagating usually from the central region in three



INCO 787 - 1/2"

Fig. 27

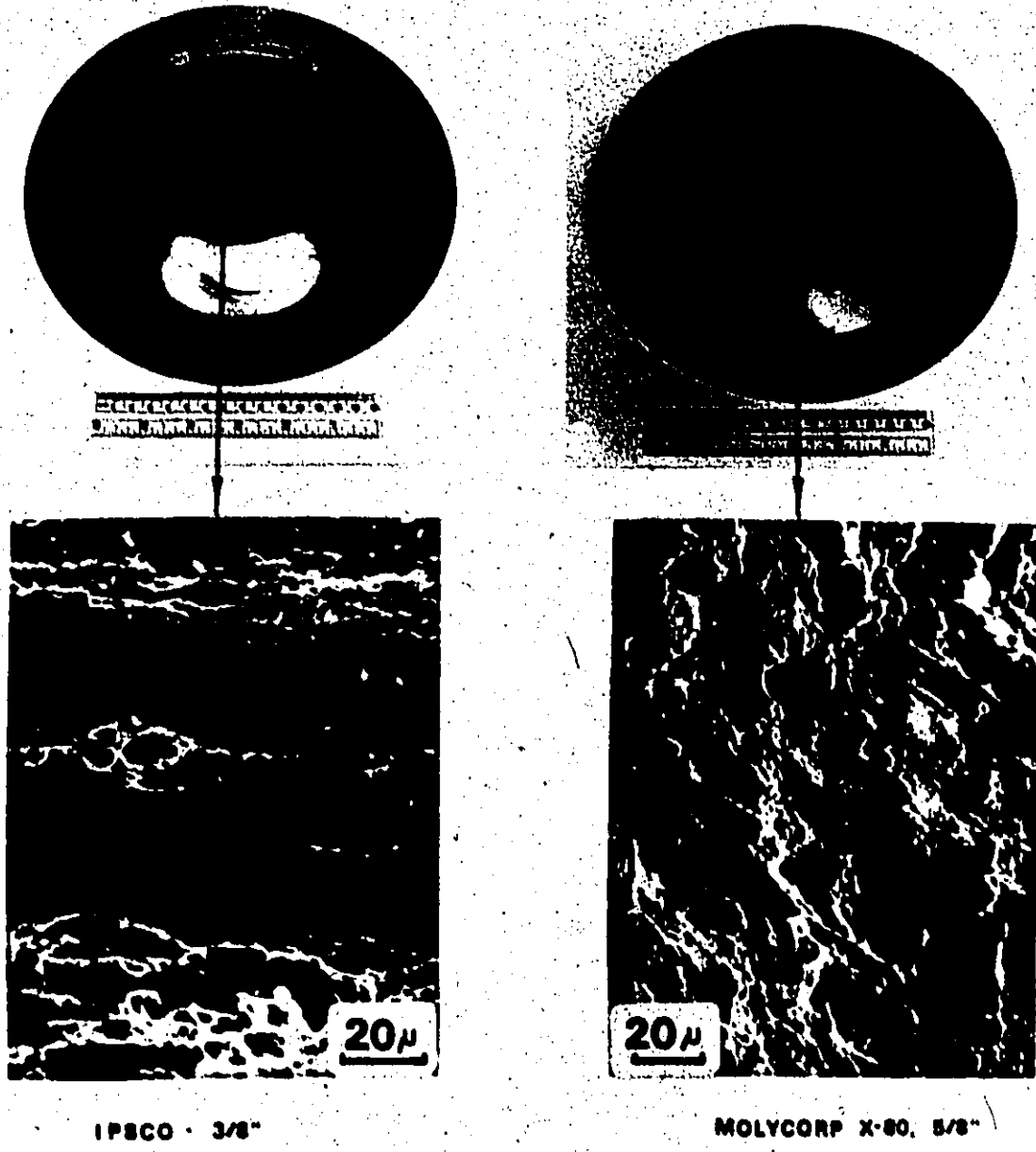


Fig. 28

directions, as indicated in Figure 28. Again in this test, catastrophic shear failure occurred at relatively low strain. The dimples are small indicating that very little void growth took place before shear occurred.

3) FAILURE MECHANISMS IN STRETCH-BEND TEST

At the more complex stress state, in the stretch-bend test, with a strain gradient through the thickness, the void nucleation occurs at the interface between the hard transformation products and the ferrite. Due to the highest tensile strain, fracture initiates at the centre of the outer surface as shown in Figure 29. Similarly to the failure mechanisms discussed earlier, islands, consisting of martensite-retained austenite become highly damaged at relatively small strain due to the accumulation of the strain at the boundaries. These damaged regions full of small microcracks and voids, later link by localized shear along the loci of planes of the maximum shear stress. Linkage occurs at relatively small overall crack-opening displacements (or strains).

An example of void nucleation in regions of mixtures of the hard transformation products and the path of cracks formed by shear between these regions, is shown in Figure 30 - an SEM micrograph of Molycorp X-80, 5/8" stretch-bend sample.

In Ipsco 3/8" material, in stretch-bend tests, an important role is played by the orientation of the large and elongated inclusions. In the case where the inclusions are oriented in the tensile direction of the test, splitting along

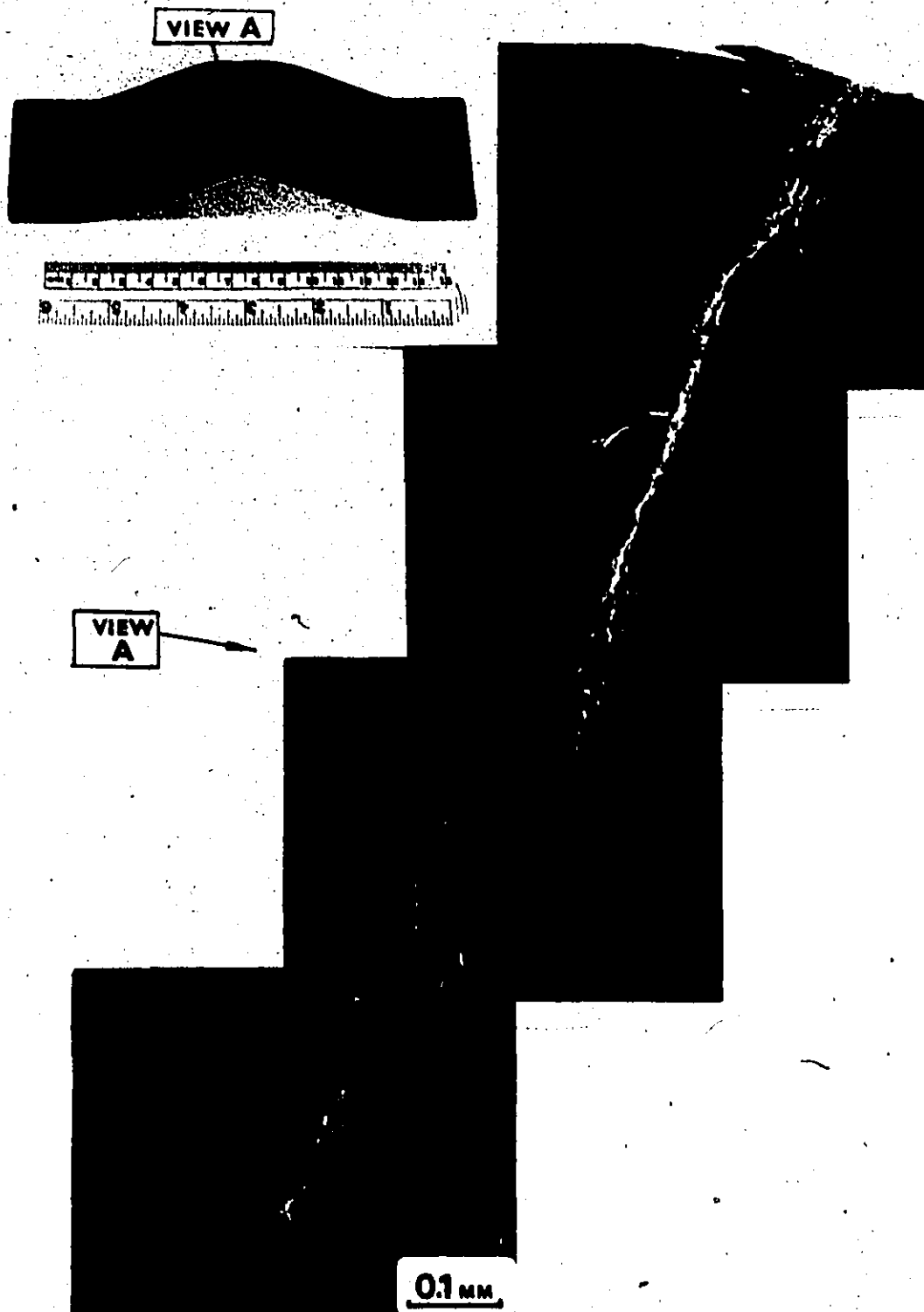
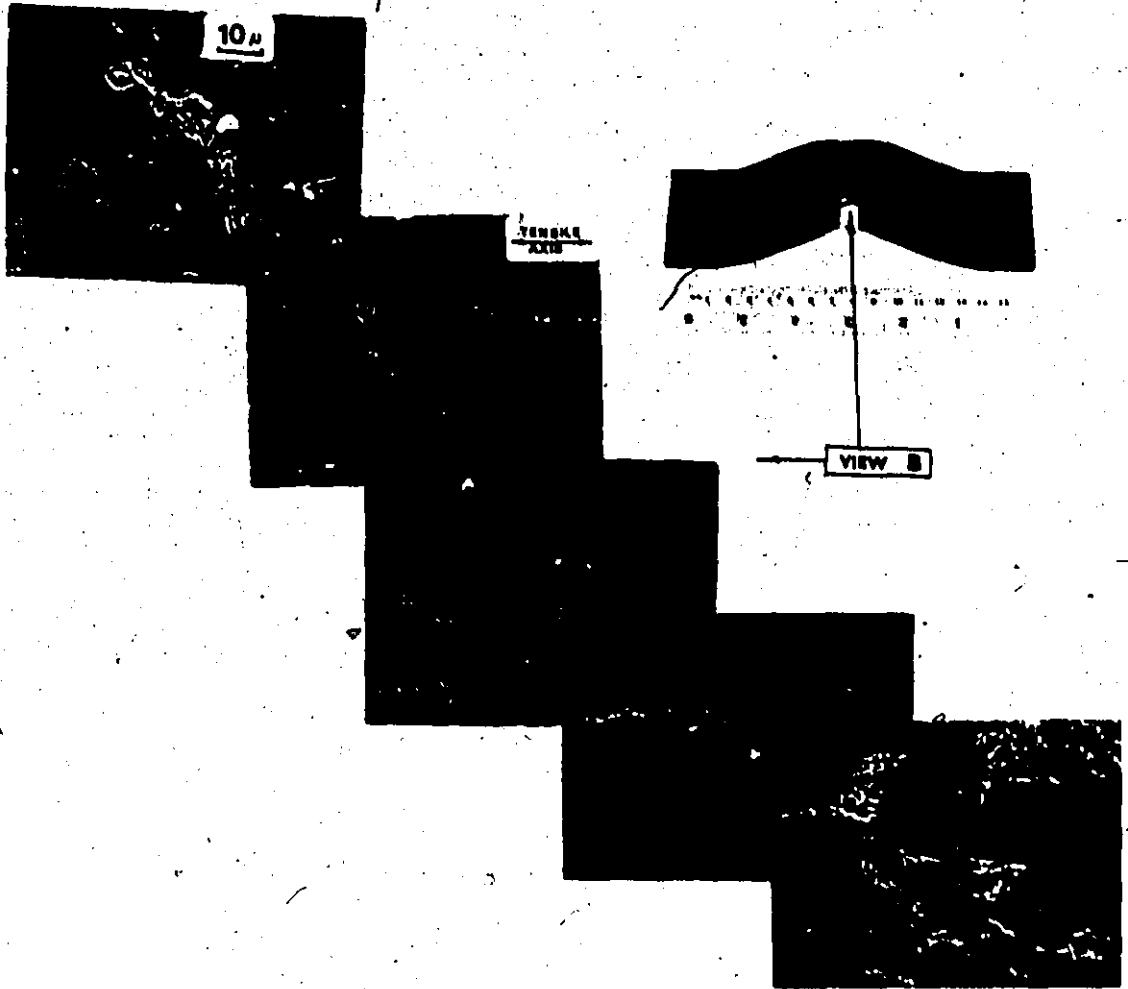


Fig. 29



MOLYCORP X-80, 5/8"

Fig. 30.

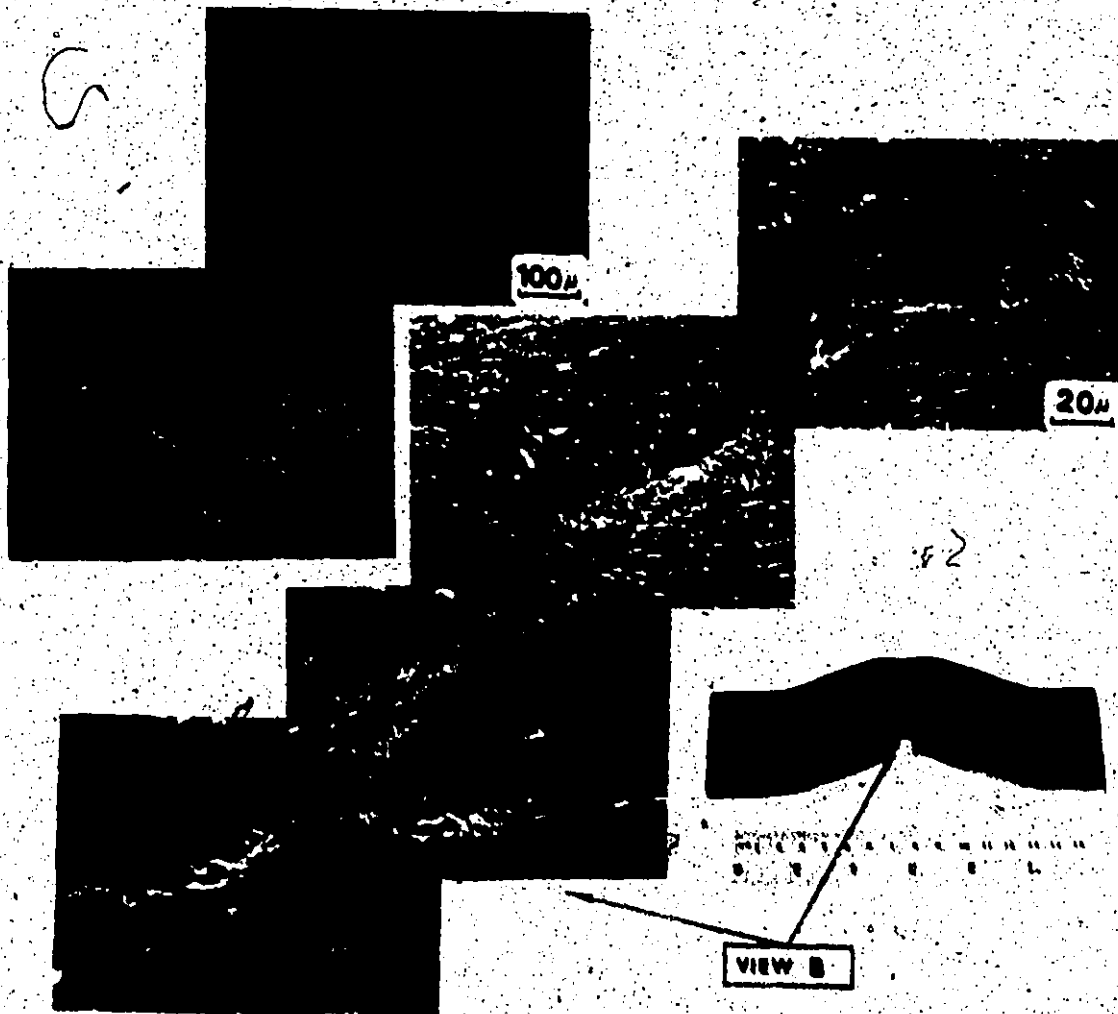
the inclusions first takes place, due to the development of the triaxial stress-state. At higher strains void nucleation at the hard phases is followed by linkage of the most damaged regions. In this case, the already present delamination could stop propagating shear band, or change its orientation from one plane to another, as shown in Figure 31.

After careful examination of the failure mechanisms in the stretch-bend test, it was found that during deformation at the boundaries between the hard regions present in HSLA steels and the relatively soft ferrite matrix, damage accumulates, producing large voids and cracks, which at critical conditions, link by localized shear. As the small cracks open, these hard regions, if damaged enough, could split apart or could be seen as a solid island in the middle of the crack, as shown in Figure 31 and Figure 32.

In general, the failure process in HSLA steels can be considered as consisting of the following steps:

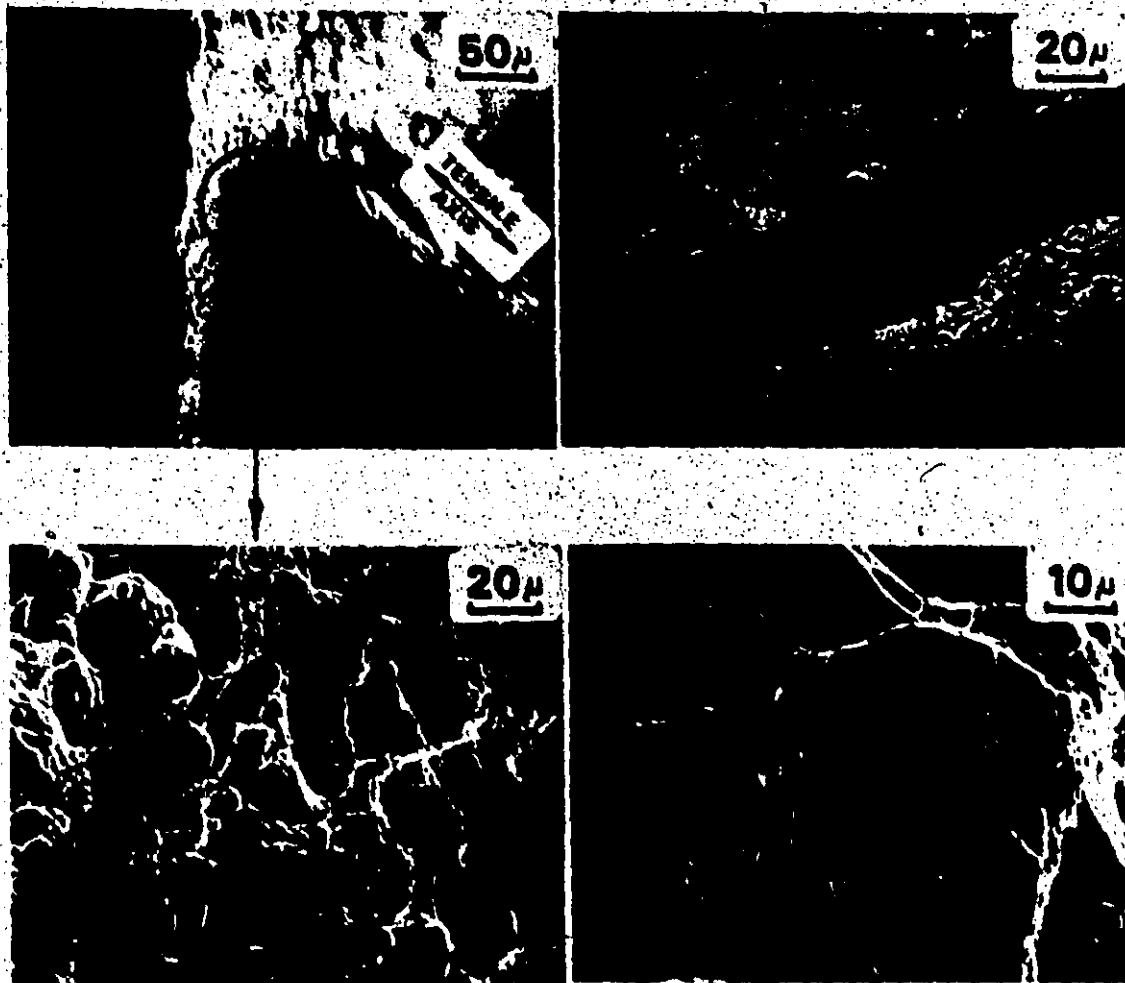
- 1) Local, brittle fracture of non-metallic inclusions or hard-rigid phases, such as M/A microconstituents or carbides.
- 2) Void nucleation on hard particles.
- 3) Void growth and joining at higher strains.
- 4) Delamination along certain planes.
- 5) Failure by localized shear, when the critical conditions for shear-band formation are satisfied.

The number of cracks nucleated by the brittle fracture of hard particles is directly proportional to the volume



IPSCO - CLIMAX, 3/8"

Fig. 31



MOLYCORP X-80, 5/8"

Fig. 32

fraction of such phases. Examples of these hard particles are:

- a) non-metallic inclusions,
- b) carbides, and
- c) complex M/A constituents.

The non-metallic inclusions, for example, MnS, affect the Ipsco Steel. The carbides, especially at grain boundaries, affect all the steels. In materials such as Molycorp X-80, where desulphurization and sulphide shape control reduce the effect of sulphides, the complex M/A constituents are the important hard particles.

In a ductile fracture, the nucleation and growth of voids, described earlier, in terms of a simple geometrical model, strongly depend on volume fraction of hard particles. The equation expressing the relationship between the growth strain to fracture and the volume fraction of hard particles

$$\epsilon_g^* = \left(\frac{1}{8}\right)^{\frac{1}{2}} f^{-\frac{1}{2}} - 1$$

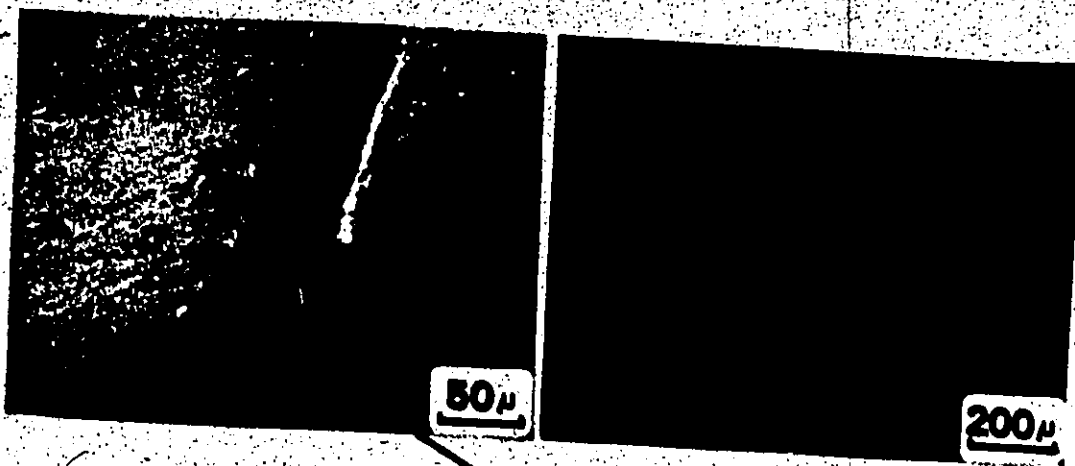
shows that increasing the amount of inclusions will cause a reduction in the true strain to fracture.

As indicated in the literature⁽¹⁶⁾, the strain to failure, ϵ_f^* , under a defined stress state should be related quantitatively in some form to the volume fraction of inclusions present in the material. An attempt was made to relate the volume fraction of the non-metallic inclusions to ϵ_f^* for the tested HSLA steels. It showed clearly that the material with the lower volume fraction of non-metallic inclusions gave the same or lower ϵ_f^* as the other materials. This indicates that

in discussing the failure process in HSLA steels the presence of the hard M/A constituents has to be considered in addition to the other inclusions.

As discussed earlier, delamination, a commonly found failure mode in HSLA steels, occurs at a relatively early stage of the deformation. In Ipsco 3/8" material with a high sulphur content, delamination failure arises due to the presence of MnS stringers and carbides along the grain boundaries. On the other hand, in Molycorp X-80, 1/4" thick plate, with a low sulphur content and rare earth additions, delaminations are found to be intergranular tear fractures, parallel to a rolling plane. According to Herp et al⁽⁷⁾, this is due to the precipitation of cementite on the ferrite grain boundaries, where banding consisting of pearlite and carbides was observed. Molycorp X-80, 5/8" plate did not display delamination. This could be explained in terms of microstructural differences. As discussed, this material contains complex M/A constituents rather than pearlite and cementite.

As a general and usually final failure mode in the tested HSLA steels, shear seems to have the most important role. This mode of localization of plastic strain and fracture initiation has been partly investigated but still, the critical conditions for shear band (shear crack) nucleation and propagation are not well understood. From the results discussed earlier in this work, it was observed that in control-rolled HSLA steels with a low inclusion content and rare earth treatment, low strains to failure were found to be due to the rela-



NORMAL TO R.D.

PARALLEL TO R.D.

IPSCO-CLIMAX, 3/8"

Fig. 33

tively early activation of the shear failure mode. In this case, the critical conditions for the formation and catastrophic propagation of unstable shear bands are reached at an early stage of the deformation. As explained earlier, the complex M/A regions with residual stresses in their vicinity, behave as large, hard inclusions in the soft matrix. During deformation, these regions become highly damaged (Figure 30).

Cracks and voids nucleated in those regions continue to grow. Due to the relatively large volume of damaged material, the work-hardening capacity of the matrix is reduced. This leads to the formation of unstable bands in the planes of reduced work-hardening capacity and high shear stress. As shown in Figure 30 and Figure 33, the shear bands are formed along the loci of velocity discontinuities and between such highly damaged regions or voids. The velocity of the shear band increases as the length increases. Due to the highly localized deformation within the band, new voids are formed prior to complete separation. Thus, the presence of hard, complex M/A regions seems to have a major effect on the strain localization and development of unstable shear failure at an early stage in the deformation history.

CHAPTER 6

REVERSE STRAINING AND THE BAUSCHINGER EFFECT

It was reported first by Bauschinger in 1882 that all metals and alloys, after plastic deformation, have a higher yield stress in the direction of the initial deformation than in the reverse direction⁽²¹⁾. This phenomena is of great importance in practice, particularly in cases where designs are based on the yield strength and materials are subjected to reverse deformation.

Although this phenomenon has been recognized for a long time, comparatively little work has been done to define the influence of basic microstructural features on the magnitude of the Bauschinger Effect (BE) in industrially important materials.

Presently, most industrial designs are based on the yield strength of the starting materials prior to forming. This is often due to difficulties in monitoring changes in the yield strength of the components during forming. However, the presence of the BE particularly in microstructurally complex materials, results in marked changes of the yield strength of the materials in each part of the production sequence. Consequently, complete characterization of the BE and an under-

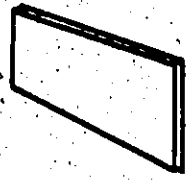

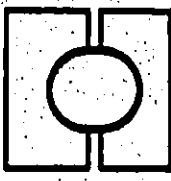

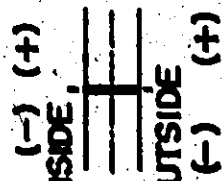
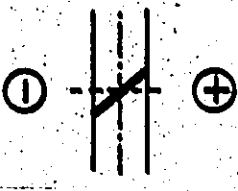
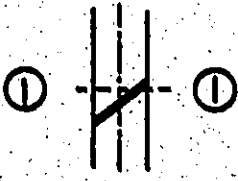
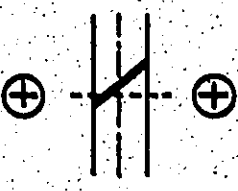
STAGE	A	B	C	D
PROCESS	PLATE 	U - PRESS 	O - PRESS 	EXPANDER 
FORMING	—	BENDING	COM-PRESSION	EXPANDING
STRAIN DISTRIBUTION	(-) (+) INSIDE  OUTSIDE (-) (+)			

Fig. 34.

standing of the microstructural features influencing its magnitude become very important and valuable factors in practice. This has great importance in the fabrication of high strength materials such as in pipe-forming, where any reduction in a Bauschinger loss (the difference in the flow stress in forward and reverse directions of straining) would lead to more efficient designs, better fabricating procedures or changes in methods of material specification.

It is the objective of the present work to investigate some factors that may influence the magnitude of the BE in HSLA steels. The investigation has considered the following problems:

- a) The study of the dependence of the BE on the extent of the forward plastic strain, ϵ_p .
- b) The study of the BE as a function of the direction of straining with respect to the rolling direction, i.e. its relation to the planar anisotropy of the materials.
- c) The study of the BE as a function of the initial sense of deformation (initial straining in tension followed by compression or compression followed by tension).

Quantitative measurements of the BE and its dependence on the variables outlined above have been done on two types of HSLA steels, Molycorp X-80, 5/8" and Ipsco 3/8" in both as-received and annealed conditions.

For clarity of presentation, the discussion is divided

into sections dealing with:

- 1) Theoretical aspects of the BE.
- 2) Factors influencing the BE.
- 3) Methods of measuring the BE.
- 4) Experimental details.
- 5) Experimental results.

1) THEORETICAL ASPECTS OF THE BAUSCHINGER EFFECT

If the direction of straining during plastic deformation of metals and alloys is reversed, some part of the work-hardening, developed in the first mode of straining is lost in the reverse straining, due to the presence of the BE. Generally, the BE is explained in terms of the action of elastic back stresses, developed in the material during inhomogeneous plastic deformation in one direction, or during local phase transformation. These back stresses oppose further deformation in the forward direction but aid it in the reverse direction.

In a plastically deformed matrix containing strong, rigid particles, the particles act as a barrier to dislocations during deformation and dislocation loops are built up around the particles which suffer purely elastic strain. The elastic stress thus produced is, of course, in a sense to help the plastic deformation in a reverse direction.

Brown and Stobbs⁽²²⁾ have produced a model to relate the magnitude of the BE to the scale of the microstructural features such as volume fraction and size of second phase

particles and the magnitude of the prestrain, for two phase materials, with no residual stresses prior to the initial straining. They introduced an image stress which is produced by misfits due to differences in the degree of deformation in the matrix and in the particles. With the assumption that the flow stress consists of three additive components: an Orowan stress (σ_0), a forest hardening stress (σ_{for}) and a back stress (σ_{back}), they predict a flow stress in the form:

$$\sigma = \sigma_0 + \sqrt{3} \alpha \mu V_f^{\frac{1}{2}} \left(\frac{8bc_p}{\pi r} \right)^{\frac{1}{2}} + \alpha \mu V_f \left(\frac{8\pi b}{\alpha^2 \epsilon_p r} \right)^{\frac{1}{2}} \left(\frac{8bc_p}{\pi R} \right)^{\frac{1}{2}} \quad (1)$$

where α is a constant of the order 0.2 - 0.3.

This model provides the most quantitative treatment for the problem of work-hardening in materials with hard spherical particles in a soft matrix. They do not consider the effect of particle shape in their calculations. However, the material often contains complex-shaped particles and residual stresses which also affect the flow process. This is particularly important at small plastic strains.

Following the model of Brown and Stobbs, Ibrahim and Embury⁽²³⁾ developed an approximate model which treats the magnitude of the forward and reverse flow stresses. As measurements of the BE must reflect the magnitude of the back stresses, they attempted to define "a parameter" which involves the back stress. For both single- and two-phase materials, they approximate the forward flow stress σ_F as the linear sum of:

$$\sigma_F = \sigma_0 + \sigma_{for} + \sigma_B \quad (2)$$

where

σ_0 is an initial yield stress (a friction stress in single-phase or an Orowan stress in two-phase materials),

σ_{for} is contribution of the forest hardening, and

σ_B is a back stress due to elastic stresses supported by the obstacles which tend to aid reverse plastic flow.

Assuming that σ_0 and σ_{for} are symmetrical in their action with respect to both forward and reverse deformation, only σ_B is polarized and will act to help reverse flow, so that the reverse yield stress σ_R can be expressed as:

$$\sigma_R = \sigma_0 + \sigma_{for} - \sigma_B \quad (3)$$

From Eqs. (2) and (3) we have:

$$\sigma_F - \sigma_R = 2\sigma_B \quad (4)$$

Dividing both sides of Eq. (4) by the total amount of work-hardening, we get:

$$\frac{\sigma_F - \sigma_R}{\sigma_F - \sigma_0} = \frac{2\sigma_B}{\sigma_F - \sigma_0} \equiv \text{BEP} \quad (5)$$

This expression (5) is then called the Bauschinger Effect Parameter (BEP), which Ibrahim and Embury⁽²³⁾ defined as "the reversible fraction of work-hardening", i.e. twice the fraction of total work-hardening due to the back stress. Hence, the BEP is not a direct indication of the local value of σ_B in the vicinity of some plastic inhomogeneity such as second phase particles, and is only a measure of the fraction of the total work-hardening due to elastic back stress.

Following work by Brown and Stobbs⁽²²⁾, σ_{for} and σ_B could be expressed as:

$$\sigma_{for} = \sqrt{3} \alpha \mu V_f^{\frac{1}{2}} \left(\frac{8b\epsilon_p}{\pi r} \right)^{\frac{1}{2}} \quad (6)$$

$$\sigma_B = \left(\frac{8\pi b}{\epsilon_p r \alpha^2} \right)^{\frac{1}{2}} \alpha \mu V_f \left(\frac{8b\epsilon_p}{\pi r} \right)^{\frac{1}{2}} \quad (7)$$

and

$$\frac{1}{BEP} = \frac{C_1}{V_f^{\frac{1}{2}}} + C_2 \quad (8)$$

$$\frac{\sigma_B}{\sigma_{for}} = C_3 V_f^{\frac{1}{2}} \quad (9)$$

From these equations, the BEP should be independent of the extent of the forward strain, but is dependent on the choice of σ_R and σ_0 parameters. The ratio between the elastic back stress and the forest hardening term is proportional to the square root of the volume fraction of hard particles. These relationships have been investigated by Ibrahim⁽²⁴⁾ for a range of steels and his results are shown in Figures 35 and 36.

In this simple model the BEP is very sensitive to the value of σ_0 used. This is particularly important for materials which show a Stress-Differential effect (S-D). This stress is the occurrence of different initial yield stresses in tension and compression. As reported⁽³³⁾, possible sources of the S-D effect could be the presence of residual stresses caused by;

- a) the expansion that accompanies the austenite to martensite transformation,
- b) thermal gradients during cooling,
- c) deformation at low temperatures.

Based on the data reported in the literature⁽³²⁾, the S-D effect

seems to be greatest for a microstructure consisting of weak ferrite and strong martensite. This is a very important factor for the accurate determination of the BEP in HSLA steels which are usually composed of a mixture of soft and hard phases.

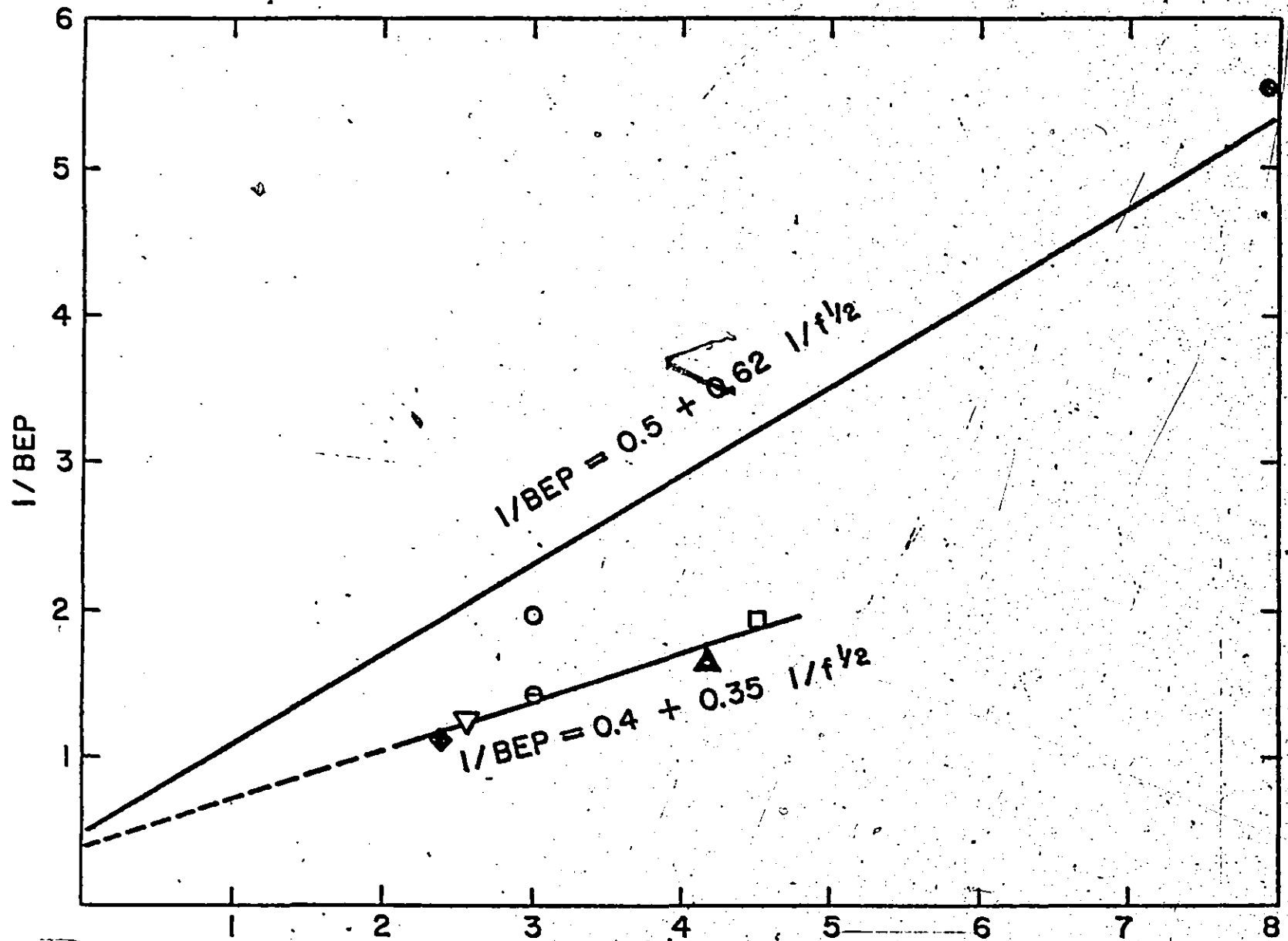


Fig. 35. Relationship between $\frac{1}{BEP}$ and $\frac{1}{f^{1/2}}$ for steels Ref. 24

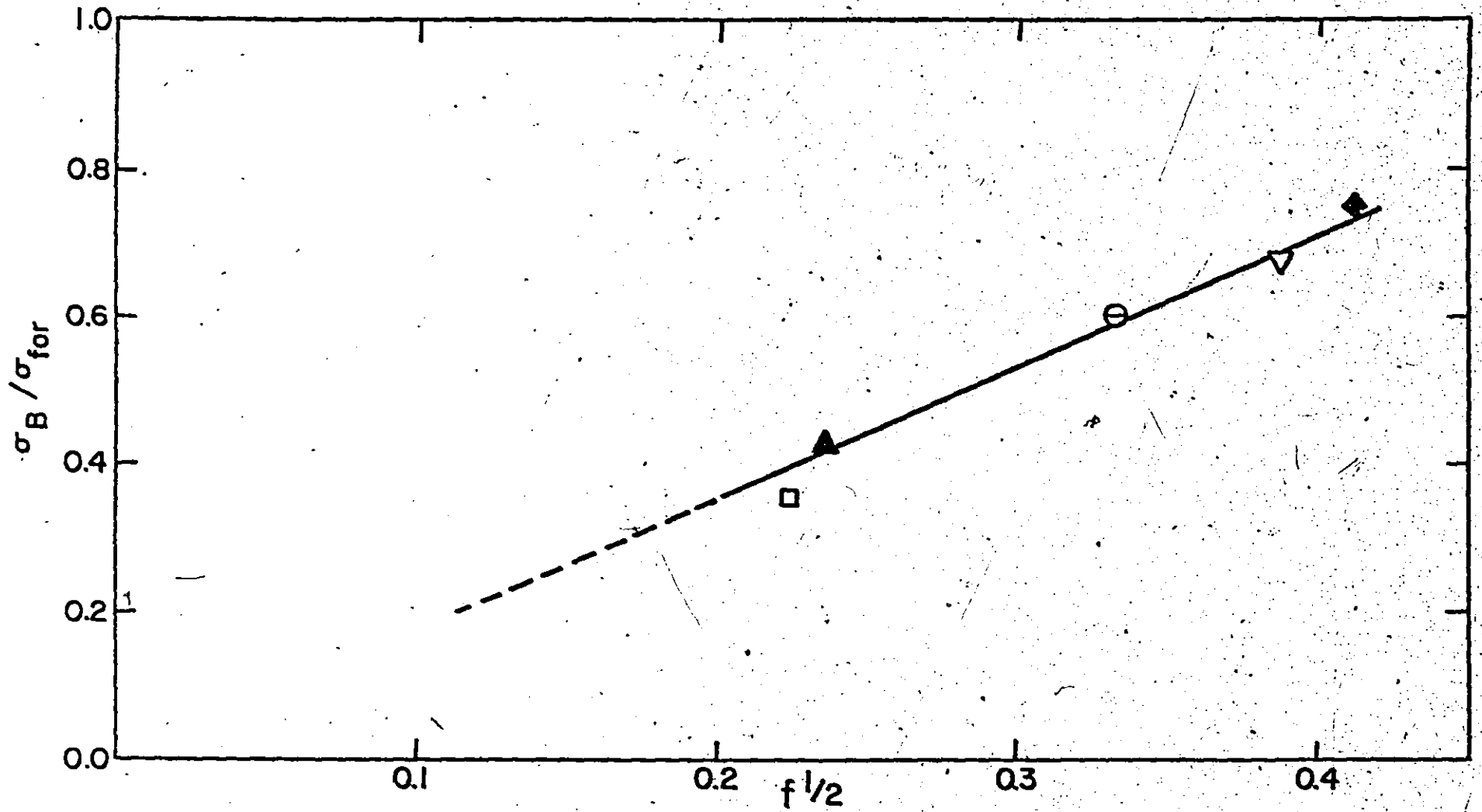


Fig. 36. Relationship between σ_B / σ_{for} and $f^{1/2}$ for various steels. (Ref. 24)

2) FACTORS INFLUENCING THE BAUSCHINGER EFFECT

Several workers^(22,24,25,26) have found that the magnitude of the back stress, and hence the BE, increases with increasing volume fraction of rigid particles. From the data shown in Figure 37, it can be seen that the magnitude of the back stress is directly proportional to the volume fraction of second phase particles, for a given size, shape and prior strain. From the data presented in Figure 35 and Figure 36 for the steels investigated, some observations can be made.

A linear relationship between $\frac{1}{BEP}$ and $\frac{1}{f_p}$ in the form of $\frac{1}{BEP} = C_2 + \frac{C_1}{f_p}$ can be seen for a range of steels. For steels containing spherical particles, Brown and Stobbs⁽²²⁾ predicted values for C_1 and C_2 to be 0.62 and 0.5, respectively, while Ibrahim⁽²⁴⁾ defined $C_1 = 0.35$ and $C_2 = 0.4$ for carbon steels containing nonspherical particles of roughly the same lamellar shape. The results show that materials containing plate-like particles exhibit very high back stress; for example, the cementite lamellar in pearlite steels. An influence of the shape of hard particles on the magnitude of the BEP was investigated in this work for a eutectoid steel (1085) and the results are shown in Figure 38.

Jamieson and Hood⁽²⁷⁾ showed that changes in the grain size do not significantly influence the magnitude of the BE in HSLA steels, as shown in Figure 39.

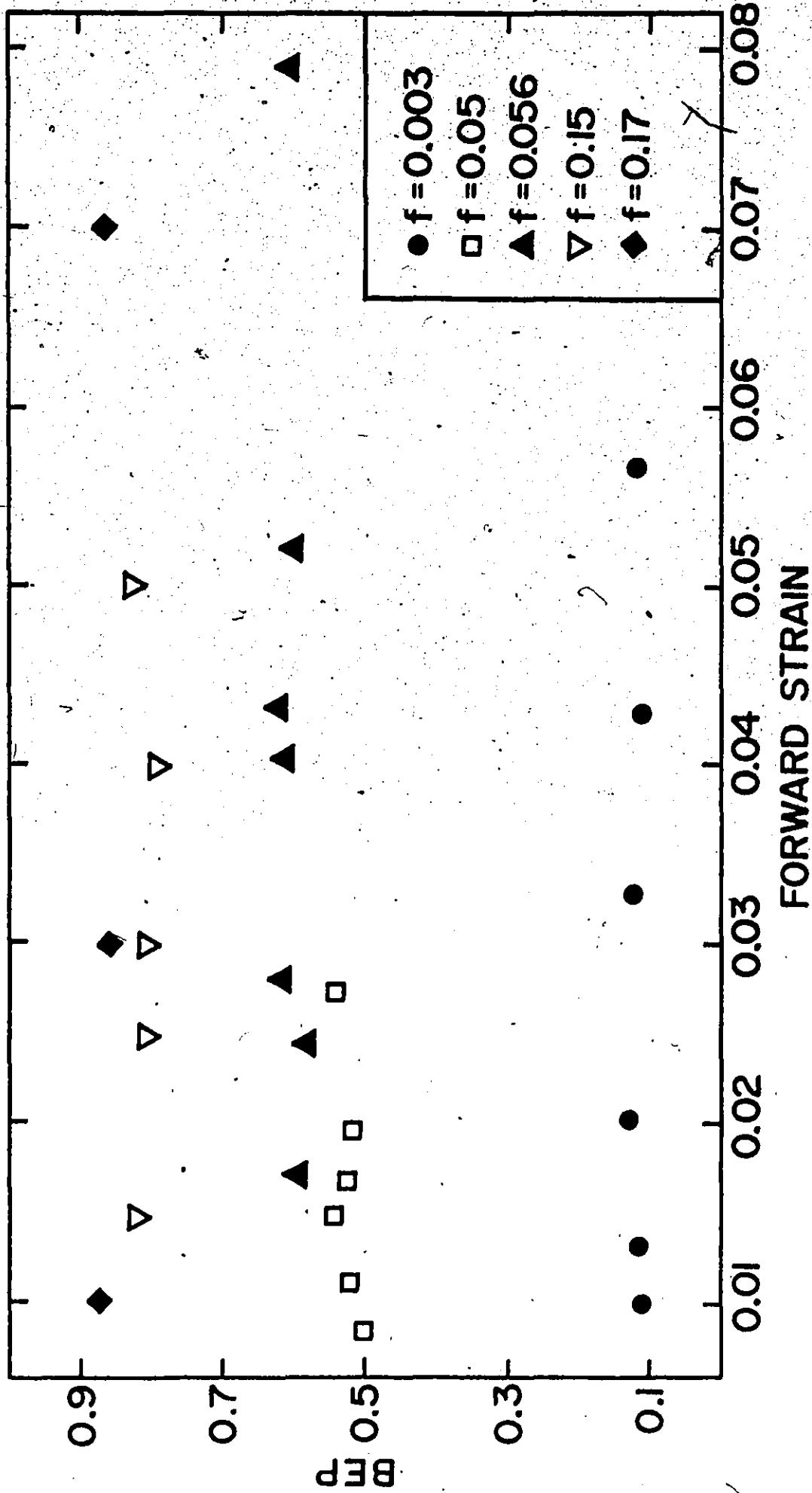


Fig. 37.

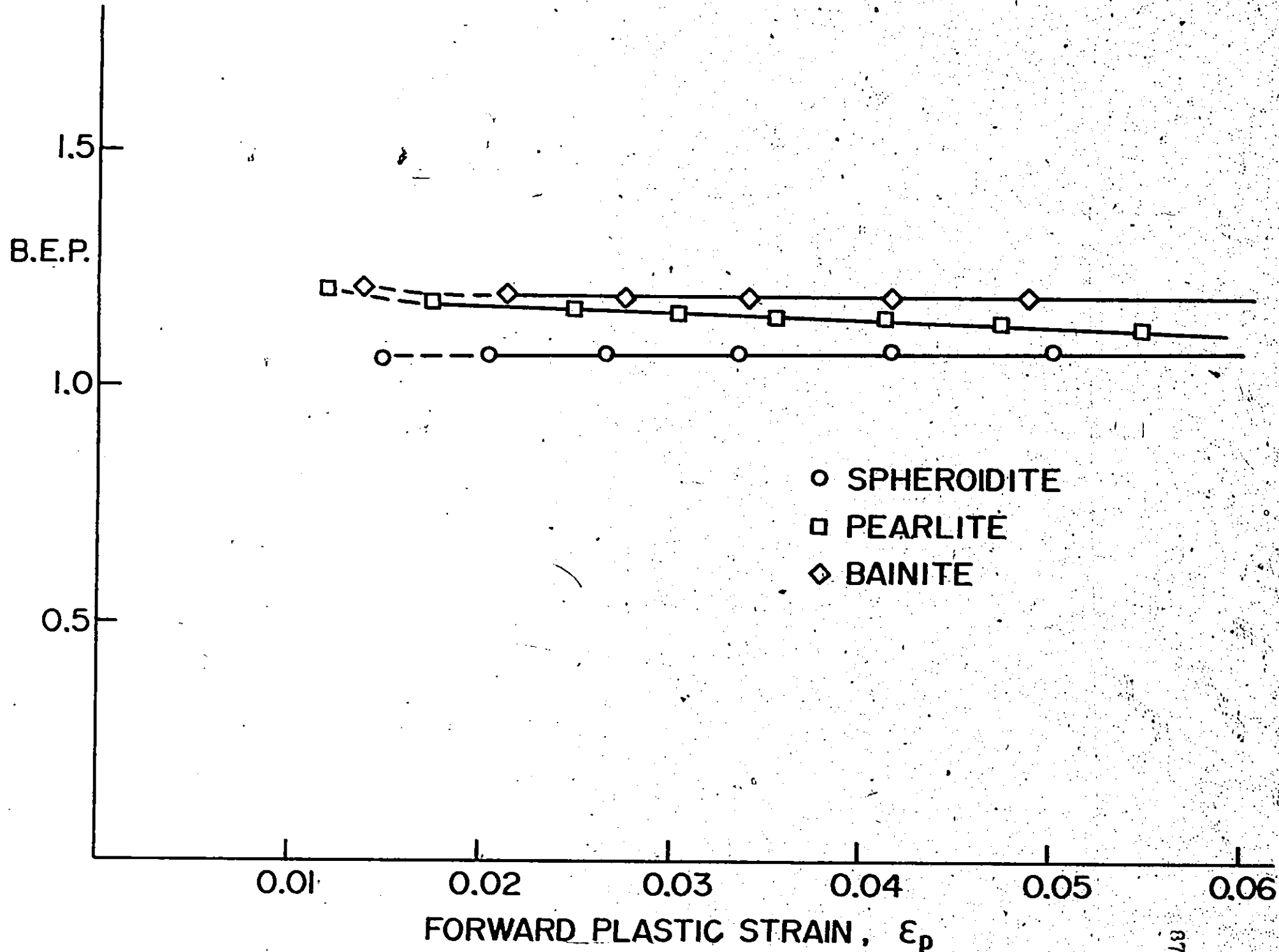


Fig. 38.

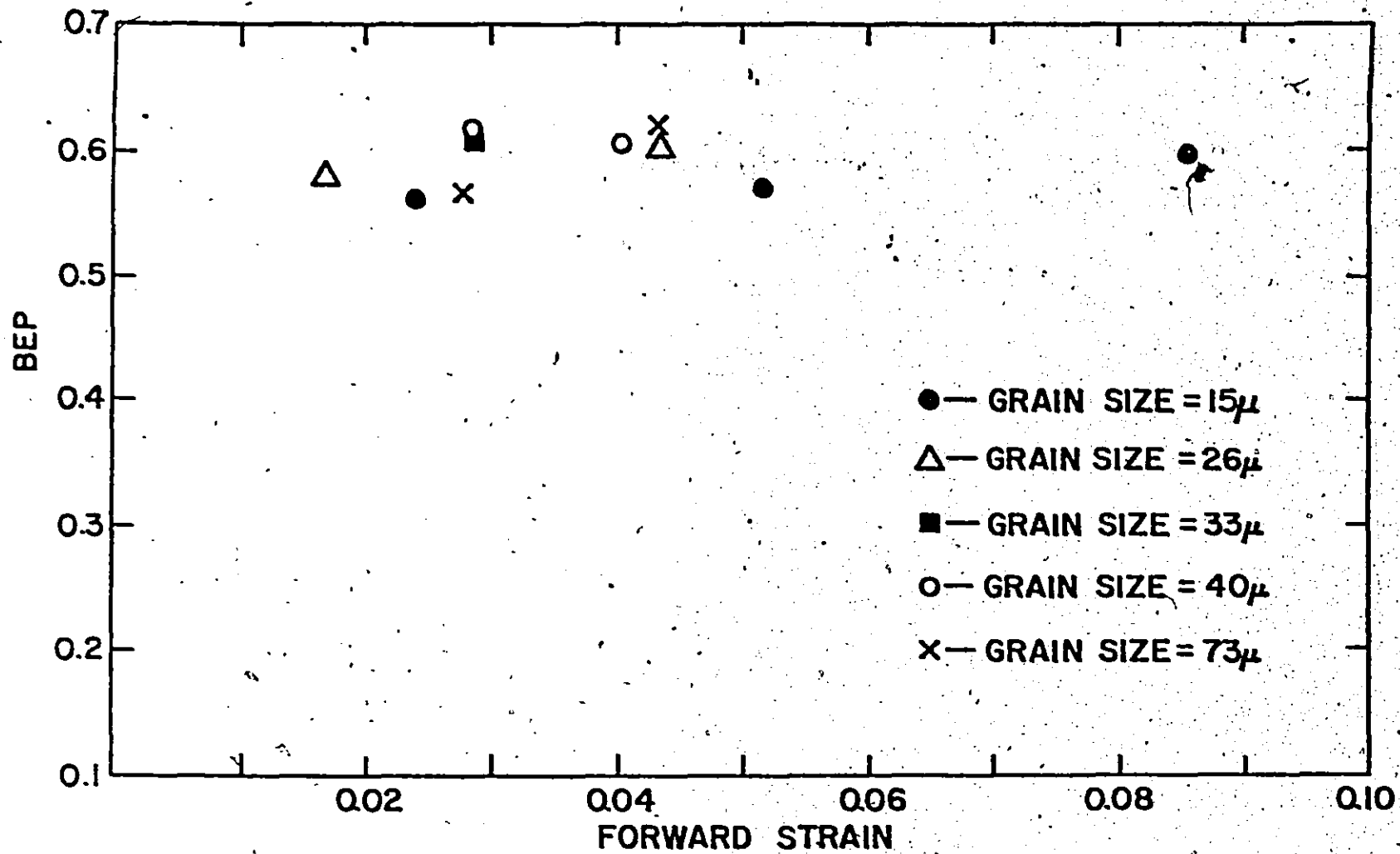


Fig. 39. Effect of grain size on the BEP calculated for the furnace cooled C-Mn steel of Harrison et al. (1972)

3) METHODS OF MEASURING THE BAUSCHINGER EFFECT

A number of authors (28, 29, 30, 23) have proposed methods for describing the BE, such as:

- a) The Bauschinger Stress:-representing the difference between yield stresses in forward and reverse deformation (Polakowski⁽²⁸⁾).
- b) The Bauschinger Strain:-defined as the amount of strain required to raise the stress level in the reverse direction to that of the forward direction (Figure 40) (Buckley and Entwistle⁽²⁹⁾).
- c) The Bauschinger Effect Factor:-in the form $\frac{\tau_F - \tau_R}{\tau_F}$, where τ_F is the flow stress after a certain amount of prestrain, and τ_R is the yield stress in the reverse direction (proposed by Janiche et al.⁽³⁰⁾).
- d) The Bauschinger Effect Parameter:-defined as "the reversible fraction of work-hardening" (proposed by Ibrahim and Embury⁽²³⁾). This parameter will be used throughout my investigation to account for the magnitude of the BE in all the materials studied. Schematic diagram showing the method used to evaluate the BEP is shown in Figure 41.

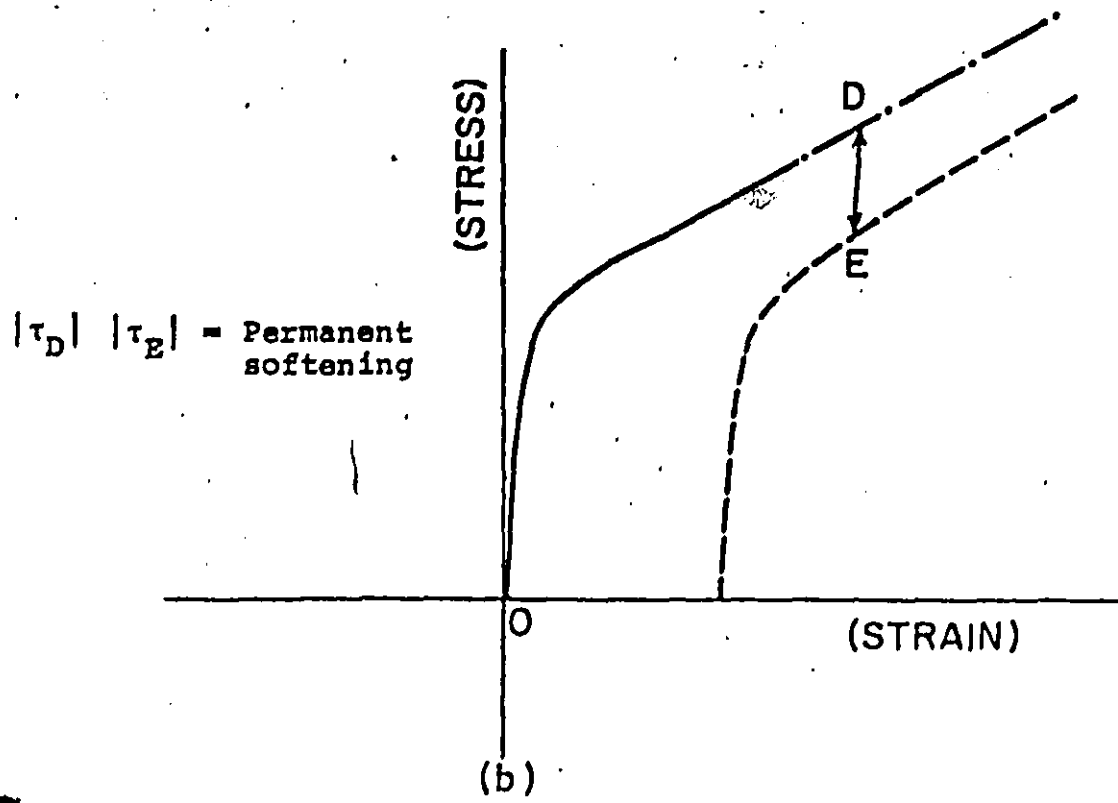
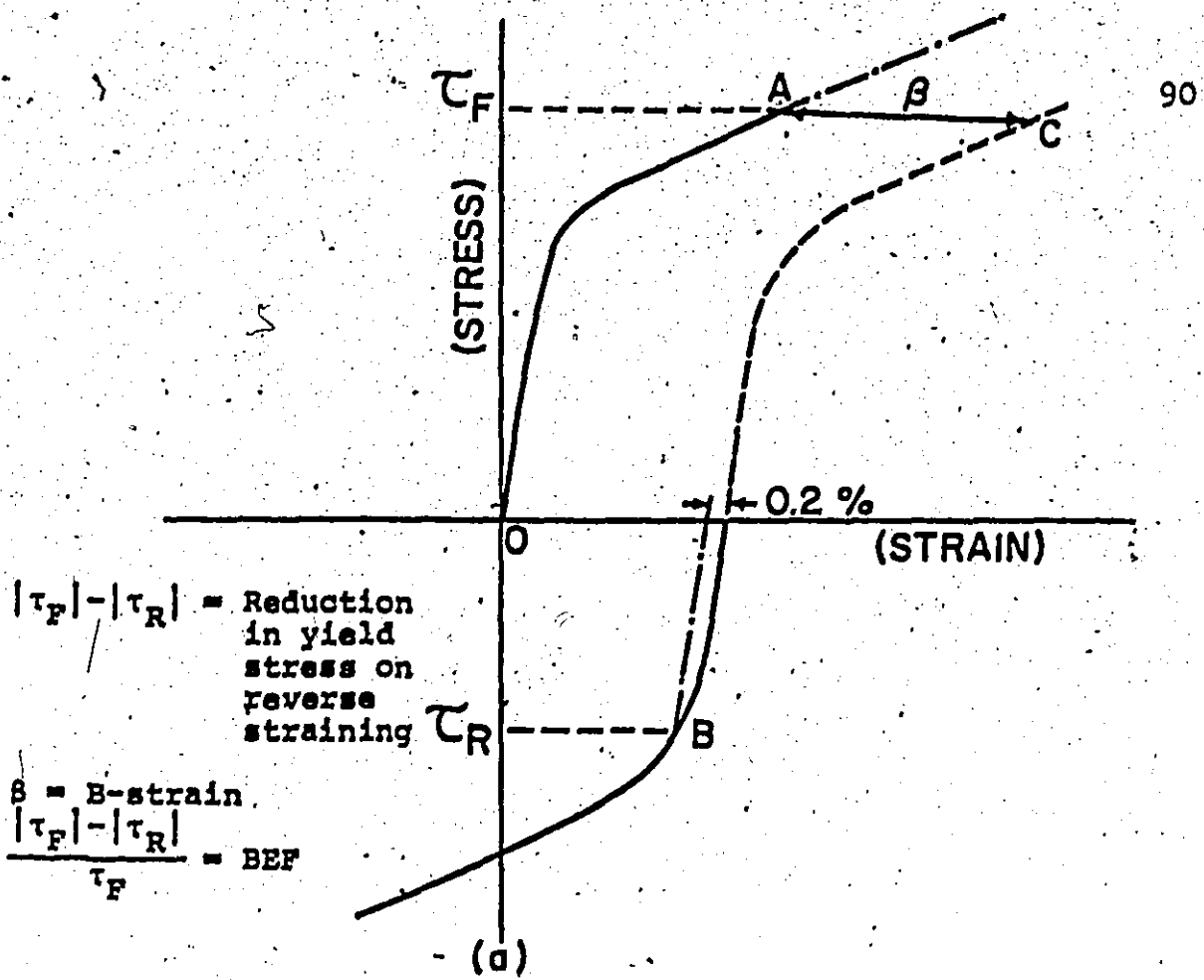


Fig. 40. Schematic illustration of methods commonly used to account for the Bauschinger effect

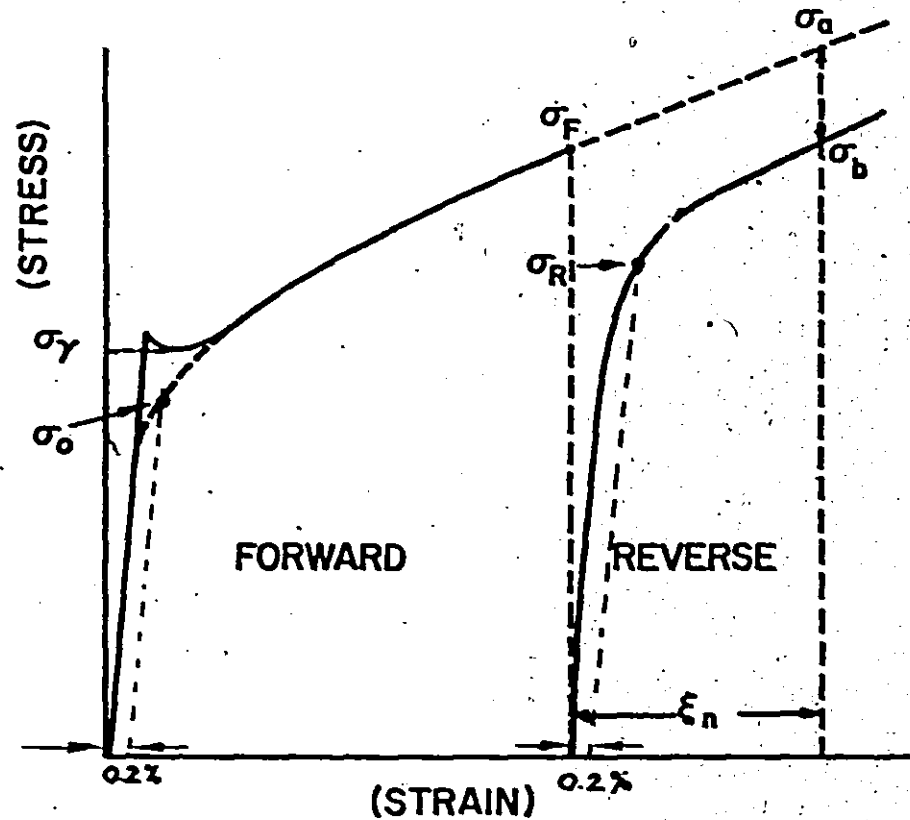


Fig. 41. Schematic diagram showing the method used to evaluate BEP. " σ_0 was estimated by extrapolating the part of the stress-strain curve corresponding to homogeneous deformation back to zero plastic strain using a log-log plot"

4) EXPERIMENTAL DETAILS

a) Materials and Testing Procedure

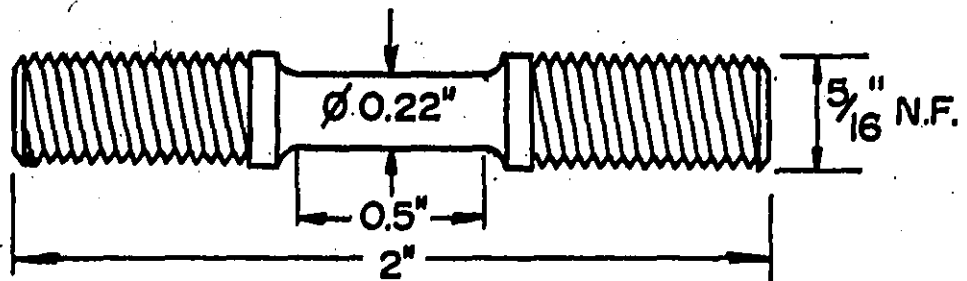
In order to study the effects of prior strain, the direction of straining with respect to the rolling direction, and the initial sense of deformation on the magnitude of the Bauschinger Effect in HSLA steels, specimens of Molycorp X-80, 5/8" and Ipsco 3/8" materials were used in both the as-received and annealed conditions. The chemical compositions and metallography of these materials are presented earlier along with detailed studies of their forming properties and failure mechanisms.

From the central region of the as-received plates, and parallel to specified directions (with respect to the rolling direction) specimens, shown in Figure 42 were machined. In order to eliminate any surface damage due to machining, the specimen surface was polished.

All tests were performed on an Instron tensile testing machine using a rig shown in Figure 43 and designed so that:

- i) the change from tension to compression was smooth, with no delay, and
- ii) the specimen axis could be accurately aligned along the rig axis.

In order to study the effect of prestrain on the BE, a range of strains from 0.005 to 0.07 were used in both tension-compression and compression-tension sequential cycling. The sample was deformed in the forward direction (tension or compression) up to a certain strain, usually starting with 0.005



SCALE 2:1

Fig. 42.

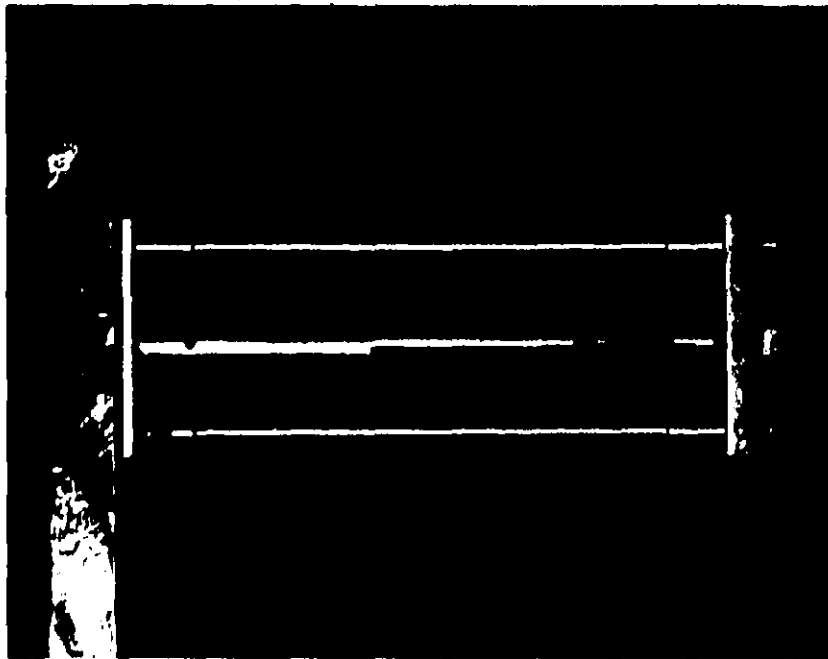
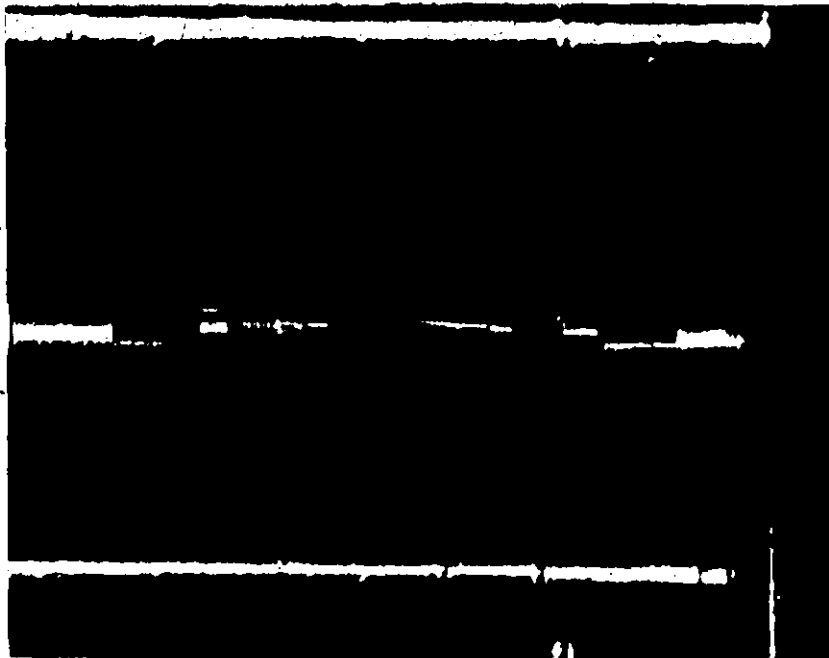


FIG. 43.

strain, and then the direction of straining was reversed (compression or tension). In this process, the sample was strained back from the forward plastic deformation to the zero total plastic strain, completing one BEP loop as shown in Figure 44. In order to reduce the number of samples needed, the same specimen was used to obtain the data for a wide range of pre-strains by sequential cycling through as many as ten loops. It was assumed that taking the sample to zero total plastic strain in each loop, produced a negligible strain hardening, even though some strain accumulation may have occurred. The amount of deformation for each loop was increased by 0.005 strain, approximately.

In order to study the influence of the sense of the initial straining (tension or compression first) on the magnitude of the BE, experiments were performed in both tension-compression and compression-tension cycles.

Also, an attempt was made to study the effect of the direction of straining with respect to the rolling direction. For this reason, specimens were taken from the plate, oriented at 0° , to 5° and 90° to the rolling direction.

All the tests were conducted at room temperature and at a crosshead speed at 0.05 in/min.

The geometry of the samples is shown in Figure 42 and all the specimens were taken approximately from the middle of the plate. The specimen dimensions were chosen to avoid buckling during compression. Strain was measured using an Intstron 1/2" strain gauge, fitted with special arms to have 1/4" gauge.

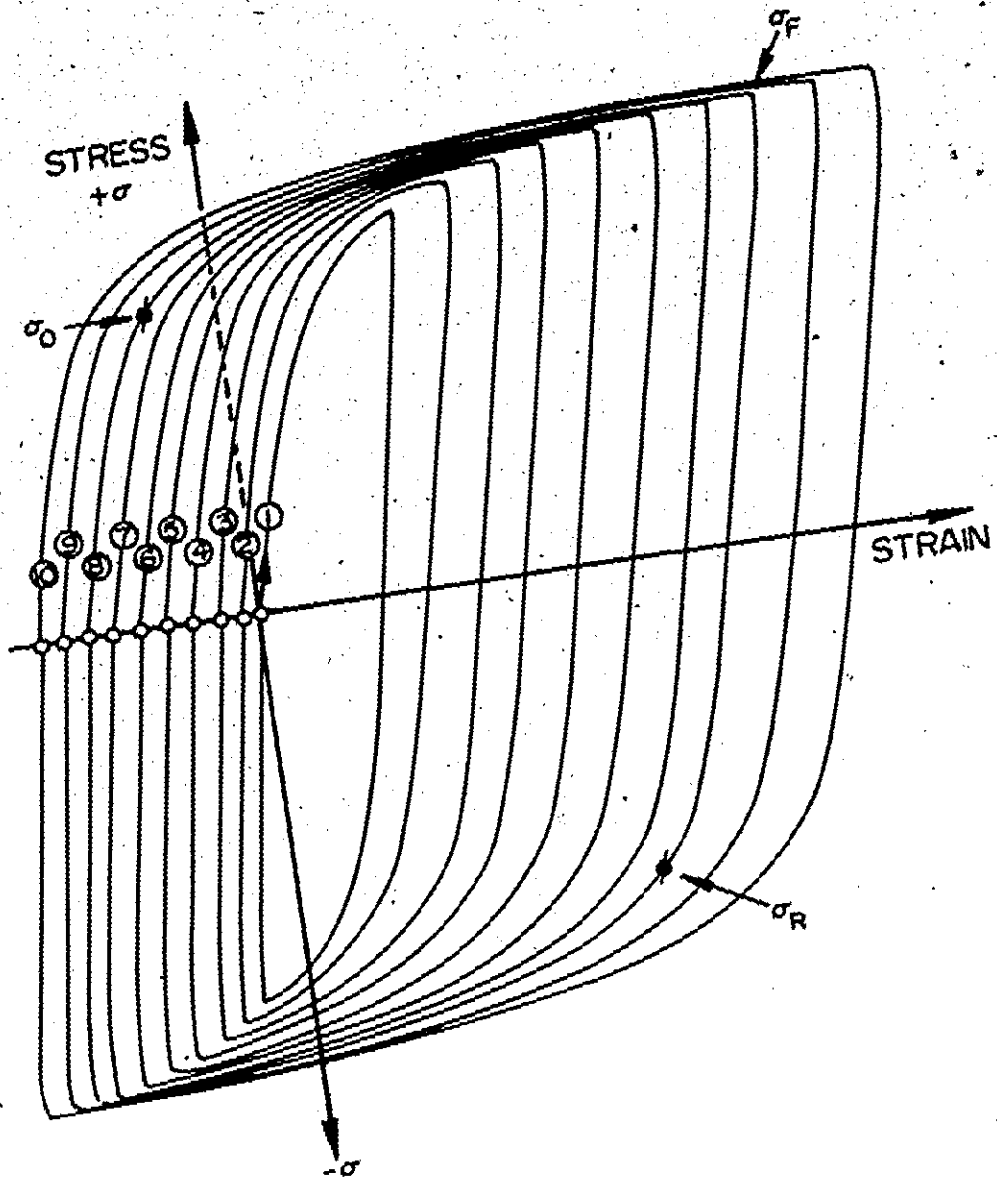


Figure 44.

b) Methods of Measuring σ_0 and σ_R

Having analyzed the factors involved in the BEP equation, it was clear that the reproducibility of the BEP data depended critically on the accuracy and consistency of measurements of the parameters σ_0 and σ_R . This requirement for a consistent definition of σ_0 and σ_R was particularly important in the comparison of test results of the different materials and conditions, each of which showed characteristic tensile stress-strain flow curves at the point of initial yielding. For instance, some materials showed continuous yielding with a highly rounded tensile flow curve. In this case, a small variation in strain caused a large difference in the measured flow stress. Other materials or test conditions clearly showed discontinuous yielding.

In order to circumvent this problem, for the determination of the yield stress, σ_0 , in forward flow, the tensile load-elongation curves were observed to fall into three distinct categories, namely;

- (i) an initial discontinuous plastic yielding;
- (ii) a prior elastic loading path followed by continuous yielding, and
- (iii) a curve with little or no elastic portion followed by continuous yielding.

For discontinuous yielding, the true stress-true strain curve was first completely plotted for the region of homogeneous plastic deformation. Then, this curve was extrapolated to zero plastic strain. The 0.2% offset stress was then obtained in the usual way. In the second case where plastic flow immediately followed a prior elastic path with no

observed discontinuity; it was possible to measure the 0.2% offset stress directly. In the final case, the required offset stress was extrapolated from a logarithmic plot of true stress-true strain data.

The measurement of the reverse yield stress σ_R was comparatively easier as the reverse flow curves all showed the behaviour previously characterized under case (ii) in the discussion above. However, all the reverse curves also showed some level of micro yielding of the order of 0.1% or less. Micro yielding has been attributed to the previously bowed and bent dislocations straightening out under the action of their own line tension and the applied reverse load. The offset stress was measured as in case (ii) above.

At this stage, it should be pointed out that for a consistent evaluation of the BEP equation, both σ_R and σ_0 should be computed from the same value of offset plastic strain. It is clear that the deformation in the reverse direction immediately after the prestrain in the forward direction can only show the net effect of both forward and reverse straining. As the reverse strain increases, the back stress produced during forward straining, decreases to zero and a new back stress is developed in a sense to oppose continued reverse deformation. Thus, if the BEP is evaluated using respectively different offset strains for σ_R and σ_0 , the established independence of the BEP with respect to the pre-strain is lost, particularly in the small pre-strain regime. This point is illustrated in Figure 44(a) from test results of Molycorp X-80, 5/8" plate. In each case, σ_0 is consistently evaluated as 0.2% offset

stress while σ_R is computed as 0.1, 0.2, 0.5 and 1.0% offset stress. Clearly, if for instance, σ_R and σ_0 are both evaluated as 0.5% offset stress, the independence of BEP of pre-strain as predicted by the equation $1/\text{BEP} = C_1 + C_2 f^{-1/2}$ once again returns.

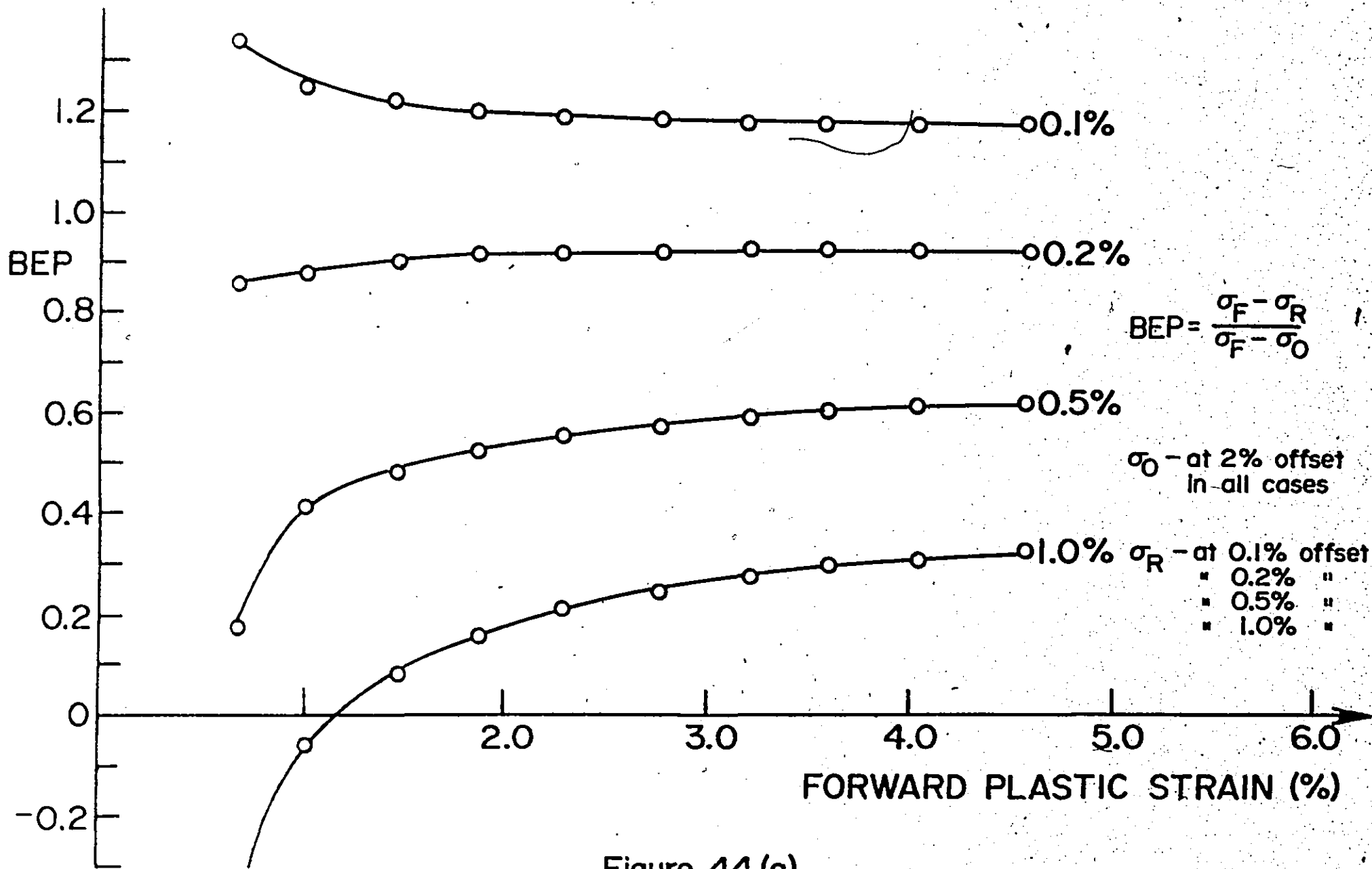


Figure 44 (a)

5) EXPERIMENTAL RESULTS

As stated earlier, the studies of reverse flow and the BE were performed on two HSLA steels, Molycorp X-80, 5/8" and Ipsco 3/8", in both the as-received and annealed conditions. Annealing experiment was conducted on finally prepared specimens in an evacuated glass tube at 550°C for 1 hour. The samples were deformed to a prestrain, followed by reverse straining as explained in the previous section. Using the data from each BEP loop, the magnitudes of the BEP were calculated. The results obtained are presented in Figures 45 to 56, which show the BEP versus forward plastic strain, ϵ_p .

The Figures show that the BEP is essentially independent of the extent of the forward plastic strain, for both types of HSLA steels and in both the as-received and annealed conditions. In general the magnitudes of the BEP for the tested materials are found to be in the order of 1 or more, showing that according to the proposed model⁽²³⁾, approximately one-half of the work-hardening in the forward deformation is involved in building up the back stress on the hard, rigid particles. Such a high magnitude of the BEP is not expected for the material containing a relatively small volume fraction of hard phases. According to the optical micrographs of these materials, for Molycorp X-80, 5/8", the volume fraction of non-ferritic phases is of the order of 0.13 - 0.15, while the measured volume fraction of these phases in Ipsco 3/8" is even lower, of the order of 0.07 - 0.10. Applying the relationship between the BEP and the volume fraction of non-ferritic phases

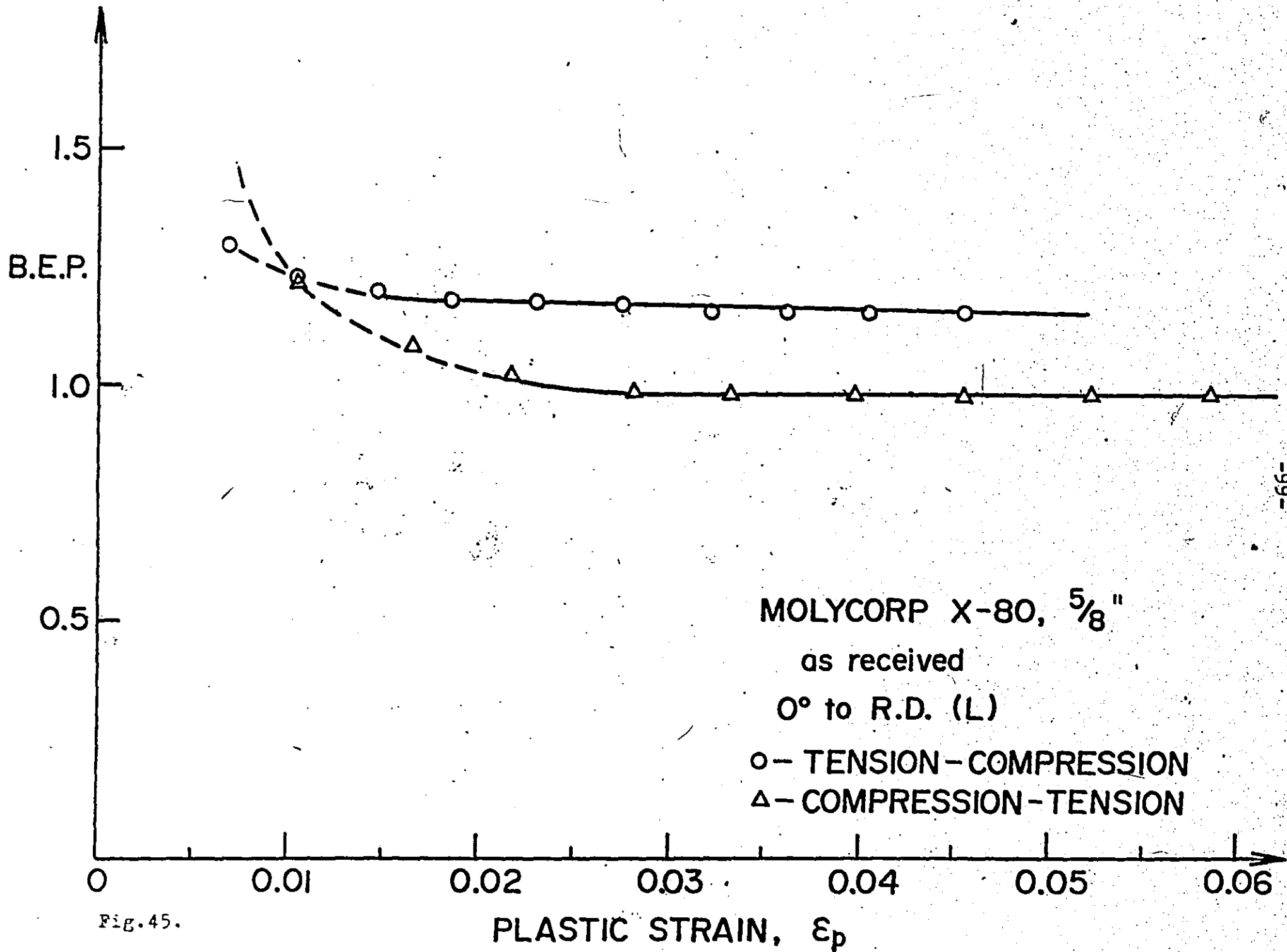


Fig.45.

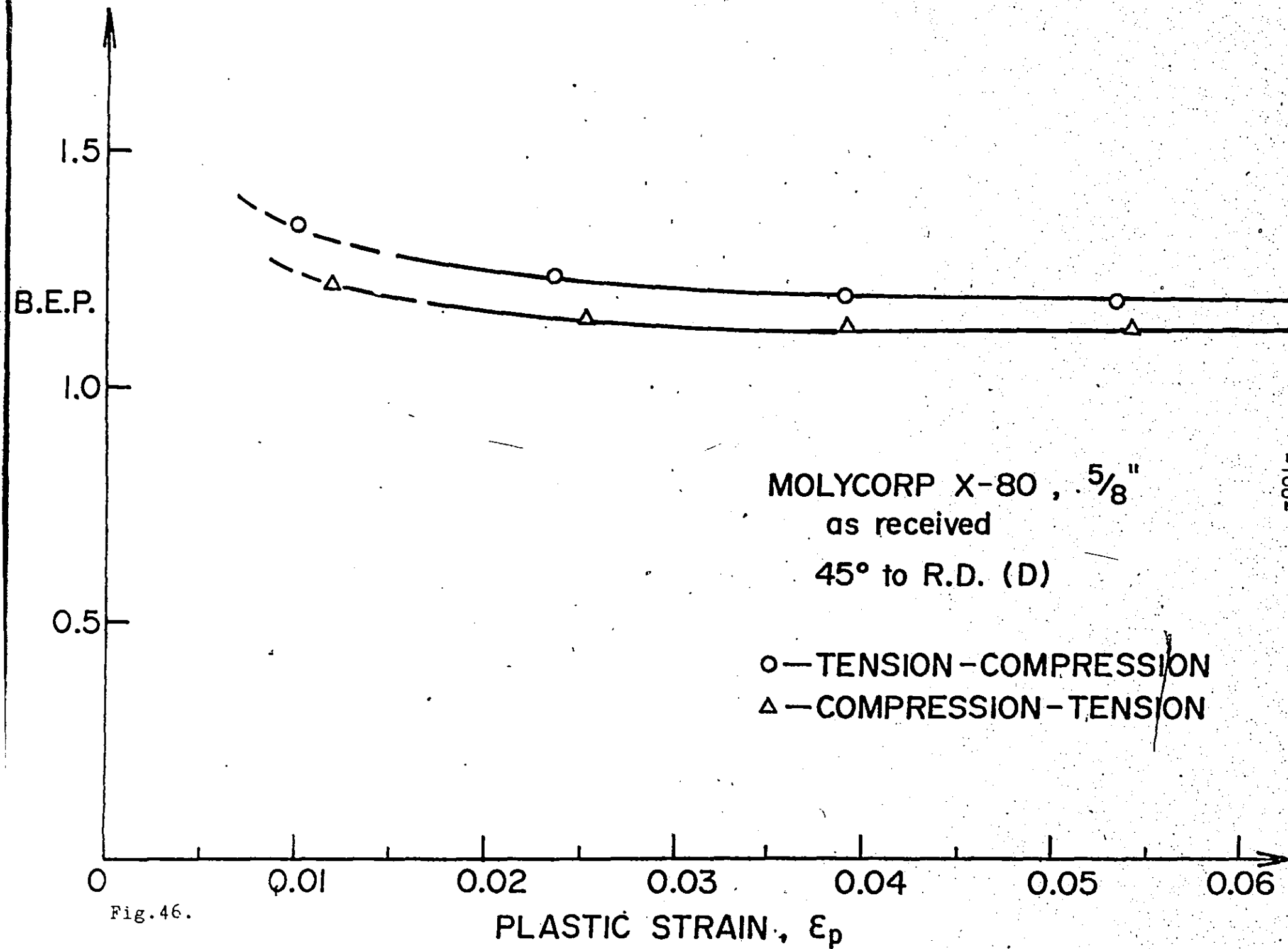


Fig. 46.

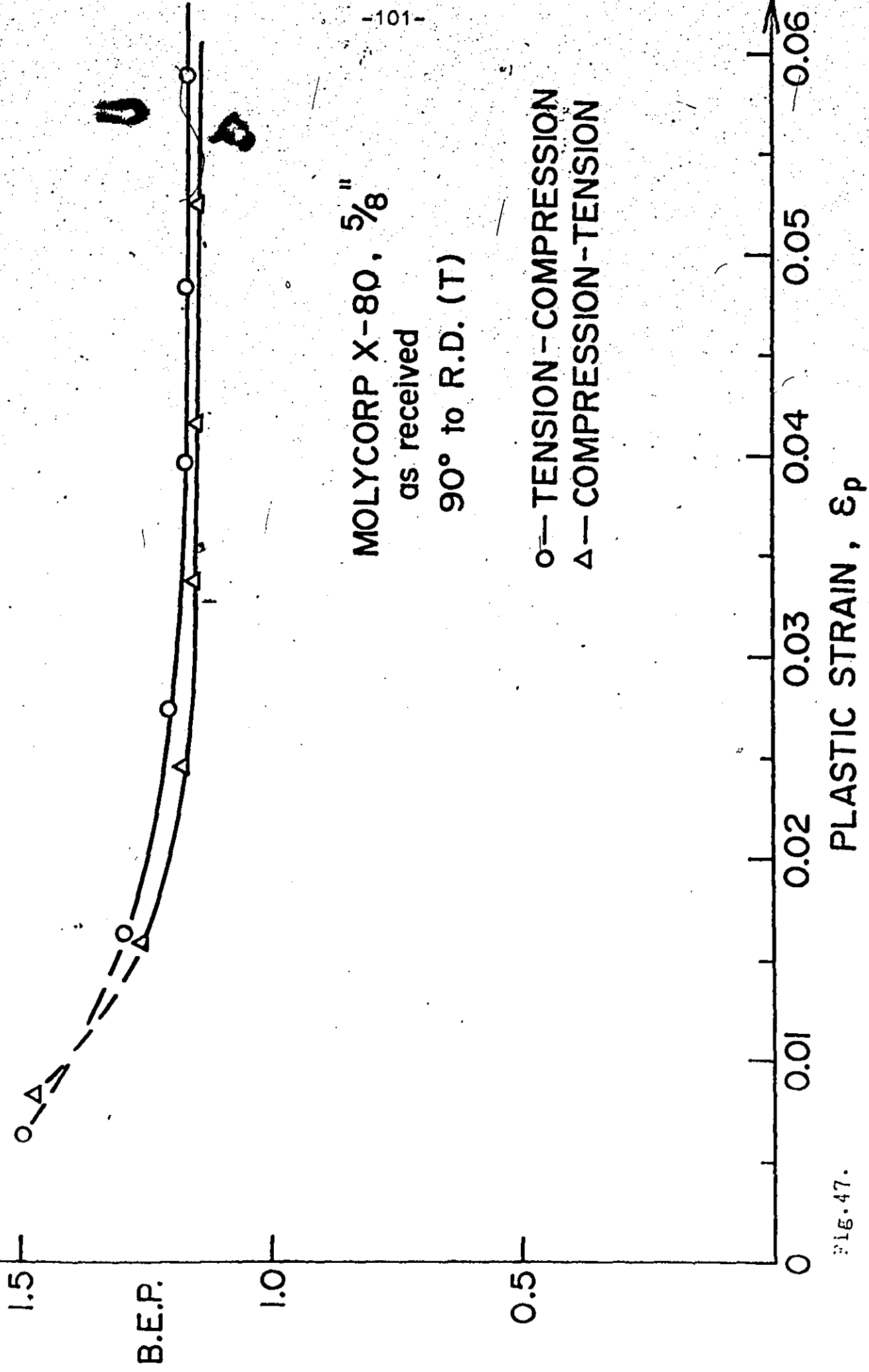


FIG. 47.

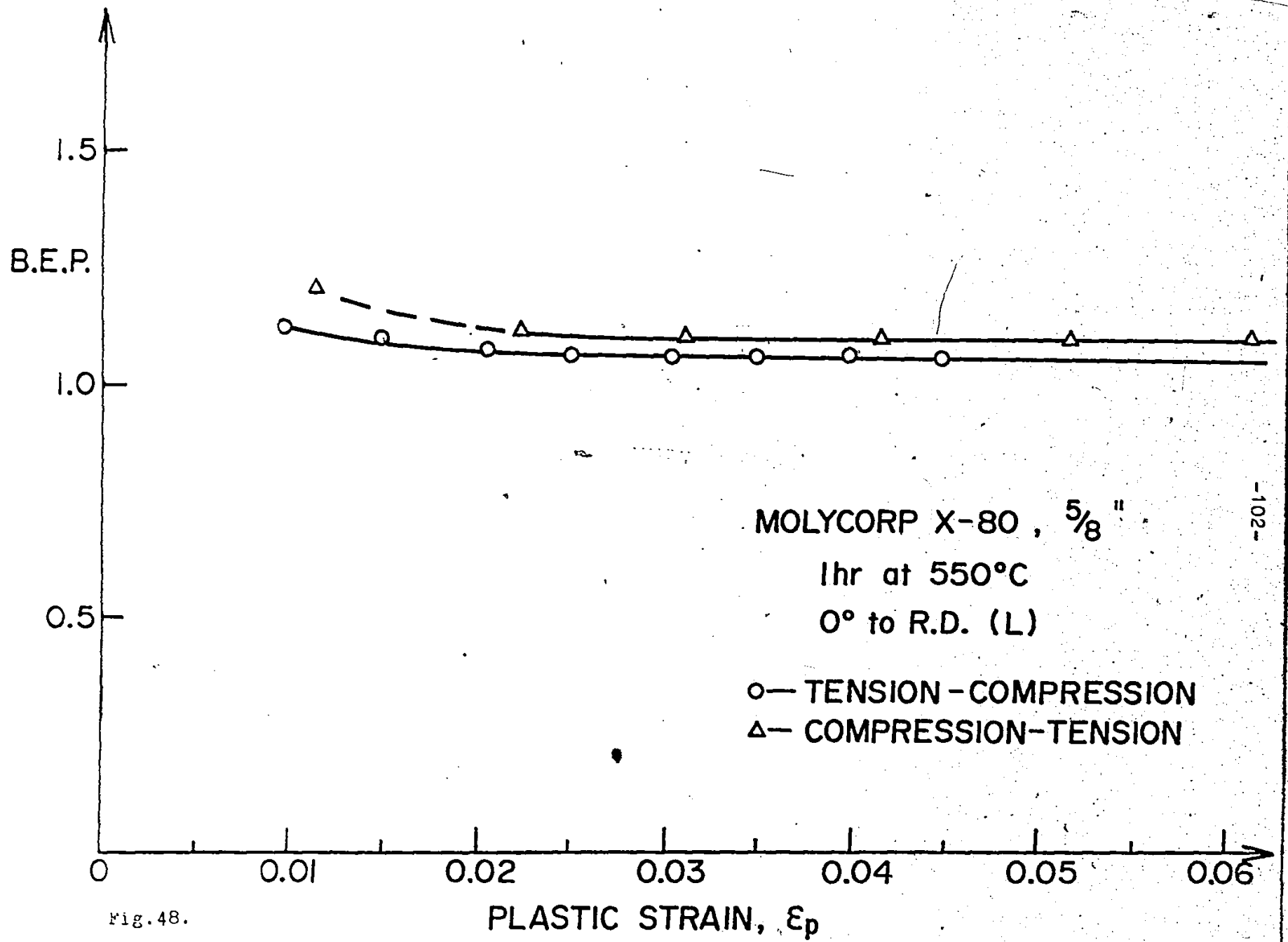


Fig. 48.

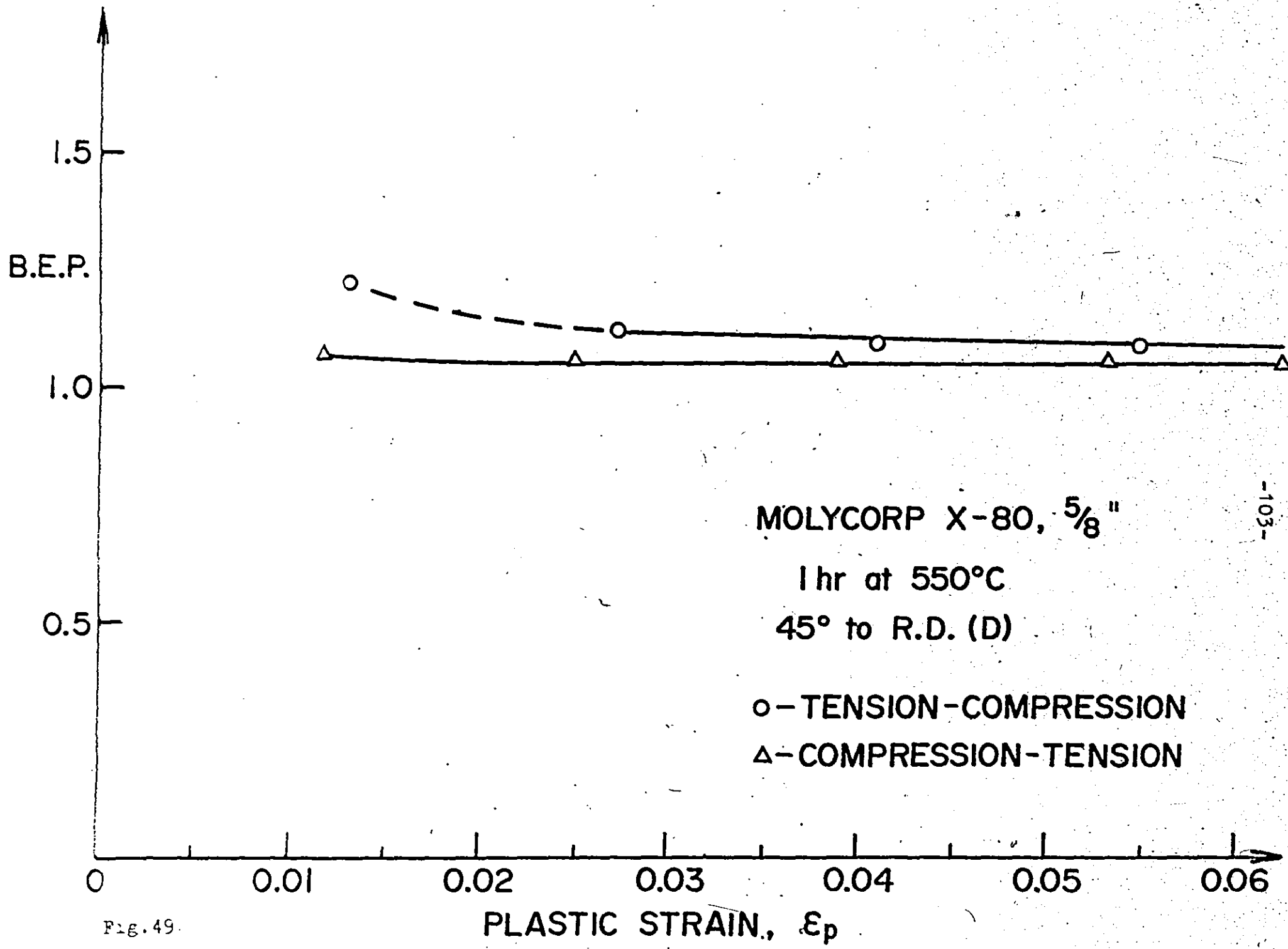


Fig. 49.

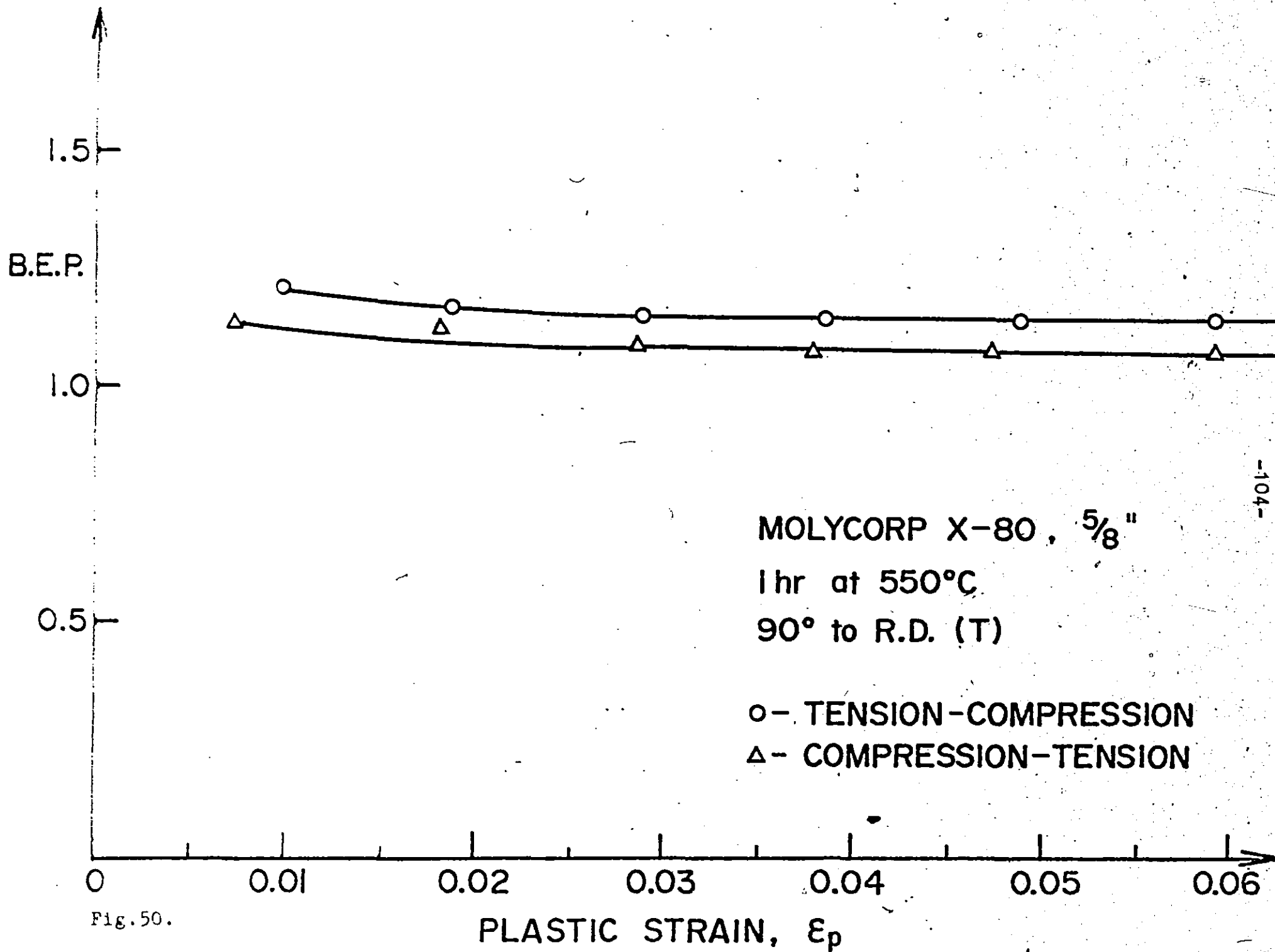


Fig. 50.

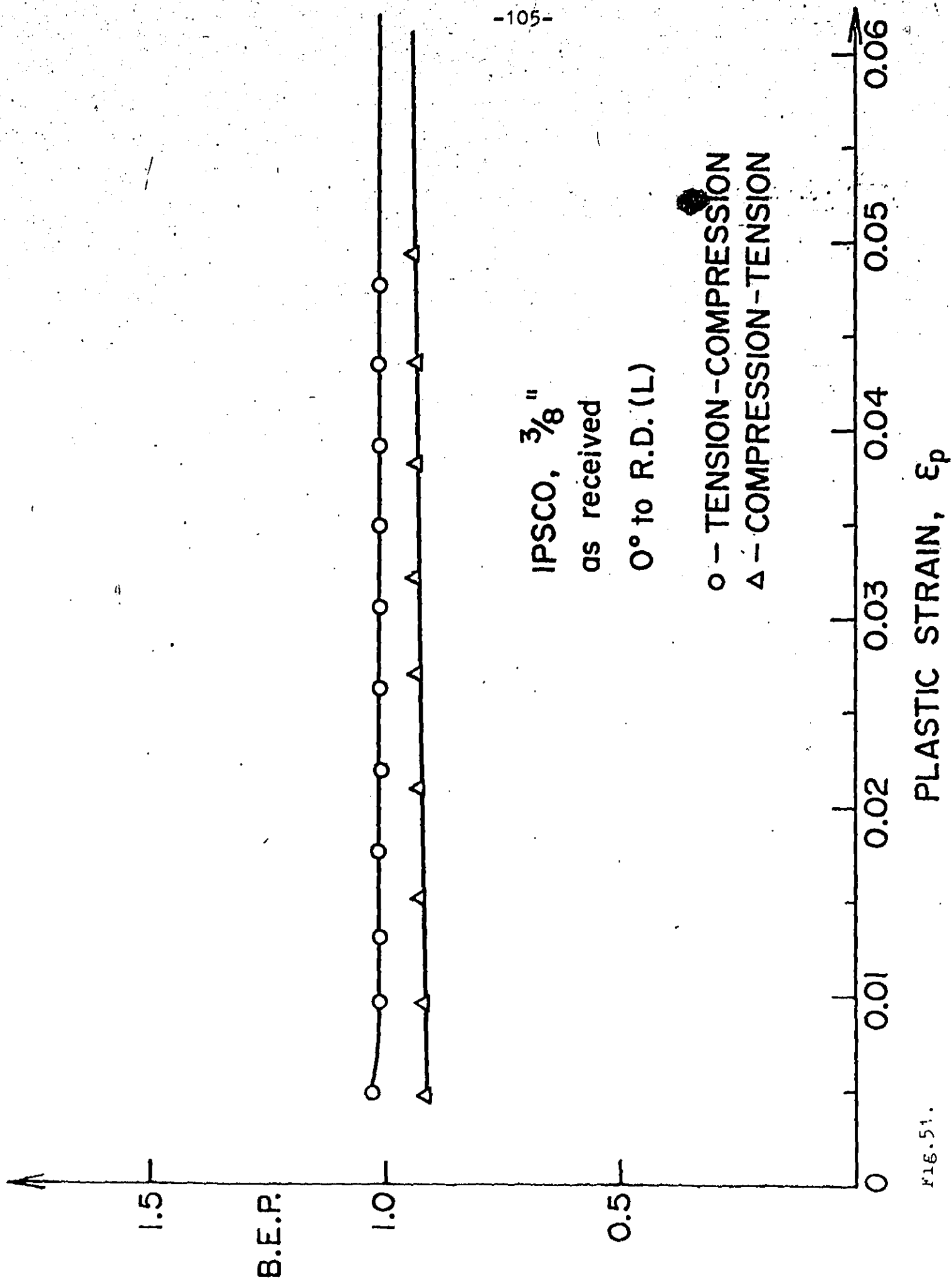


FIG. 51.

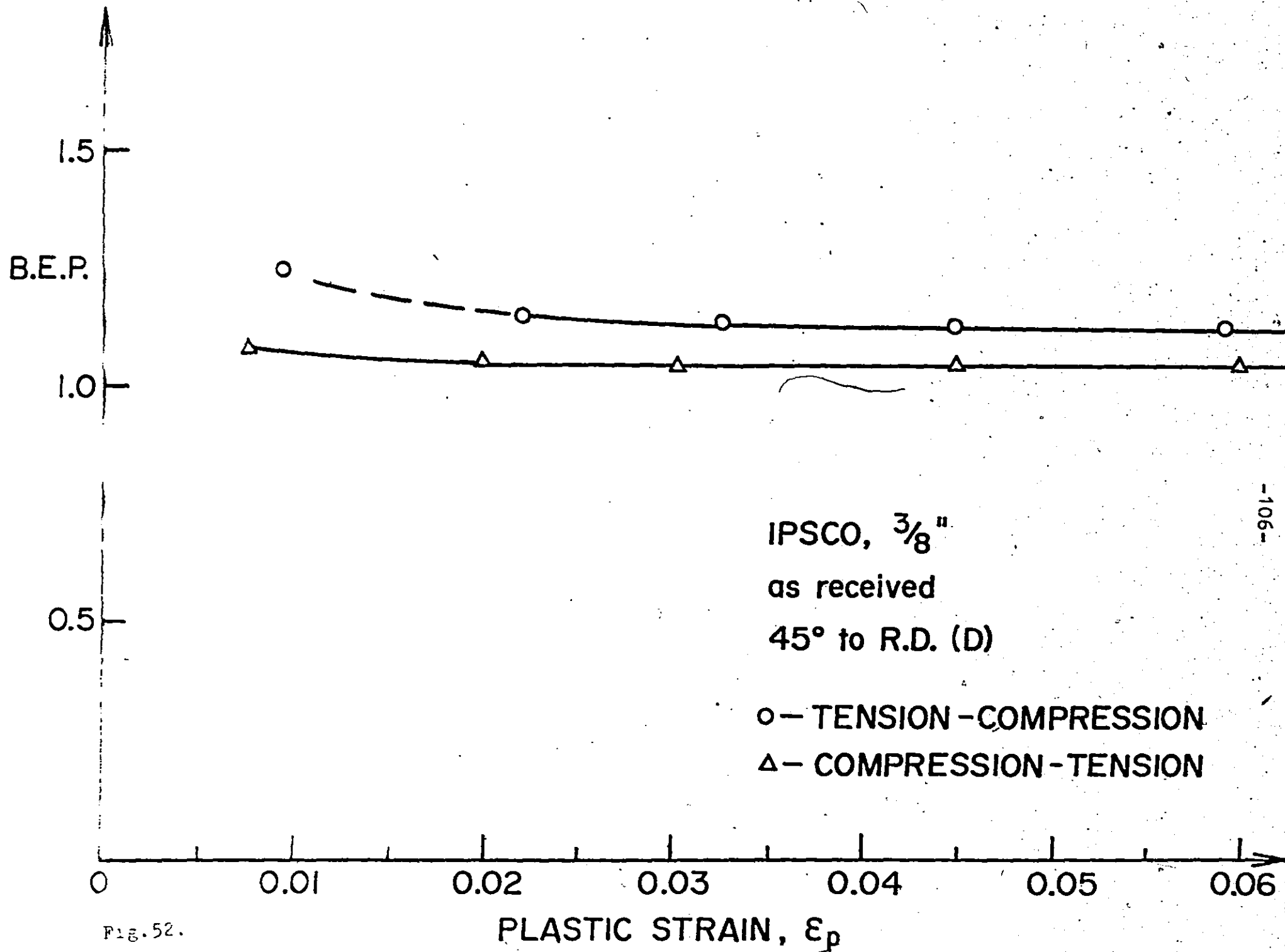


Fig. 52.

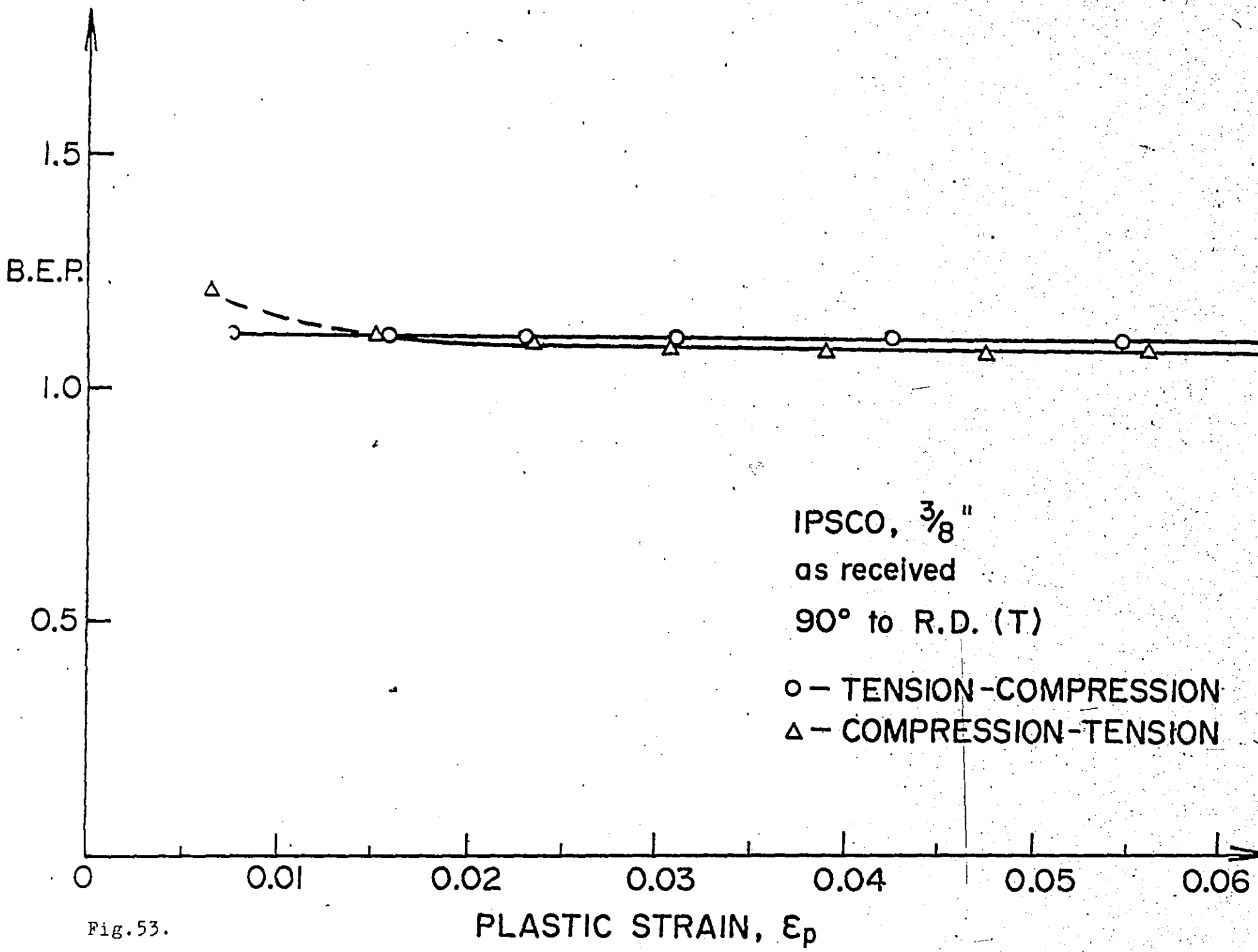


Fig. 53.

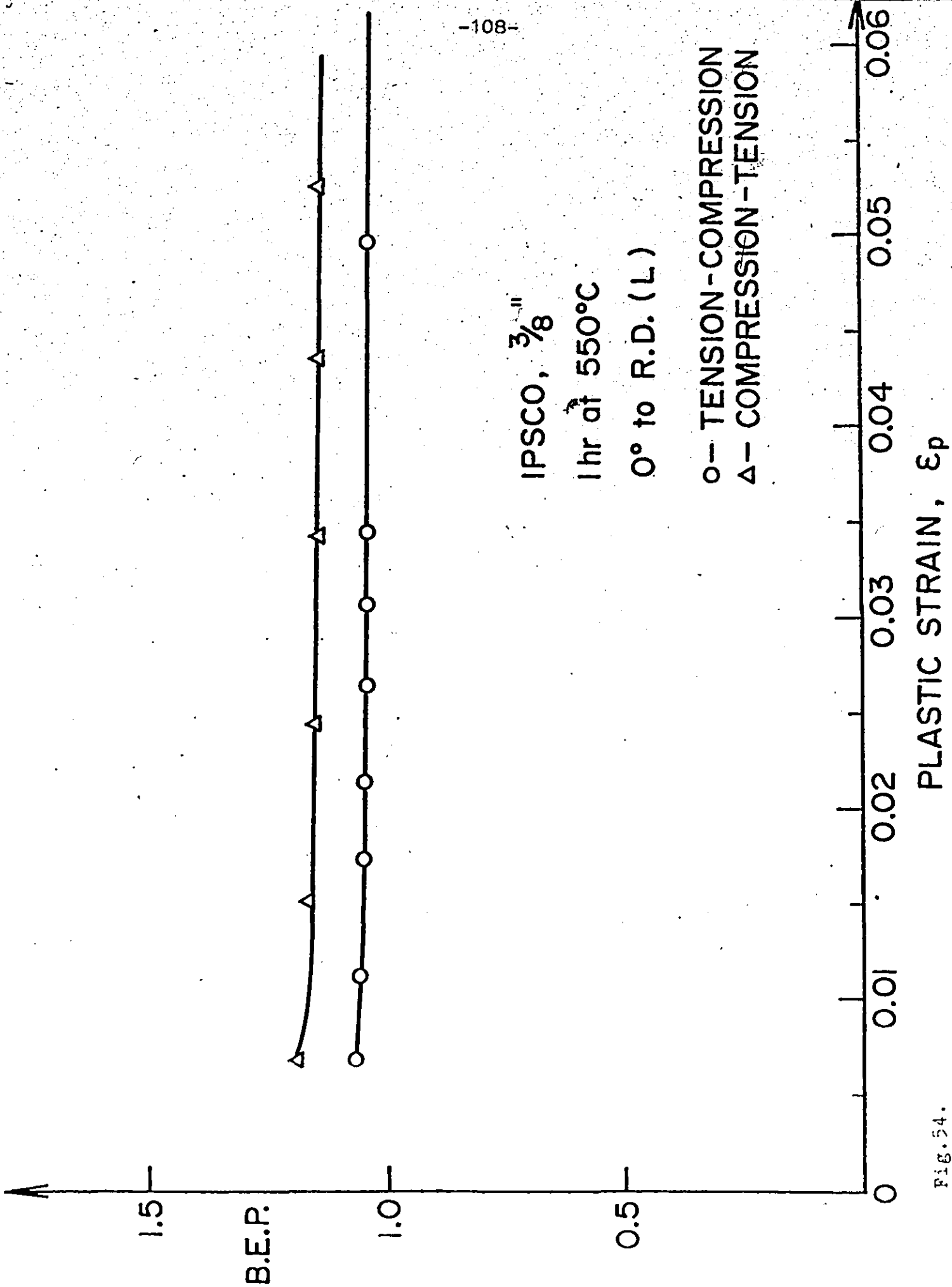


FIG. 54.

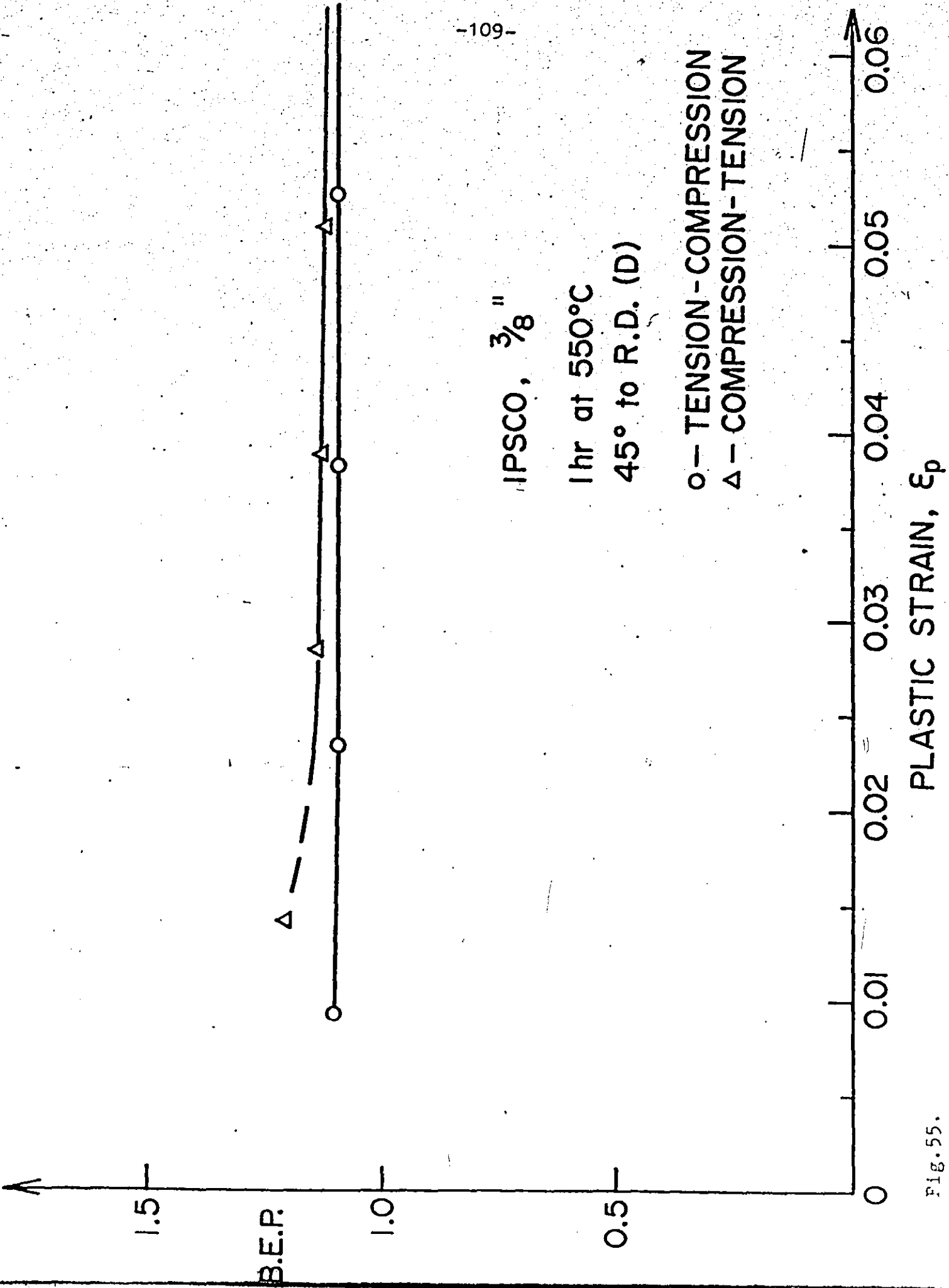


Fig. 55.

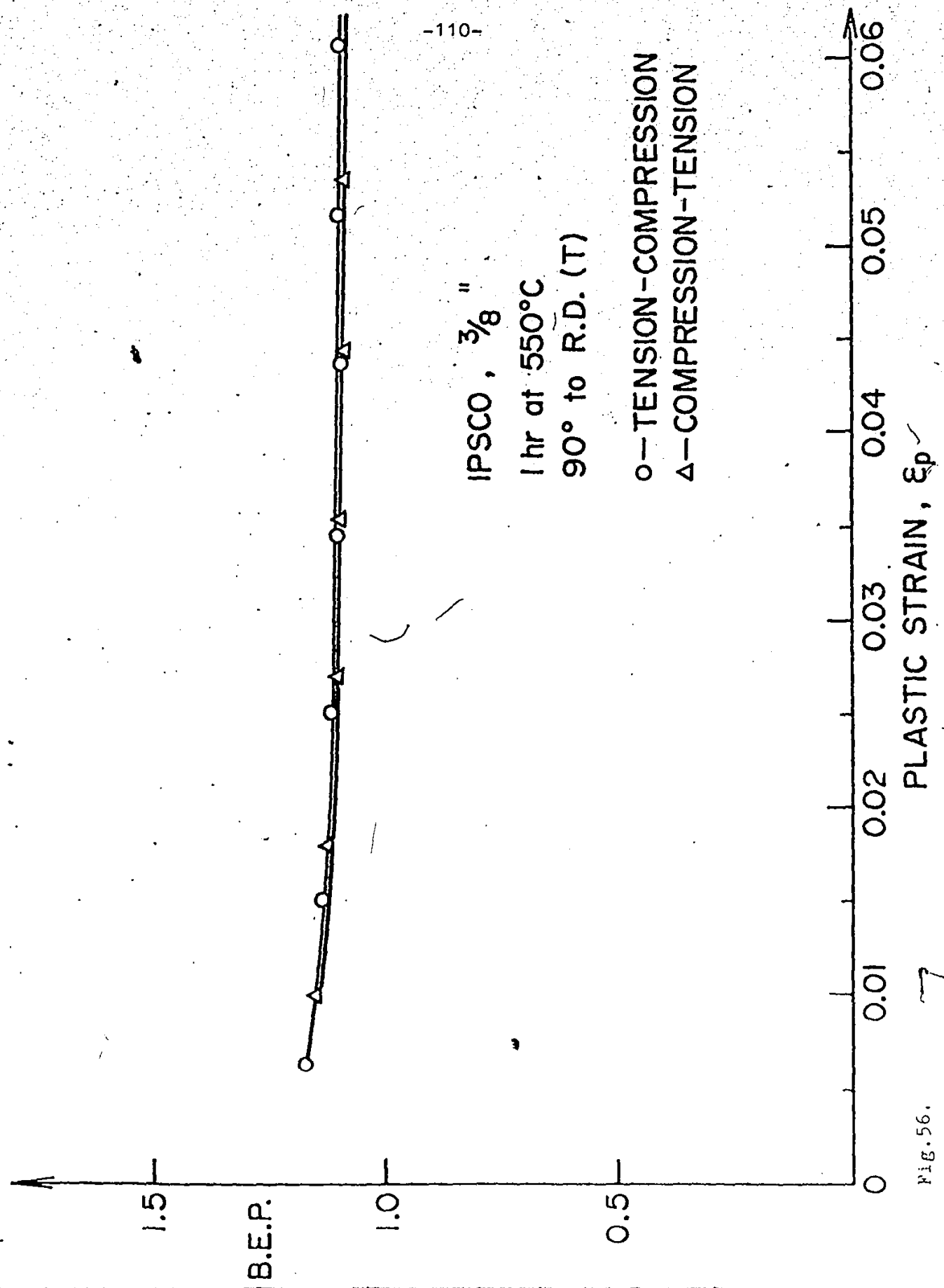


FIG. 56.

for a range of steels presented by Ibrahim⁽²⁴⁾, Figure 35 for these volume fractions, the expected magnitudes of the BEP are much smaller. This fact shows that a simple relationship between the BEP and volume fraction of second phase particles found for a wide range of carbon steels cannot be simply applied for HSLA steels systems. Using data obtained in this study for these two HSLA steels, a new relationship between these factors is found to be

$$\frac{1}{\text{BEP}} = 0.3 + 0.27 \frac{1}{f^2} \quad (10)$$

and is represented in Figure 57.

From existing data shown in Figure 57 it can be seen that the magnitude of the BEP is increasing as the shape of the second-phase particles becomes more complex. This indicates that the effective shape of the non-ferritic phases in HSLA steels is very complicated with complex stress fields around the particles. Also, the unexpected high values of the BEP in materials with relatively small measured volume fractions of non-ferritic phases lead us to the conclusion that the volume fractions measured by optical microscopy are not the effective volume fractions.

Besides the small precipitates not measurable optically, the measured volume fraction could be increased by residual stress fields in the vicinity of the particles. This seems particularly important for Molycorp X-80, 5/8" where the M/A constituent with residual stresses in its vicinity was documented in previous chapters. Residual stresses in the mater

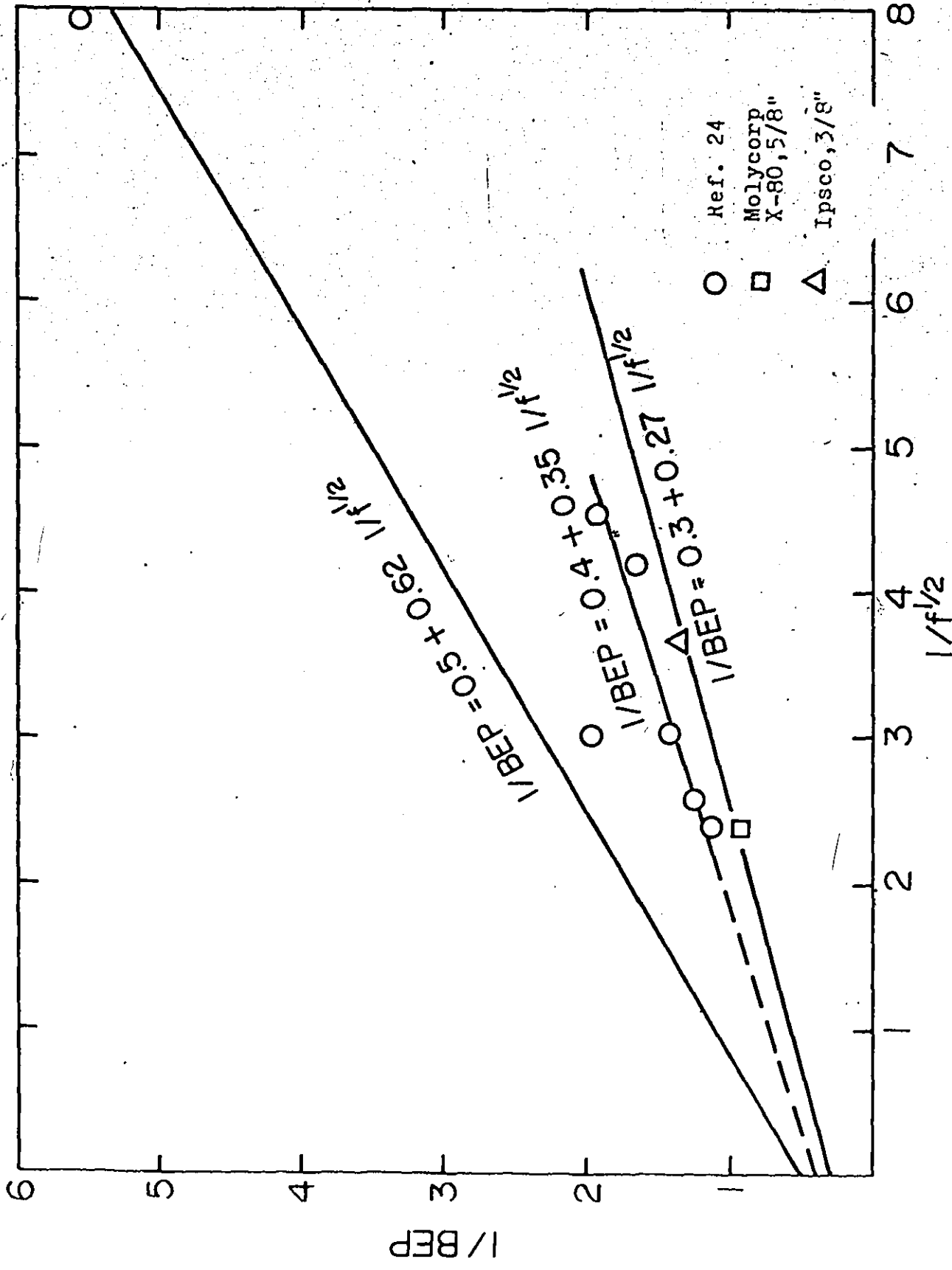


Fig. 57

ials could result from processing at low temperatures, or as a result of the transformation (volume accommodation of the microconstituents such as retained austenite or martensite).

To investigate the presence of the residual stresses in these materials, their sense and scale, experiments were conducted in tensile-compressive and compressive-tensile cycling deformation. From the results shown in Figures 45 to 56 it is found that in both tested HSLA steels, Molycorp X-80 and Ipsco, in the as-received conditions, the magnitudes of the BEP for tension-compression type of deformation are well above those for compression-tension tests. This leads to the conclusion that in the as-received materials there already exists some tensile residual stress, which opposes deformation in tension and aids the deformation process in compression. According to the simple model for the BEP, used in this investigation, very small differences in the initial flow stress, σ_0 , are needed for marked changes in the BEP in the tested materials. It was found in this work that the yield stress in compression is lower than it is in tension by approximately 1 - 4 ksi, depending on the specimen orientation with respect to the rolling axis. By annealing for 1 hour at 550°C, the difference in the BEP in both materials is reduced, showing that the probably existing residual stresses are removed by this heat treatment.

Knowing that the presence of the residual stresses could result from the controlled rolling at low temperatures or from the transformation, an attempt was made to investigate if the

nature of the residual stresses has any relationship to the rolling direction.

Studies of the BEP were conducted on specimens taken at 0° (L-longitudinal), 45° (D-diagonal) and 90° (T-transverse) from the rolling direction. All the experiments were again done in tension-compression and compression-tension, and the results are shown in Figures 45 to 56. For clarity, all the results for the BEP are summarized in Figure 58 for Molycorp X-80, 5/8" and in Figure 59 for Ipsco 3/8".

From the data, a general conclusion can be made that the largest difference in the magnitudes of the BEP in tension-compression and compression-tension tests is found for the samples taken parallel to the rolling direction. This difference decreases as the orientation of the samples rotates towards the transverse direction. This indicates polarization of the residual stresses in the rolling direction and can be explained in two ways. Firstly, the largest portion of the residual stresses in the as-received materials could result from the rolling at low temperatures. Secondly, alignment of the second-phase particles in the rolling direction during processing could provide maximum resistance to the flow processes in specimens parallel to the rolling direction.

It is important to note that the difference between the magnitudes for the BEP in tension-compression and compression-tension for Molycorp X-80, 5/8" during annealing, is decreased in longitudinal samples while the magnitude of the BEP for transverse orientation is almost unchanged. This means that

MOLYCORP X-80, 5/8"

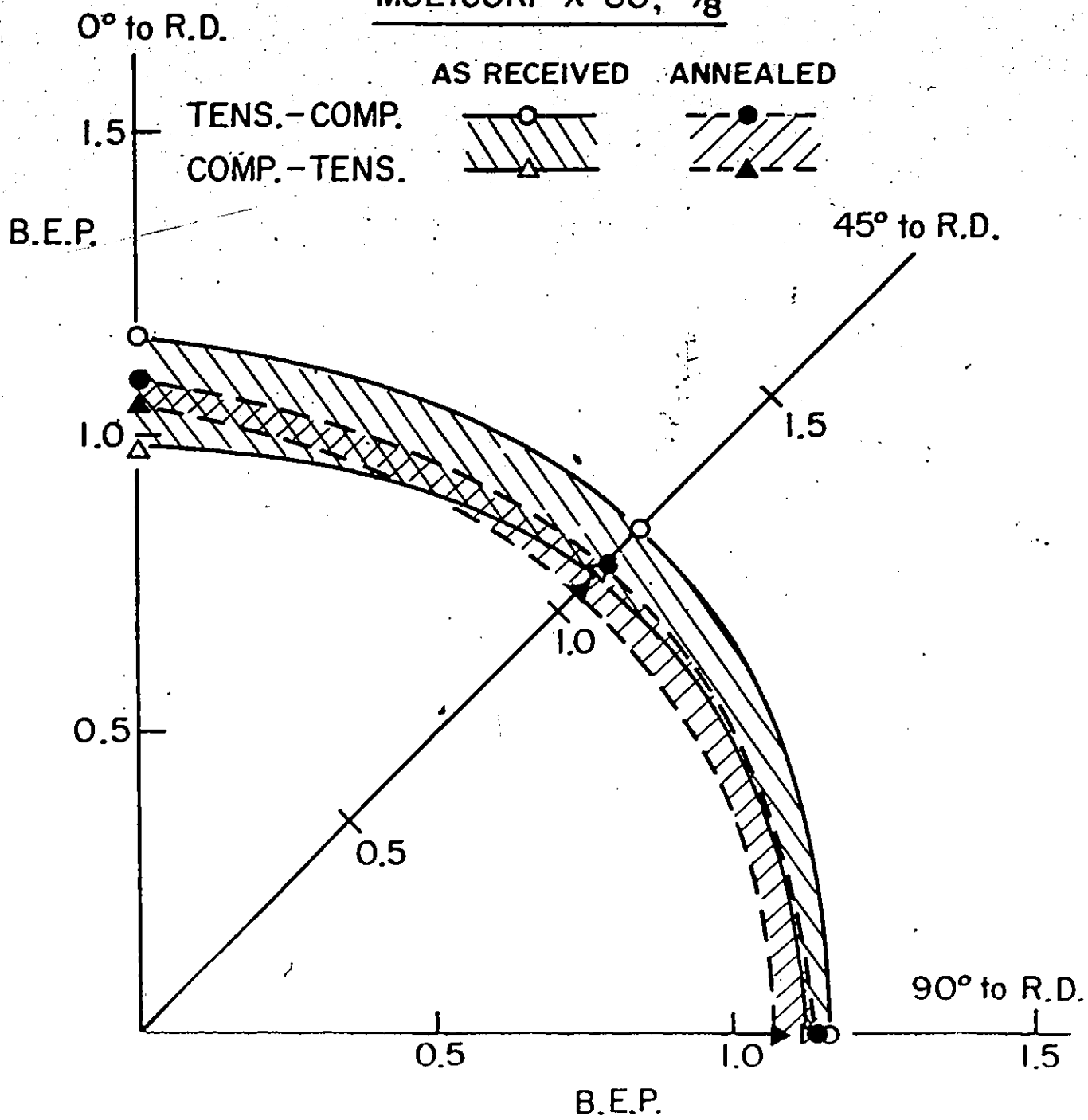


Fig. 58.

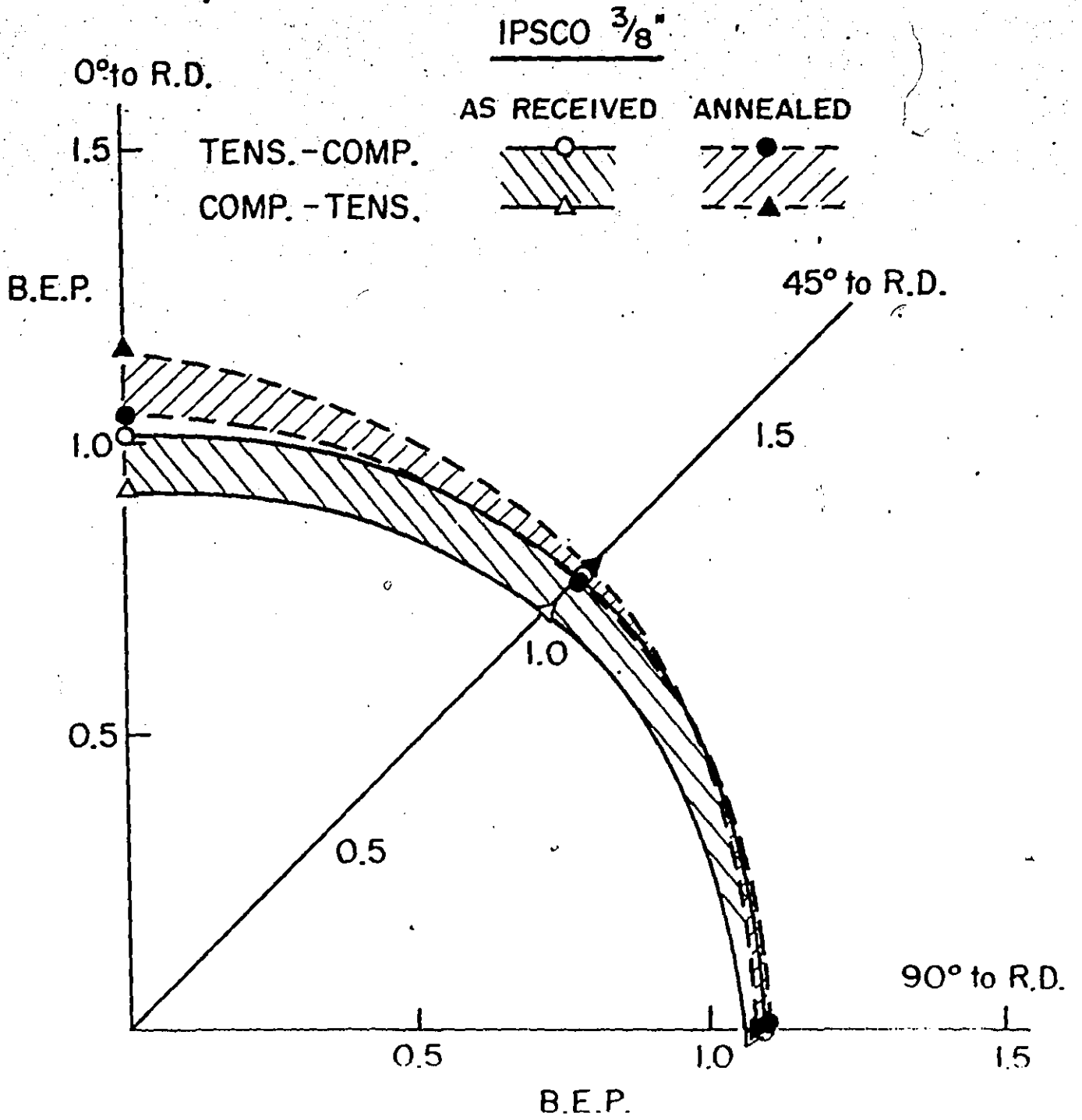


Fig. 59.

the observed anisotropy in Molycorp X-80, 5/8" in the as-received condition is removed by annealing, bringing the BEP magnitudes to almost the same values in any orientation. The data for Molycorp X-80, 5/8" supports the theory that the presence of the residual stresses are due to the rolling at low temperatures and due to localized transformation. Knowing that the presence of the residual stresses in the as-received condition could affect the shape of the initial yielding, the stress-strain curves for Molycorp X-80, 5/8" for the tested orientations, in both tension and compression are compared, and are presented in Figure 60.

It can be seen from the initial part of the stress-strain curves, that there exist some differences in the work-hardening rates and these also cause the differences in the measured 0.2% offset yield stresses. The roundness of the presented tensile stress-strain curves, increases as the orientation of the sample rotates from the transverse to the rolling direction, indicating that the most effective tensile residual stresses are polarized parallel to the rolling axis⁽³¹⁾. In compression tests, the roundness of the stress-strain curves is almost the same in all orientations.

From the summarized data for Ipsco 3/8" shown in Figure 59, it can be seen that the largest difference in the BEP values between tension-compression and compression-tension was observed in the samples taken from the rolling direction, while almost no difference was found for the samples in the transverse direction. It was interesting to notice that, after

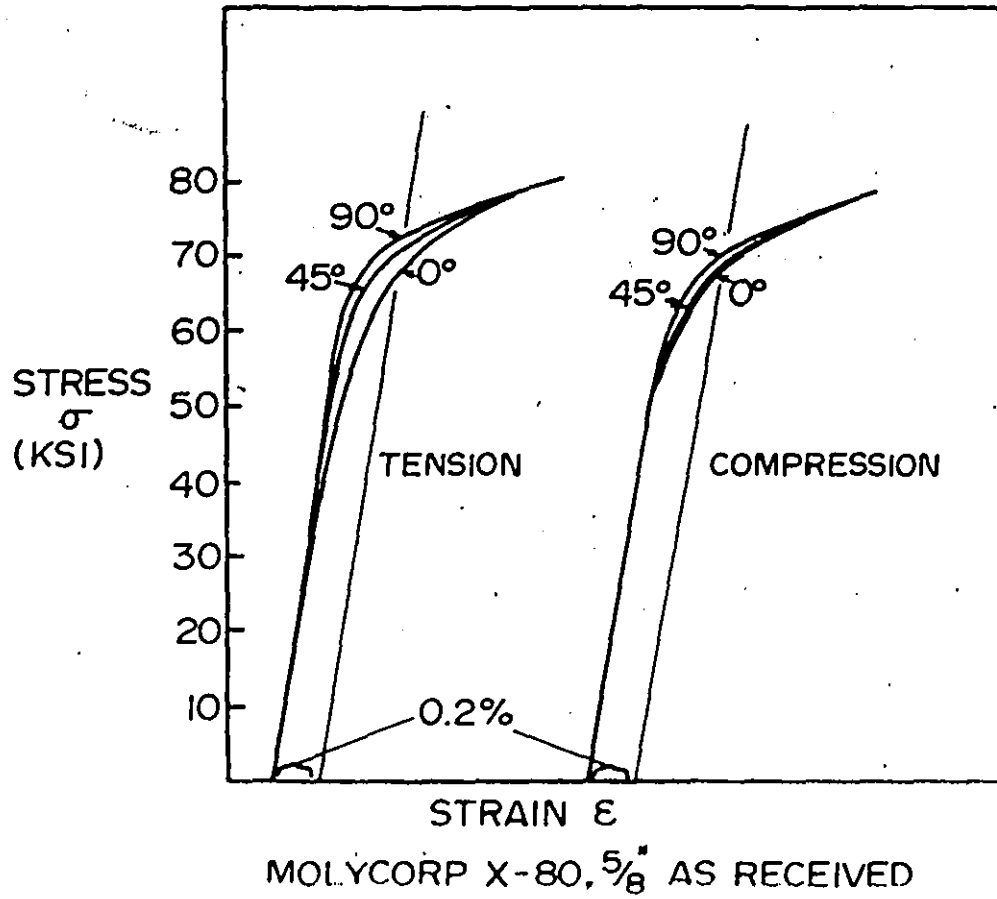


FIG 60.

annealing (1 hour at 550°C), the magnitude of the BEP for compression-tension test for the longitudinal samples was increased while the values for this parameter for tension-compression was almost unchanged. It is possible that during annealing some precipitation hardening occurred, and the increased volume fraction influences the magnitude of the BE. At the present time it is not understood why such a difference in the BEP for different orientations exists after annealing.

It was documented in previous chapters that the presence of residual stresses in HSLA materials plays an important role in the failure mechanisms and in a similar manner it could be stated here that the presence of any residual stress fields greatly increases the Bauschinger loss. To reduce these effects, more work is needed for a fully quantitative analysis of all the factors that could cause a residual stress field in the materials.

As reported earlier, in these complex materials, the S-D effect is observed and is of the order of 1-4 ksi. This is particularly important for the accurate characterization of the BE as a function of the direction and sense of the initial deformation. This may account for the observed planar anisotropy and the differences obtained in the BE.

According to the literature⁽³²⁾, this is an indication of the presence of polarized residual stresses in the material. These stresses could be related to the preferred orientation of the second phase particles in the rolling direction and could be caused by the volume expansion that accompanies the austenite

to martensite transformation and by the thermal gradients present during cooling. As reported, these materials, consisting of a mixture of soft and hard phases could show a large S-D effect. To characterize the S-D effect and its relationship to the BE for the tested materials, more work is needed for the precise determination of the yield stress, σ_0 , in various directions and senses of deformation.

As a general comment, the magnitude of the BE in HSLA steels is very large even though these are materials with very low carbon levels and relatively low inclusion levels.

The main microstructural features in HSLA steels influencing the BE are found to be a number of complex, hard, rigid and relatively large regions such as M/A constituents and carbides, along with some residual stresses in their vicinity.

CHAPTER 7
CONCLUSIONS

The present thesis has been concerned with the mechanical properties, the forming characteristics, the fracture behaviour and their relationship to the microstructural features of the commercially processed HSLA steels. In addition, an effort has been made to describe the behaviour of these materials in reverse straining.

From the data presented in this thesis, the following conclusions can be formulated:

1. In spite of the very low carbon content, the microstructures of the tested HSLA steels are complex and can be represented as mixtures of the soft (ferrite) and the hard (M/A, inclusions) phases. In the materials with very low inclusion content, the critical microstructural quantity seems to be the complex M/A constituent.
2. The work-hardening exponents, n , and the corresponding values for the uniform strains in uniaxial tension are relatively low. Soon after the geometrical instability is reached, the samples failed along shear zones.
3. The strain to failure for the HSLA steel with a very low inclusion content is almost the same as or less

than the failure strain for the HSLA steel with a high inclusion content. In the first case, the M/A constituent present in this material plays the role of inclusions.

4. The Forming Limit Diagrams produced show relatively low forming potentials, predicting difficulties in the forming of more complex components from these materials.
5. The results from the stretch-bend tests show a good correlation with the forming characteristics. It is a very sensitive method of evaluating the transverse formability and the effectiveness of sulphide shape control.
6. A number of failure modes is observed in this study, and the most critical seems to be the development of unstable shear bands at an early stage in the deformation history. The presence of hard, complex M/A regions with residual stresses in their vicinity could have a major influence on the strain localization and the formation of unstable shear bands.
7. The magnitude of the BE in the tested HSLA steels is very large, even though these are materials with very low carbon levels and relatively low inclusion contents.
8. The magnitude of the BEP for these materials is found to be independent of the extent of the forward plastic strain, but is dependent on:
 - a) the direction of straining with respect to the rolling direction,
 - b) the initial sense of deformation (initial straining in tension or compression).

REFERENCES

- (1) J.M. Gray, "Metallurgy of HSLA Pipeline Steels", Molybdenum Corp. of America, Rep. No. 7201 (1972).
- (2) J.D. Boyd, Canada Centre for Mineral and Energy Technology, Report No. ERP/PMRL - 75 - 13(R), June 1975.
- (3) V. Biss and R.L. Cryderman, Met. Trans. 1971, 2, 2267.
- (4) J.L. Michelich and R.L. Cryderman, "Low Carbon Mn-Mo-Nb Steel for Gas Transmission Pipe", 72 - Pet - 36, published by ASME, 1972.
- (5) K. Cooper and J.D. Embury, Can. Met. Quart., 1975, 14, 69.
- (6) J.M. Gray and W.G. Wilson, "Molycorp Develops X-80 Arctic Pipeline Steel", Pipeline and Gas Journal, December 1972.
- (7) H. Herø, J.D. Evensen and J.D. Embury, Can. Met. Quart., 1975, 14, 117.
- (8) International Nickel Company of Canada, private communications.
- (9) J.M. Gray, "Metallurgy of HSLA Steels: Present and Future Possibilities", Molybdenum Company of America, 1972, Report No. 7201.
- (10) T. Butler, Sheet Metal Ind., 1964, 9, 703.
- (11) D. Black and H. L'Herbier, Met. Proc., 1965, 6, 62.
- (12) D.P. Clausing, Int. J. Fract. Mech., 1970, 6, 71.
- (13) S.P. Keeler, "Understanding Sheet Metal Formability", Issue of Machinery Magazine, 1968, 4, 5.
- (14) D.K. Uko, Master's Thesis, McMaster University, 1975.
- (15) A.S. Argon, J. Im and R. Safoglu, presented at Third Int. Conf. on Fracture, Munich, 1973.
- (16) L.M. Brown and J.D. Embury, Proc. Third Int. Conf. on Strength of Metals and Alloys, page 164, Cambridge, 1973.
- (17) E. Miyoshi, M. Fukuda, H. Iwanaga and T. Okazawa, Proc. Inst. Gas. Eng. Conf., Crack Prop. in Pipelines, Newcastle, 1974.
- (18) I. Kozasu, T. Shimizu and H. Kubota, Trans. I.S.I. Japan, 1973, 13, 21.

- (19) R.F. Dewsnap, R. Pearce and J.R. Branson, B.S.C. Report, MG/24/72, reported at Proc. of BDDRG, 1972.
- (20) J.D. Embury, J.D. Evensen and A. Filipovic, "The Mechanical Properties of HSLA Steels", Proc. of the Battelle Colloquium on "Fundamental Aspect of Structural Alloy Design", September, 1975.
- (21) J. Bauschinger, J. of Civil Eng., N.F. 1881, 27, 289.
- (22) L.M. Brown and W.M. Stobbs, Phil. Mag. 1971, 23, 1201.
- (23) N. Ibrahim and J.D. Embury, Mat. Sci. Eng., 1975, 19, 147.
- (24) N. Ibrahim, Ph.D. Thesis, McMaster University, 1974.
- (25) D.V. Wilson and Y.A. Konnan, Acta. Met., 1964, 12, 617.
- (26) W. Janiche et al, Tech. Mitt. Krupp, Forschungsber, 1975, 23, 117.
- (27) R.M. Jamieson and J.E. Hood, JISI, 1971, 209, 46.
- (28) N.H. Polakowski, JISI, 1951, 169, 337.
- (29) S.N. Buckley and K.M. Entwistle, Acta. Met., 1956, 4, 352.
- (30) W. Janiche, E. Stolte and J. Kagler, Tech. Mitt. Krupp, Forschungsber, 1965, 23, (4), 117.
- (31) J. Friedel, "Internal Stresses and Fatigue in Metals", edited by G.M. Rassweiler and W.L. Grube, p.220, published by Elsevier, Amsterdam 1959.
- (32) Hirth and Cohen, Trans. Met. Soc., 1970, 1, 1.
- (33) Salwe and Willner, Naval Ship Research and Development Centre, 1972, Report No. 3701.